ANALYSIS OF PARTICLE DEFORMATION MECHANISMS AND COMPACT EXPANSION DURING COMPACTION ON A HIGH SPEED ROTARY TABLET PRESS

by

SARVAJNA KUMAR DWIVEDI

B.Pharm., Banaras Hindu University, 1984
M.Pharm., Banaras Hindu University, 1986
M.Sc., The University of British Columbia, 1988

A THESIS SUBMITTED IN PARTIAL FULFILLMENT OF

THE REQUIREMENTS FOR THE DEGREE OF

DOCTOR OF PHILOSOPHY

in

THE FACULTY OF GRADUATE STUDIES

(Pharmaceutical Sciences)

We accept this thesis as conforming

to the required standard

THE UNIVERSITY OF BRITISH COLUMBIA

October, 1992

In presenting this thesis in partial fulfilment of the requirements for an advanced degree at the University of British Columbia, I agree that the Library shall make it freely available for reference and study. I further agree that permission for extensive copying of this thesis for scholarly purposes may be granted by the head of my department or by his or her representatives. It is understood that copying or publication of this thesis for financial gain shall not be allowed without my written permission.

Department of PHARMACEUTICAL SCIENCES

The University of British Columbia
Vancouver, Canada

Date Oct. 08/92

DE-6 (2/88)

ABSTRACT

Pharmaceutical tablets are the most widely used dosage form and are prepared by the high speed compaction of powders or granules in a die on a rotary tablet press. The tablets produced must be coherent and capable of withstanding the stresses of handling and transportation. Successful compact formation depends on the ability of the particles to deform and form interparticulate bonds during compression in the die and the ability of these bonds to withstand elastic expansion during decompression and ejection from the die.

Compaction on the high speed rotary presses used in the pharmaceutical industry normally occurs in less than 50 ms. The mechanisms of particle deformation during compaction are often analysed using presses operating at slow speeds or by using specialised equipment which perform tests on either preformed compacts or on single crystals.

In the present work a sixteen-station rotary tablet press - a Manesty Betapress - was used to analyse high speed compaction. The analysis involved a study of the relationship between punch force and machine deformation, and its use in understanding the deformation of powder particles during compression and the elastic expansion of compacts during decompression. Rotary presses have been used to analyse compaction previously but either the materials were compressed under static conditions, or the results were obtained by complex viscoelastic modeling. These results were in error because the machine deformation was ignored when the punch displacement was calculated from the machine and punch-head geometry.

In contrast, the relationship between machine deformation and punch force was used in this work to calculate punch displacements on the

Betapress from the measurements of upper punch force. A previously reported method of calculating the punch displacement (Oates and Mitchell, 1989, 1990) was refined and simplified. This requires only the force versus time data where the force was measured by a strain-gauged upper roll support pin. Since it is relatively easier to measure punch force on a rotary press than make direct measurements of punch displacement, this method offers accurate punch displacement analysis without using complex instrumentation and/or geometric calculations.

Over forty solids were studied on the Betapress. The solids were characterized for various physicochemical properties including true and bulk densities, and melting and/or decomposition temperatures. Powder X-ray diffraction, melting points and a two-component melting point-composition phase diagram of R and S-ibuprofen showed that racemic ibuprofen is a one phase 'racemic compound' as opposed to a two phase 'racemic mixture'. Thus, the USP description of ibuprofen as a '± mixture' is misleading. All solids, including the commercially available S-ibuprofen and racemic ibuprofen, were compressed on the Betapress under speed.

The force signals from the upper roll support pin were collected as a function of time on a desk-top computer via an analog to digital converter. The compaction cycle was divided into compression and decompression phases by the dead centre position at which the punches are vertically aligned with the centres of the compression roll support pins. The force-time data were analysed using specially written software to obtain several parameters from the compaction cycle. Parameters obtained from the compression phase included peak offset time, decrease in punch pressure during peak offset time, porosity changes, work of compression and yield values of the solids.

These parameters related particle deformation to pressure. The relationship between force and machine deformation was used to subtract the machine recovery from the total recovery during decompression. This gave a novel method of estimating tablet expansion during decompression. The tablet expansion data was used to calculate the work of tablet decompression and to estimate the Young's modulus of several pharmaceutical solids.

Since particle deformation during compression is dependent on strain rate, the strain rate during compaction was approximated by using the decrease in volume of the powder bed in the die during compaction, and this, along with the above parameters, was used to ascertain the deformation mechanism of each solid.

The solids were categorised into groups ranging from low yield-strength ductile solids such as acetylsalicylic acid, ibuprofen and their formulations to high yield-strength brittle solids such as the various calcium phosphates. The tableting parameters of formulated drugs and processed excipients were different from the parent samples. Racemic ibuprofen and S-ibuprofen showed little difference in their tableting parameters, hence a decision to use S-ibuprofen instead of racemic ibuprofen in tableting should be based on differences in other properties such as solubilities and pharmacokinetic differences.

A simple and inexpensive method of analysing the behaviour of powder particles during compaction on a high speed rotary press using only force-time measurements is presented. This method is potentially applicable to any tablet press, and can be used for the in-process validation of compaction, for the quality control of raw materials, and for the development of new tablet formulations.

LIST OF CONTENTS

LIST OF SYMBOLS

σ	Stress
σ_T	Stress at the points of interparticulate contact: true stress
σ_y	Yield stress or yield value
ϵ	Strain
$\dot{\epsilon}$	Strain rate
$\epsilon(fr)$	Strain as a function of fr
η	Viscosity
ρ_r	Relative density
ΔD_m	Change in machine deformation in response to ΔF
$\Delta D_m(fr)$	ΔD_m as a function of fr
$\Delta D_{mfr=0}$	ΔD_m at fr = 0, i.e., the dead centre position of punches
$\Delta D_{mF=0}$	ΔD_m at F = 0, i.e., at the end of decompression
D_m	Machine deformation
D	Distance between the punch faces during compaction
D(fr)	Distance between the punch faces during compaction as a function of fr
D(F)	Distance between the punch faces during compaction as a function of punch force
D(t)	Distance between the punch faces during compaction as a function of time during compression
E	Young's modulus
E_p	Modulus of elasticity of a tablet with a certain porosity
fr	Fraction of a turret revolution
$fr_{F=0}$	fr at F = 0, i.e., at the end of decompression
ΔF	Change in punch force during the compaction cycle
F	Punch force during the compaction cycle
$F_{fr=0}$	F at fr = 0, i.e., at the dead centre position of punches

ΔH	Change in the height of compacts during decompression
$\Delta H(fr)$	Change in the height of compacts during decompression as a function of fr
ΔH^f_R	Heat of fusion of a racemic compound
H_{max}	Value of the Heckel term $\ln(1/p)$ at P_{max}
$H_{F=0}$	Compact height at F = 0, i.e., at the end of decompression
$H_{fr=0}$	Compact height at fr = 0, i.e., at the dead centre position of punches
K^{-1}	Machine deformation constant (2.3×10^{-6} cm/N)
p	porosity
$\Delta P/V_T$	Decrease in pressure during peak offset time normalised for true volume of the material
P	Pressure
P_{max}	Maximum pressure or peak pressure
R	Gas constant
t	Time during the compaction cycle
T^f	Absolute temperature on liquidus curve of the binary phase diagram of an enantiomeric system
T^f_R	Absolute melting point of racemic compound
T_m	Melting point
t_{off}	Peak offset time
V_T	True volume
W_C	Work of compression
W_D	Work of decompression
x	mole fraction enantiomeric composition

LIST OF TABLES

LIST OF FIGURES

ACKNOWLEDGEMENTS

I am thankful to the following people:

My research supervisor Prof. A.G. Mitchell, for his continuous support, encouragement and advice during my studies at The University of British Columbia, and for providing a laboratory atmosphere congenial to independent thinking and research. His guidance over the years has been an invaluable experience for me. I will cherish his friendship for a long time to come.

Dr. J. A. Lund of the Dept. of Metals and Materials Engineering at UBC for critical evaluation of most of the work presented in this thesis and for his thoughtful suggestions at various times during the course of this work. His continued support as a member of my supervisory committee is specially acknowledged.

Dr. J. G. Sinclair, Dr. H.M. Burt, and Dr. A.H.L. Chow (now at Glaxo Canada Inc.) for their valuable support as members of my supervisory committee throughout the course of this work.

My friend and research colleague Mr. R.J. Oates for insightful discussions and ideas, and for writing the excellent computer software without which much of this work would be incomplete.

My colleague Mr. Ibrahim El-Bagory for his help when needed, and Mr. Charles Winternitz and Ms. Marion Wong for their sincere technical assistance as summer students during the initial part of this work.

Gifts of samples from the various suppliers, and Graduate Awards from the Berlex Foundation and the Novopharm Group (Stanley Drugs) are gratefully acknowledged.

TO

SADASHIV

1. INTRODUCTION

Tableting by powder compaction can be described as a process of increasing the density of a powder bed with the intent of creating a certain degree of bonding between the powder particles, thereby obtaining a coherent compact capable of withstanding the stresses of handling and transportation. Compaction is the general process of application of mechanical force to a powder bed. The densification of the powder bed during compaction is called compression and an increase in the mechanical strength of the powdered material due to bonding is called consolidation (Marshall, 1986). The compaction process involves application of force, or pressure, on the powder bed by confining the powder to a gradually diminishing volume between two punches within a die (the compression phase), and then releasing this force (the decompression phase) to allow the removal of the tablet from the die. The most commonly used machines in the manufacture of tablets by powder compaction are rotary tablet presses which compress the powders by a biaxial compression process. On a rotary tablet press the complete compaction cycle usually occurs in less than 50 ms. Industrial scale tableting is therefore a high speed process.

1.1 THE COMPRESSION PHASE

During the compression phase, the powder particles rearrange under the applied force and, above a certain force, undergo deformation. The process of rearrangement causes an initial densification of the powder bed during which some particle deformation may occur. The success of powder compaction in producing strong, coherent tablets depends, at least in part, on the extent of deformation of the particles (crystals, crystalline aggregates, or granules containing some type of binder) during the

compression phase. Deformation exposes new, uncontaminated surfaces where bonding readily occurs since these surfaces are in close proximity to each other.

Train (1956), Toure *et al.* (1980), and Parrott (1985) discussed the various stages which a powder bed goes through during compression. The actual events are complex since the behaviour of the powder particles during compression is governed by factors such as pressure (or stress), the amount of deformation (or strain), and the rate of deformation (or strain rate) at the particulate level. Hence knowledge of stress, strain and strain rate is important in understanding particle behaviour during compression. The nature of the equipment used, the physicochemical properties of the solid, and the ambient conditions of temperature and humidity, are among the factors that can influence the stress-strain behaviour of the particles during compression.

1.1.1. Elastic, viscous and viscoelastic stress-strain behaviour

Two important mechanisms by which materials may deform under stress are elastic deformation and viscous flow. These are described by the following theories:

(1) The theory of elasticity, according to which the stress in elastic solids is always directly proportional to strain but is independent of the rate of strain. This is the basis of the Hooke's law of elasticity, which can be expressed as,

$$\sigma = E \cdot \epsilon \qquad (1)$$

where, σ = stress, ϵ = elastic strain and E is the modulus of elasticity, or the Young's Modulus, of the solid assuming an isotropic nature. The elastic strain is completely recoverable upon the removal of stress.

(2) The theory of hydrodynamics, according to which the stress in viscous materials (fluids) is always directly proportional to the rate of strain but is independent of the strain itself. This is described by Newton's law of flow of viscous fluids:

$$\sigma = \eta \cdot \dot{\epsilon} \qquad (2)$$

where, $\dot{\epsilon}$ = rate of strain, and η is the coefficient of viscosity. The strain in viscous materials is non-recoverable upon the removal of stress.

The above two categories of deformation represent ideal stress-strain behaviour. Real solids deviate from ideality and combine the elastic solid-like behaviour with the viscous liquid-like behaviour. Such materials, unlike elastic solids, do not maintain a constant strain under a constant stress, but go on slowly deforming under this stress. If deformed to a constant strain, these materials will require gradually diminishing stress to maintain the deformation. The phenomenon of gradually increasing strain under constant stress is called creep, while the phenomenon of gradually diminishing stress under a constant strain is called stress relaxation. Materials which show these deviations from ideality may not be able to recover their deformation instantaneously and/or completely upon

the removal of stress and are called viscoelastic materials (Popov, 1968; Ferry, 1980).

The nature of viscoelastic materials is described by the theory of viscoelasticity which is based on models combining one or more ideal elastic solid element (a spring) with one or more ideal viscous fluid element (a dashpot). The most simple is the combination of a spring and a dashpot in series, giving a Maxwell model, or in parallel, giving a Voigt-Kelvin (or Kelvin) model. A combination of these simpler models in series or in parallel with each other and/or with the ideal elastic or viscous elements gives more complex models. Equations relating the stress, strain, and the strain rate in these models can be derived for each configuration of the elastic and viscous elements (Bland, 1960; Flugge, 1975). The equations can be derived assuming unidimensional linear viscoelastic behaviour, or can be based on the more complex three dimensional linear viscoelastic behaviour. The general purpose of these equations is to explain the rate and extent of creep and stress relaxation phenomena when materials deviating from the ideal elastic or viscous behaviour are subjected to stress.

1.1.2. Creep and stress relaxation in pharmaceutical solids under pressure

The ability of a material to undergo creep or stress relaxation is related to its ability to deform by flowing under stress. Therefore an estimate of the rate and extent of creep or stress relaxation under compression can be used as an estimate of the ability of the powder particles to deform by a flow process. Creep and stress relaxation in pharmaceutical powders have been studied by compressing the powders for varying lengths of time using various types of compression equipment.

The phenomenon of creep in pharmaceutical powders has been investigated by measuring the change in strain as a change in the powder bed height under a constant stress, measured as the stress on the punches. Among the first reports was that by Okada and Fukumori (1975) who examined the creep properties of a number of inorganic salts by maintaining a constant upper punch pressure on an isolated punch and die assembly for up to 10 hours. The thickness of the powder bed decreased and levelled off during this period of time, suggesting that the particles of these solids undergo some type of time-dependent deformation by flow under stress. Travers *et al.* (1983) and Celik and Travers (1985) used a hydraulic press and recorded creep as 'strain movements', i.e., change in the height of the compacts within the die, when the stress was maintained at a constant level for up to 60 s. Based on the amount of strain movement, selected pharmaceutical solids were divided into compressible and poorly compressible classes. Staniforth *et al.* (1987) used a similar testing procedure to measure the creep behaviour of microcrystalline cellulose when it was formulated with different amounts of water. They concluded that, while it differentiated the formulated material from the parent material, the creep analysis could not explain the differences between the tablet strengths before and after formulation with water.

Contrary to the assumption that the peak punch pressure occurs at maximum punch displacement, Ho and Jones (1988a) reported the phenomenon of 'punch travel beyond peak force' on a compaction simulator and related it to the plastic flow of materials during compression. This can be interpreted as creep provided the peak force (or the stress) remains constant while the punches travel beyond the peak force. Doroudian (1991) recorded punch travel beyond peak pressure on a hydraulic press, but this

observation was complicated by a decrease in the pressure when the punches travelled beyond the peak pressure. Hence, it seems that the punch travel beyond peak pressure neither represents creep nor stress relaxation, since neither stress nor strain is constant.

The study of creep during powder compaction requires the conditions of constant stress, which can be attained under static conditions on slow speed compaction equipment such as a hydraulic press. Creep analysis by the above methods therefore differentiates the flow properties of materials over time intervals uncharacteristic of real tableting conditions. During the highly dynamic process of tableting on a rotary tablet press it will be almost impossible to obtain the condition of constant stress. It is possible that the differences in the flow properties, as indicated by differences in the creep behaviour under static conditions may either disappear, or may become more pronounced, under dynamic conditions.

During high speed tableting, stresses change rapidly in response to the rapidly changing volume between the punch faces within the die. Deformation of powder particles by flow will occur within the confines of the die and the punch faces over a time period which is determined by the type of compression equipment used. Since, during tableting, it is relatively easier to measure the change in pressure as a function of time, the analysis of the stress relaxation phenomenon has received greater attention than has the analysis of creep. For example, Shlanta and Milosovich (1964) observed a decrease in punch stress with time for a number of pharmaceutical solids on an instrumented hydraulic press. Cole *et al.* (1975) reported differences in the extent of stress relaxation of sodium chloride, potassium chloride, lactose and potassium citrate when these substances were compressed on a device specially developed to

simulate a rotary tablet machine. Using a hydraulic press similar to the one used by Shlanta and Milosovich (1964), Hiestand *et al.* (1977) found that materials, the tablets of which fail by capping or lamination, showed slow stress relaxation. David and Augsburger (1977) quantitated stress relaxation on a Stokes RB-2 rotary tablet machine under static conditions by recording the decrease in pressure over a period of several seconds for some direct compression excipients. Rees and Rue (1978) measured stress relaxation on a Wilkinson STD 1 reciprocating tablet machine. They also indicated that a rotary tablet machine, such as the one used by David and Augsburger (1977), may not be a deflection-free system and therefore the strains during the period of stress relaxation may not be constant. Peleg and Moreyra (1979) studied the effect of moisture on the stress relaxation pattern of powders under pressure using an Instron Universal Testing Machine. Caspar and Muller (1984) used a single punch eccentric press to obtain the stress relaxation data over a period of up to 60 s and found differences between the behaviour of selected pharmaceutical materials. More recently, using an Instron Physical Testing Instrument, Cutt *et al.* (1987) demonstrated the effect of wet granulation on the stress relaxation of a model system consisting of glass bellotini granulated with different binders. The granulated glass showed significantly enhanced stress relaxation over a period of 6 minutes compared with non-granulated glass. Ho and Jones (1988b) studied the stress relaxation of a number of pharmaceutical materials on a modern compaction simulator.

These reports indicate both qualitative and quantitative differences in the stress relaxation behaviour of various substances. Relative to the high speed operating conditions of rotary presses, the decrease in stress was followed over long periods of time ranging from a few seconds to

several minutes. Only some of these studies provided evidence of constant strain.

To establish the relevance of stress relaxation in tableting on rotary presses, where compression normally occurs in less than 50 ms, evidence is required that stress relaxation indeed occurs at the speeds encountered on such machines and that the condition of constant strain is satisfied over the period of stress relaxation. To provide such evidence it is necessary to investigate the relationships between stress and strain on a rotary tablet machine or on a compaction simulator. Stress relaxation studies on a compaction simulator require an input of the punch displacement profile from the rotary tablet press in order to simulate its compaction cycle. If the deformation of the tablet press under load is ignored (section 2.3.2), the resultant errors in the displacement profiles will lead to inaccuracies in the estimation of strain during the period of stress relaxation.

1.2. THE DECOMPRESSION PHASE

During compression, the distance between the punch faces decreases as the tablet press does work on both the powder bed and the press (including the punches and die). The work done on the press deforms it elastically such that the elastic energy is recovered during decompression. By contrast, only a small portion of the work done to the powder bed is recoverable. The rest of the work is lost to friction, particle deformation, heat and other irreversible processes in forming a tablet. During the decompression phase the stresses built up during the compression phase are rapidly released and the tablets are subsequently ejected from the die. The length of decompression phase on high speed presses is

normally less than 20 ms, during which time a tablet expands in an axial direction within the confines of the die while still in contact with the punches. The rapid decompression and the resultant expansion may cause tablet failure by capping and lamination if the interparticulate bonds formed during the compression phase are too weak to withstand the stresses induced by the decompression (Ritter and Sucker, 1980).

1.2.1. Analysis of tablet expansion during decompression

Tablet expansion during decompression has been studied using isolated punch and die assemblies mounted in stress-strain analysers (Travers *et al.*, 1983; Malamataris *et al.*, 1984; Bangudu and Pilpel, 1985; Celik and Travers, 1985) and compaction simulators (Yu *et al.*, 1988). Single punch presses fitted with linear variable differential transformers (LVDTs) have been used to measure punch displacements and press deformation (Ho *et al.*, 1979; Juslin and Paronen, 1980; Lammens *et al.*, 1980; Kaneniwa *et al.*, 1984; Cook *et al.*, 1988). Since tablet expansion during decompression is very small relative to the elastic recovery of the press, it is essential that the LVDTs are mounted and calibrated such that tablet recovery can be differentiated from that of the press.

It is technically more difficult to measure the punch displacement on a rotary tablet press (Ridgway-Watt, 1983, 1988; Walter and Augsburger, 1986; Oates and Mitchell, 1990). As an alternative to direct measurements, Rippie and Danielson (1981) and Charlton and Newton (1984) calculated punch displacement from machine and punch head geometry assuming no machine deformation and recovery.

1.2.2. Use of tablet expansion in material characterisation

Rippie and Danielson (1981) and Danielson *et al.* (1983) analysed the decompression of several pharmaceutical solids on a rotary tablet press and concluded that the recovery of tablets during decompression is elastic in nature. If this conclusion is extended further, it is possible that the elastic expansion of the tablets can be analysed by using the theory of elasticity to obtain the Young's modulus of the tablet material. Young's modulus is an important fundamental material constant.

The Young's modulus, and other elastic moduli, of composites have been derived from physical models consisting of spherical or nonspherical pores homogeneously distributed in an isotropic matrix (Rossi, 1968). Tablets are anisotropic, heterogeneous bodies in which the pore shape and structure differ from the ideal nature required by the theoretical models. Therefore, their recovery and modulus at a given porosity, E_p, must be determined experimentally for each formulation and each set of tableting conditions. The E_p of various compacted pharmaceutical materials has been determined in flexure tests (Church and Kennerley, 1982, 1983; Mashadi and Newton, 1987; Bassam *et al.*, 1988; Agbada and York, 1990) and compressive tests (Kerridge and Newton, 1986). Roberts and Rowe (1987a, b) calculated E_p using yield strengths estimated from Heckel plots (Heckel, 1961) and the tablet indentation hardness values, previously determined by Jetzer *et al.* (1983), in an equation given by Marsh (1964). The modulus at zero porosity, E, was estimated by Kerridge and Newton (1986), Roberts and Rowe (1987a), and Bassam *et al.* (1988) using E_p in the equation of Spriggs (1961), and by Roberts and Rowe (1987a) using E_p in the equation of Wachtman (1969).

Problems associated with the comparison of E_p obtained from compacts of differing porosities and uncertainties in values of E obtained by extrapolating the values of E_p to zero porosity are avoided by single crystal tests. Ridgway *et al.* (1969) used a microtensile testing machine modified for use in compression and estimated Young's modulus from the stress-strain curves of a number of substances. Single crystal microindentation measurements were made by Duncan-Hewitt (1988), Duncan-Hewitt and Weatherly (1989b) and Wong and Aulton (1989) to determine E for sucrose and α-lactose monohydrate, respectively. The modulus was found to vary with crystal face illustrating the anisotropic nature of these crystals. Similar conclusions can be drawn on the basis of an earlier work by Bridgman (1948) in which compressibility data for different faces of sucrose crystals were obtained by a hydrostatic compression procedure, from which the Young's modulus for different faces can be estimated.

It would be convenient if the data from a high speed rotary tablet press could be used to characterise the decompression phase by a simple analytical procedure without having to resort to extensive viscoelastic modeling. Such analysis would not only be useful in characterising materials, but should also help in developing better formulations for problem drugs.

1.3. PARTICLE DEFORMATION UNDER PRESSURE

There are five possible mechanisms by which a particle may deform during compaction:

1. Elastic deformation which occurs by either stretching, bending, or compression of the bonds in the crystal structure. This normally

occurs below the pressure at which permanent deformation by the processes 2-5 occurs.

2. Plastic flow which occurs mainly by a crystallographic slip phenomenon, i.e. by the movement of one dimensional defects (dislocations) in the crystal structure. The presence of dislocations in crystalline solids promotes plastic flow and flow generates new dislocations with increasing strain. Dislocations on different crystallographic planes interfere with each other's movement and the stress needed to continue deformation increases. This is known as work-hardening.
3. Viscous flow which occurs normally by a bulk movement or displacement of molecules in the particle structure. Dislocations are not a prerequisite for this type of flow. Under load, solids exhibiting viscous flow behave as fluids with high viscosity coefficients.
4. Viscoplastic flow which occurs partly by plastic flow and partly by a viscous flow process. Solids exhibiting viscoplastic deformation are less readily deformed than viscous materials.
5. Fracture by a crack initiation and propagation process which occurs as a consequence of the separation of certain lattice planes in the crystals. Materials which deform by fracture are called brittle. There may also be non-crystalline materials, e.g., polymers below their glass transition temperature, which will exhibit a brittle behaviour at ambient temperature. Fracture is normally preceded by a certain degree of permanent deformation by plastic flow. Work hardening, and the related high localised stresses, due to plastic flow is one of the primary causes of fracture. Under certain

conditions of loading, some materials may fracture without prior permanent deformation.

The particles of most solids exhibit an initial elastic deformation phase followed by permanent deformation of some type as the powder bed is subjected to increasing loads during compaction. It is likely that a given material may exhibit a mixture of flow and fracture phenomena depending on the conditions of stress, strain and strain rate.

1.3.1. Viscoelastic modeling of the compression data

In several of the reports mentioned in section 1.1.2 the stress relaxation data has been fitted to the equations for a given type of viscoelastic model. For example, David and Augsburger (1977) applied the Maxwell model of linear viscoelasticity to the stress relaxation data and reported a characteristic viscoelastic constant for each material. Rees and Rue (1978) found an exponential decay of stress, contrary to the linear decay reported by David and Augsburger (1977). They argued that there could be more than one characteristic viscoelastic constant for the powders compressed. Peleg and Moreyra (1979) used stresses at the end of stress relaxation normalised for the initial stress in a modification of the Maxwell model, and obtained easily interpreted linear plots, the slopes and intercepts of which were characteristics of a given material. Caspar and Muller (1984) fitted the stress relaxation data of some pharmaceutical solids to a model with at least 5 Maxwell elements.

As mentioned above, viscoelastic materials are also characterised by strain recovery which does not occur instantaneously and which may or may not be complete. Rippie and Danielson (1981) and Danielson *et al.* (1983) analysed several pharmaceutical solids from this standpoint using the

punch-stress versus time data from the decompression phase of the compaction cycle on a rotary press, and the stress-relaxation data from the post-compression phase by leaving the tablet in a die instrumented to measure the residual die wall pressure. They fitted these data with equations derived from the three-dimensional linear viscoelastic theory, and concluded that the deformation under load could be best characterized by the Voigt-Kelvin (or Kelvin) solid model in contrast with the Maxwell model. The recovery of the compacts during decompression was elastic, while the post-compression recovery, when the upper punch was no longer in contact with the compact, was viscoelastic.

It can be seen that although the theory of viscoelasticity provides a sound theoretical ground for analysing the deformation behaviour of solids under compression, there is a lack of agreement in the literature over which particular model, if any, can best describe the behaviour of pharmaceutical solids during compression. Since most pharmaceutical solids are expected to possess some time-dependent deformation, one source of disagreement could be the difference in the rates of deformation as a result of different types of compression equipment used in the various studies. The theories of elasticity or viscoelasticity were developed for non-porous, isotropic solid bodies. Thus another, mostly ignored, potential source of variation in the results and their interpretation, is the effect of porosity of the powder bed and the effect of changes in porosity on particle deformation during compaction. A realistic analysis of the deformation behaviour should include deformation speeds (i.e., the strain rates) comparable to those encountered on a rotary press, and the effect of changes in porosity during the compaction process. One solution would be to use a high speed rotary press for the analysis.

1.3.2. Modeling of compaction using mechanical properties from single crystal microindentation methods

The actual deformation mechanism of crystals can be ascertained by using single crystal microindentation techniques, but the particle deformation behaviour in a powder bed during compaction will be different owing to the particle-particle interactions which are absent in the microindentation tests. Nevertheless, the mechanical properties of single crystals derived from such tests can be used to model the compaction of powders. Modeling of compaction using mechanical properties from indentation tests is well established in the area of material sciences, and has been recently applied to the compaction of pharmaceutical powders. Duncan-Hewitt and Weatherly (1990a, 1990b) modeled the densification of pharmaceutical powders during uniaxial compaction using single crystal properties derived from microindentation. The models differed for ductile and brittle materials, although in both cases the models required a knowledge of the change in the number of particle contacts during densification, the condition for local yielding at particle-particle contact, the average area of interparticulate contact (which depends on the particle geometry and the powder bed density), and the relationship between 'far-field stress and the local stresses at each contact'. Each of these factors were analysed using the mechanical properties, and the densification as a function of pressure was calculated and compared with the actual densification profiles according to the already established Heckel equation (Heckel, 1961).

Although the modeling of powder compaction is mathematically appealing and scientifically rigorous, its use in the routine analysis of powder behaviour under pressure may be limited. Large, well-formed crystals are required and specialised equipment is used to obtain the

single crystal properties. It may not be possible to obtain suitable single crystals and hence the mechanical properties from indentation for those pharmaceutical powders that are either non-crystalline, or are granulations containing more than one component in the same particle.

1.3.3. Use of indices of performance in characterisation of materials.

A large body of literature on the tableting of pharmaceutical solids is related to the characterisation of materials by determining various parameters which relate some measure of tablet strength to either the deformation properties of materials under pressure or to their elastic nature under given conditions of stress. These parameters are called 'indices' of performance of powders. The most commonly used indices of tableting performance are due to Hiestand (Hiestand and Smith, 1984; Hiestand, 1985). These indices, namely, 'Strain Index', 'Bonding Index' and 'Brittle Fracture Index', represent 'the relative strain during the elastic recovery that follows plastic deformation', 'the relative survival during decompression of the areas of true contact that formed at maximum compression', and the ratio of 'the tensile strength of tablets with and without a hole at their center'. The wide application of these indices is restricted because they require the use of specialized equipment, such as a pendulum impact indentation hardness tester and a special die and punch assembly to form large rectangular compacts with a small cylindrical hole in the centre. Moreover, it has been found difficult to reproduce these indices from one laboratory to another (Duncan-Hewitt and Grant, 1987a).

Malamataris *et al.* (1984) used ratios of two parameters, namely, 'elastic recovery' and 'plastic compression' as indicators of the balance between the elastic and plastic behaviour of pharmaceutical powders on a

Dartec universal tester, and related this ratio to tablet strength. Celik and Travers (1985) proposed an 'elastic recovery index' defined as the ratio of the elastic recovery of compacts to the strain movements (section 1.1.2). This index was used to ascertain the compaction behaviour of some direct compression bases on a hydraulic press. Guyot *et al.* (1986) proposed a 'tabletability index' and a 'cohesion index' to analyse the behaviour of powder mixtures on a single punch eccentric press. Ho and Jones (1988b) proposed 'rise time' as a new index of tablet compression using a compaction simulator. This time is the interval between initiation of compression and the point of maximum force.

Most of the above indices or parameters are determined on slow speed compaction equipment and therefore their conclusions may not be easily extrapolated to the high speed rotary presses.

1.4. EQUIPMENT USED FOR ANALYSIS OF POWDER BEHAVIOUR UNDER PRESSURE

While rotary tablet presses are universally used for tablet manufacturing, various other types of equipment have been used to analyse the behaviour of powders under pressure. These include various types of hydraulic presses, mechanical stress-strain analysers such as Instron Physical Testing Equipment, single station tablet presses, and the more modern and expensive compaction simulators. The most obvious problems with the use of hydraulic and single punch presses are their uniaxial compaction cycle as opposed to the biaxial cycle of the rotary presses, and their inability to reproduce the rates of compaction obtained on the rotary presses. The compaction simulators are designed to simulate the compaction cycle of the rotary presses (Cole *et al.*, 1971; Rees *et al.*, 1972; Hunter

et al., 1976; Bateman, 1988; Bateman *et al.*, 1989; Celik and Marshall, 1989). While the advantage of compaction simulators is that it should be possible to mimic the compaction cycle of any rotary tablet press by feeding the punch displacement cycles to the computer controlling the simulator, this very aspect of their use becomes their drawback. This is because the punch displacement profiles of rotary presses are difficult to determine (Ridgway Watt and Rue, 1979; Walter and Augsburger, 1986; Oates and Mitchell, 1990). The punch displacement profiles have been calculated from the machine and punch geometry (Rippie and Danielson, 1981; Charleton and Newton, 1984). However, there is a significant error in these calculations because the contribution to the total displacement by the machine deformation is ignored. Oates and Mitchell (1989, 1990) proposed a systematic way of deducing the punch displacement profiles using a relationship between the machine deformation and applied force. Unless the correct profiles are fed to the compaction simulator, the results generated are in serious error.

1.5. PRELIMINARY WORK LEADING TO THE PRESENT RESEARCH

Experiments in our laboratory indicated that the peak punch pressures on a Manesty Betapress occur prior to the vertical alignment of the punches with the centres of the upper and lower pressure rolls (the dead centre position). The time by which the peak pressures were set off from such an alignment was called the 'peak offset time' (t_{off}), the duration of which is apparently a characteristic of the compaction behaviour of the material under stress (Oates and Mitchell, 1989). Recently, Morehead and Rippie (1990) confirmed this observation on a Colton 216 rotary tablet press. The

punch stress profiles were not symmetrical about the punch displacement profiles, and this asymmetry was attributed to time-dependent viscoelastic processes occurring within the compact. For substances such as Avicel, Klucel and Mannitol, they reported 'maxima lead times' analogous to the t_{off} on the Manesty Betapress. The duration of t_{off} is presumably related to time-dependent flow, and it is pertinent to investigate whether this occurs under conditions of constant strain.

An observation of the force-time profiles on the Manesty Betapress suggested that the small differences between the decompression curves of various pharmaceutical materials might be used to calculate the in-die tablet expansion and to estimate the Young's modulus, E, of the material from this expansion by using the data obtained under normal operating conditions. As mentioned above, the machine deformation has been ignored by previous workers when calculating punch displacement on rotary presses. By contrast, the present work extends the relationship between punch force and machine deformation developed for the compression phase of the tableting cycle of a Manesty Betapress to punch force and machine recovery during the decompression phase.

1.6. OBJECTIVES OF THE PRESENT RESEARCH

In their reviews of the various techniques employed for investigation and interpretation of powder compaction, Krycer *et al.* (1982a, 1982b) indicated that 'a great deal of confusion and discrepancy' exists in the literature. This was primarily because of the 'many varied, and often unsubstantiated, techniques' used. The brief review of the literature presented in the above sections indicates that the situation has not improved greatly since these remarks were published.

In the present work a high speed rotary tablet press was used under normal operating conditions with the following specific objectives:

1. To develop an inexpensive and simple method of analysing the compaction cycle which, in principle, can be applied to the analysis of powder compaction on any rotary press.
2. To obtain parameters, under normal operating conditions, from the compression and decompression phase of the compaction cycle, which relate to permanent deformation and elastic expansion.
3. To characterise the deformation mechanism of various pharmaceutical solids using the information obtained in objective 2 with particular reference to the effect of strain rate.
4. To demonstrate the influence of processing and formulation of various direct compression excipients and drugs on their deformation mechanism.

2. MATERIALS AND METHODS

2.1. MATERIALS

The materials listed below were used as received from the various sources:

A-Tab	Anhydrous dicalcium phosphate, Rhone-Poulenc.
Acetaminophen Fine Powder	Crystalline acetaminophen USP (20% particles larger than 38 μm), Mallinckrodt.
Acetaminophen Granular	Crystalline acetaminophen USP (95% particles larger than 45 μm), Mallinckrodt.
Acetaminophen Powder	Crystalline acetaminophen USP (60% particles larger than 38 μm), Mallinckrodt.
Acetylsalicylic Acid	Crystalline sample, Monsanto.
Anhydrous Emcompress	Anhydrous dicalcium phosphate, Edward Mendell.
Anhydrous Lactose	Roller-dried β-lactose containing 73.9% β-anomer, Sheffield.
Asagran	Direct compression formulation, Monsanto.
Avicel Large	Microcrystalline cellulose (average particle size 200μm), FMC Corporation.
Avicel PH101	Microcrystalline cellulose (average particle size 50μm), FMC Corporation.
Avicel PH102	Microcrystalline cellulose (average particle size 90μm), FMC Corporation.
Avicel PH105	Microcrystalline cellulose (average particle size 20μm), FMC Corporation.
Caffeine	Crystalline sample, MCB Manufacturing Chemists.
Cal-Star	Dicalcium phosphate dihydrate, FMC Corporation.

Cellactose	A direct compression formulation with 25% cellulose and 75% lactose , Meggle.
Compap CG	90% Acetaminophen USP with 10% excipients, Mallinckrodt.
Compap Coarse 73 L	73% Acetaminophen USP with 27% excipients including lubricant, Mallinckrodt.
Compap Coarse L	90% Acetaminophen USP with 10% excipients including lubricant, Mallinckrodt.
Compap L	90% Acetaminophen USP with 10% excipients including lubricant, Mallinckrodt.
DCI-63	Direct compression formulation containing 63% ibuprofen with excipients, Mallinckrodt.
Di-Pac	Sucrose (98%) co-crystallized with dextrins (2%), Amstar.
Di-Tab	Dicalcium Phosphate Dihydrate, Rhone-Poulenc
Elcema G250	Powdered cellulose, Degussa.
Emcocel	Microcrystalline cellulose, Edward Mendell.
Emcompress	Dicalcium Phosphate Dihydrate, Edward Mendell.
Emdex	Dextrates, Edward Mendell.
Fast-Flo Lactose	Spray-dried agglomerates of fine α-lactose crystals bound by amorphous lactose (94.6% α-anomer), Foremost.
Lactose DCL 21	Roller-dried β-lactose containing 76.7% β-anomer, De Melkindustrie Veghel.
Mannitol	Crystalline sample, Atlas.
Mannitol M.G.	Direct compression form, Roquette.
Neosorb	Direct compression form of sorbitol, Roquette.
α-Lactose monohydrate	Crystalline sample containing 98.2% α-anomer, BDH.

Potassium Chloride	Crystalline sample, Fisher.
R-ibuprofen	Stereochemically 97% pure R-enantiomer of ibuprofen, Sepracor.
Racemic ibuprofen	Crystalline sample, Apotex.
Racemic ibuprofen	Crystalline sample, Upjohn Co.
Rhodapap DC-P3	Direct compression form containing 97% acetaminophen and 3% PVP, Rhone-Poulenc.
S-ibuprofen	Stereochemically 96% pure S-enantiomer of ibuprofen, Ethyl Corporation.
S-ibuprofen	99.7% pure S-enantiomer of ibuprofen, Ethyl Corporation.
Sodium Chloride	Crystalline sample, Allied Chemicals.
Spray-dried lactose	Spray-dried slurry of large α-lactose crystals with some amorphous lactose (approx. 95% α-lactose), Foremost.
STA-Rx-1500	Pregelatinized starch, Colorcon.
Sucrose	Crystalline sample, BDH.
Sugartab	Sucrose (90-93%) agglomerated with invert sugar (7-10%), Edward Mendell.
Tri-Tab	Tricalcium Phosphate, Rhone-Poulenc.
Xylitol	Crystalline sample, Roquette.

2.2. CHARACTERIZATION OF MATERIALS

2.2.1. Determination of bulk and true density

The bulk densities of various materials were determined by a procedure used in the Handbook of Pharmaceutical Excipients (1986). A known quantity (approximately 25g) of the powder was poured from a beaker into a 100 mL measuring cylinder held at an angle of approximately 45° from the horizontal. The cylinder was brought to a vertical position and gently rocked sideways to level the top surface of the powder. The volume of the powder to closest mL was noted. Dividing the mass of the powder by this volume gave the bulk density of the material.

The true density (or the particle density) of various materials was determined by helium-displacement pycnometry using a Quantachrome Multipycnometer. A 149.59 cm^3 sample cell was used for all powders as this gave density values closest to the values determined from a suspension density method (Dwivedi, 1988).

2.2.2. Differential scanning calorimetry (DSC)

The melting temperature of the various solids was determined by heating the samples in open pans using a Du Pont model 910 differential scanning calorimeter controlled by a Du Pont Series 99 thermal analyzer. The signals from the DSC were fed to an Apple II+ computer through a variable amplifier and an analog to digital converter. The DSC curves were recorded and analyzed using a data analysis software. The melting points were recorded as intersections of the extrapolated leading edge of the endotherms with the baseline extrapolated from before the endotherm. Enthalpies of fusion were determined from the DSC curves using indium as the calibration standard.

2.2.3. Determination of binary phase diagram for characterization of ibuprofen

Determination of a melting point versus composition phase diagram between the constituent enantiomers provides the most fundamental verification of the nature of the racemic substances. Since both, racemic ibuprofen and S-ibuprofen, are available for tableting the binary phase diagram of ibuprofen was determined using the nearly pure samples of R-ibuprofen and S-ibuprofen to ascertain the nature of the solid state of racemic ibuprofen.

Accurately known masses of R-ibuprofen and S-ibuprofen were weighed out directly into standard open aluminum pans to obtain enantiomeric mixtures with evenly spaced mole fractions of S-ibuprofen between 0.04 and 0.96. The total mass of each mixture was about 5 mg. The pans were heated at 10°C/min from 20°C to 90°C under a stream of nitrogen flowing at 138 kPa. The samples were cooled to room temperature and reweighed. No weight loss was detected indicating that the volatility of ibuprofen (Ertel *et al.*, 1990) was not a problem in the interpretation of the DSC results. Standard open pans were used instead of hermetically sealed volatile sample pans for quantitative DSC because of the greater contact area between the pan bottom and the constantan sample platform in the DSC cell. No significant difference was found in the enthalpies of fusion (ΔH^f) determined in standard or volatile sample pans confirming that no solid-vapor transition occurred under the experimental conditions. All samples recrystallized within 2 h of cooling, but were annealed at room temperature for 36 h before the DSC scan was repeated. Peak temperatures from the melting endotherms were plotted against the enantiomeric composition to give the binary phase diagram. The peak temperatures changed negligibly when the same samples were reheated after a storage for 6 months at room

temperature, indicating that the initial annealing of 36 h was adequate. Recrystallizing from the melt was preferred over recrystallization from solution which would require complete removal of the solvent and the possibility of solvate formation would have to be ruled out.

The phase diagram was verified by the thermal analysis of mixtures of racemic ibuprofen with R-ibuprofen and S-ibuprofen and confirmed by calculating the melting point at various enantiomeric compositions using an equation derived from the Prigogine and Defay equation (Prigogine and Defay, 1954).

2.2.4. Powder X-ray diffraction patterns of ibuprofen samples

Powder X-ray diffraction provides information supplemental to the phase diagram. Powder X-ray diffraction patterns of the racemic ibuprofen and enantiomers of ibuprofen were obtained on a Rigaku Geigerflex X-ray diffraction system. The system was operated by an IBM compatible computer via a Rigaku D/MAX-B controller. The diffraction patterns were recorded at a continuous scanning rate of 5°2θ/min using CuK_{α} radiation (40 kV, 20 mA) with the intensity of diffracted X-rays being collected at intervals of 0.05°2θ. A Ni-filter was used to remove CuK_{β} radiation.

2.3. COMPRESSION OF THE MATERIALS ON A ROTARY PRESS

2.3.1. Equipment

A Manesty Betapress was used for all experiments. This is a sixteen station rotary tablet press. One of the sixteen stations of the press was fitted with a die with 1/2" (1.270 cm) flat-faced upper and lower punches, and the remaining fifteen stations were blanked off. No force was applied

to the punches by the precompression pressure rolls. The hopper and feed-frame were removed for easy access to the tooling.

Two types of punches, namely, IPT and Manesty, were used. The Manesty punches are supplied by the makers of the machine, and conform to the European standards. The IPT punches conform to the specifications of the Industrial Pharmaceutical Technology Section of the Academy of Pharmaceutical Sciences, American Pharmaceutical Association (Swartz, 1969). The Betapress can be fitted with appropriate lower cam tracks to accommodate the differences in the geometrical design of the two types of punches. The most important difference between these punches is in the geometry of their heads. The IPT punches have a larger flat portion on the head relative to the Manesty punches (Fig. 1).

2.3.2. Instrumentation and calibration of Betapress to obtain force and displacement

Analysis of the tableting compaction cycle requires measurements of both punch force and the distance between the upper and lower punches (punch displacement) during powder compaction and consolidation as a function of time, t, or fractional turret position, fr. Punch force measurements are relatively easy to make using strain gauges or load cells mounted either directly on the punches or on other, remote parts of the machine. Measurement of punch displacement, however, poses serious problems, arising mainly from the technical difficulties and expense of recovering signals from rapidly moving punches. An important objective in instrumenting the Betapress, therefore, was to develop a method of determining both punch force and displacement from measurements of punch force only.

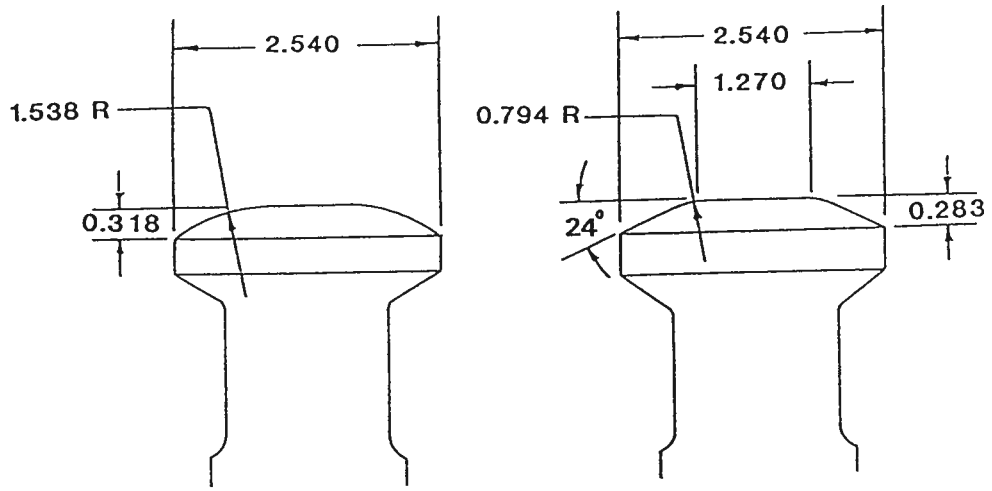

FIG. 1. Schematic illustration of geometrical differences between punch head profiles of Manesty and IPT type punches. The IPT punch heads have a relatively larger flat area. All dimensions are in cm.

This required an analysis of the relationship between the applied force and punch displacement during the compaction cycle. The procedures developed by Oates and Mitchell (1989, 1990) were refined and simplified as outlined below to measure force and then calculate displacement as a function of the force exerted on the powder bed during the compression phase of the compaction cycle. The method used to analyse expansion of the compacted powder during the decompression phase is described in section 2.6.

The roll pin supporting the upper pressure roll and the cross beam supporting the lower pressure roll were strain gauged to determine the upper and lower punch forces respectively (Oates and Mitchell, 1989). The signals from the strain gauged upper compression roll pin were calibrated against known loads before placing the pin in position. The signals from the strain gauges on the lower cross-beam were calibrated against the upper roll pin.

To establish the relationship between punch force and displacement, punch displacements during the compression of selected materials using both Manesty and IPT punches were measured directly by a linear variable differential transformer (LVDT) whilst running the machine under speed. The LVDT was inserted in an empty punch hole in the turret, next to the hole in which the punches were placed, and its actuator arm was connected to the punches by a specially designed linkage (Fig. 2). The signals from the LVDT were retrieved through a set of slip-rings mounted on the outer surface of the upper flange of the turret. To eliminate errors due to possible tilting of the punches as they travel between the upper and lower pressure rolls, the LVDT was mounted in leading and trailing positions on both the upper and lower punches. Thus, the net measured punch

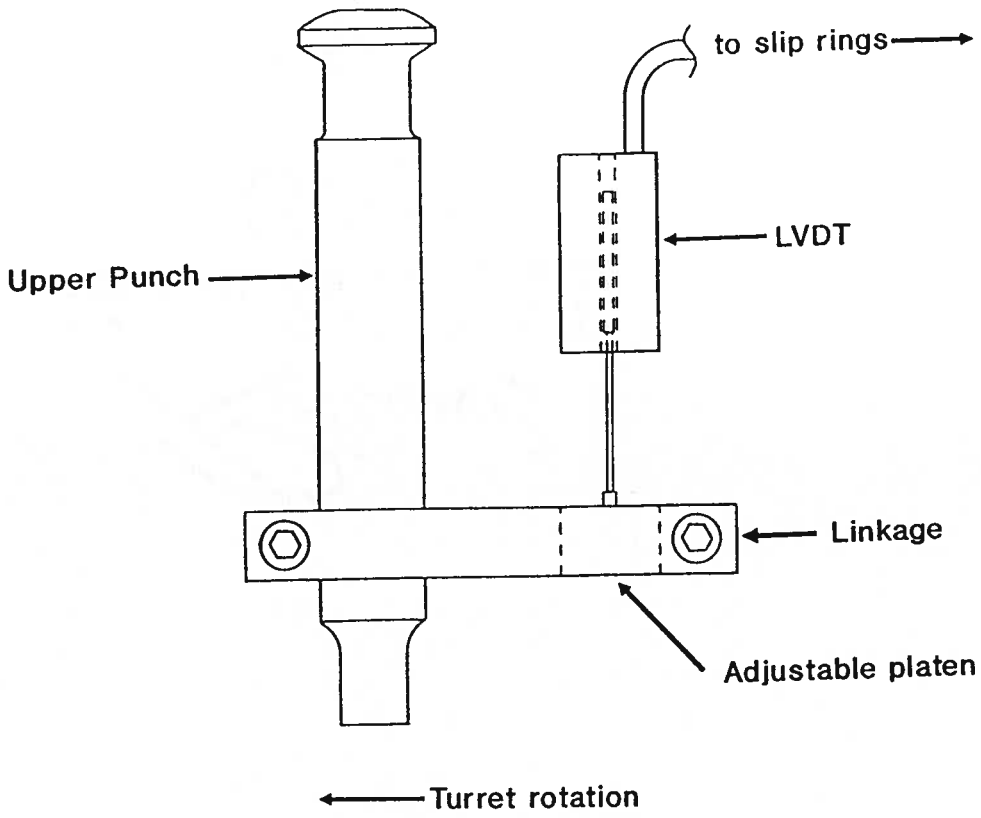

FIG. 2. Drawing illustrating attachment of a linear variable differential transformer (LVDT) to an upper punch for direct measurement of punch displacements using an LVDT-slip ring system on the Betapress.

The armature of the LVDT rests on the adjustable platen which is a part of a linkage between LVDT and punches. Signals from the LVDT were retrieved through slip rings mounted on the upper flange of the turret. The linkage is shown in a trailing position relative to the punch as it rotates with the turret, but was also mounted in a leading position. Measurements in both leading and trailing positions were used to annul errors in displacement due to tilting of the punches with respect to their vertical axis as they passed between the upper and lower compression rolls.

displacement was a combination of four separate measurements. Typical upper and lower punch displacements profiles obtained in this manner are given in Fig. 3.

The net punch displacement, expressed as the distance, D, between the two punch faces during the compression phase was found to be a function of three independent variables:

(a) the fractional turret position, fr, of the punches as they move against the respective compression rolls under a negligible force, and hence under a negligible machine deformation,

(b) the punch force, F, during compression, which causes significant machine deformation (punch contractions + machine deflections; section 3.3.1) throughout the compression phase, and

(c) the time, t, during which the punches accelerate from their initial resting positions. Hence there is a time-dependent change in displacement during the initial part of the compression phase.

The contributions to the displacement from these variables can be represented as D(fr), D(F), and D(t), respectively. D is then given by:

$$D = D(fr) + D(F) + D(t) \qquad (3)$$

The terms on the right hand side of equation 3 were determined as follows:

(1) To obtain D(fr), displacement was measured using the LVDT-slip ring system under speed with the die cavity completely filled with a high viscosity oil. The oil was squeezed out of the die during compression, while maintaining sufficient force ($\approx$ 1 kN corresponding to a pressure of $\approx$ 8 MPa) for the punches to follow the contours of

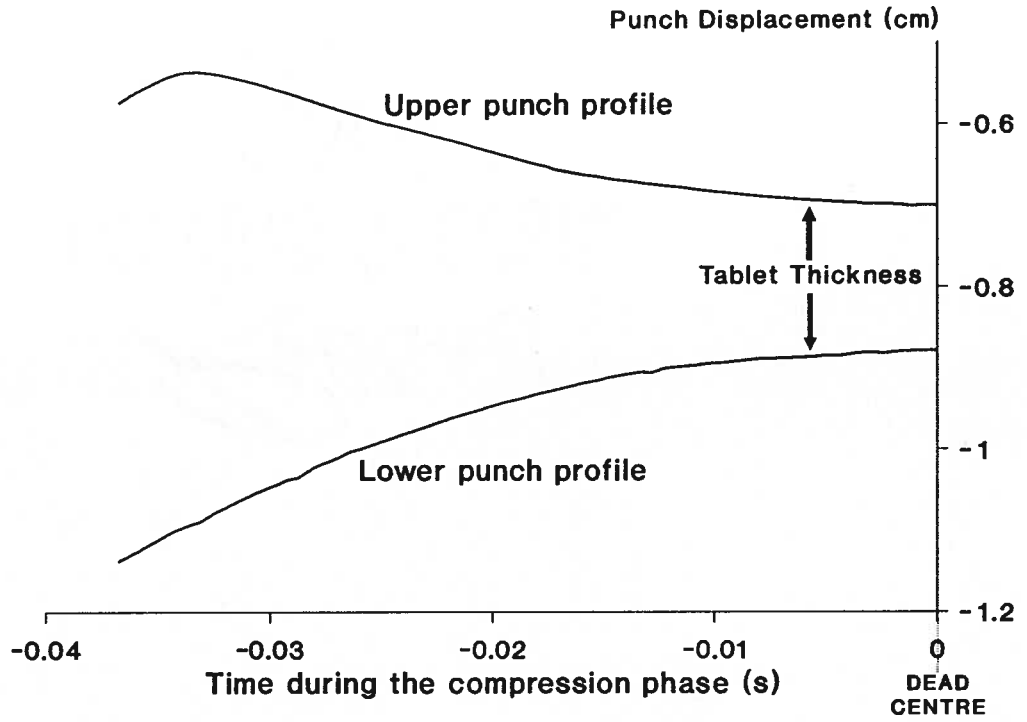

Fig. 3. Representative upper and lower punch displacement profiles measured using an LVDT-slip ring system. Compression times are expressed as negative values since the dead centre position is assigned a value of zero time.

The initial part of the upper punch displacement profile shows an upward movement because the upper punch resting on the powder bed under gravity is initially pushed up by the lower punch until it comes in contact with the upper compression roll and subsequently begins moving down along the roll.

the compression rolls, but not to cause significant machine deformation. The measured displacement profiles (Fig. 4a) were curve-fitted using polynomial regression and the constants of the polynomial were used to calculate the D(fr) component of D during compression.

Rippie and Danielson (1981) and Charleton and Newton (1984) calculated the punch displacement profile from the geometry of machine and the shape of the punch heads. This is equivalent to saying that D = D(fr) and is therefore in considerable error since machine deformation is neglected.

(2) When a solid is compressed under speed, the displacement not only changes with fr, but also with F since the punches contract and bearings carrying the compression rolls, as well as the lower cross-beam, are deflected away from the powder bed together with the upper and lower punches. Thus additional changes in displacement, D(F), occur as a result of the machine deformation when solids are compressed. To separate D(F) from D(fr), the D(fr) curves from Fig. 4a were subtracted from the total punch displacement profiles of various particulate solids measured using the LVDT-slip ring system. The resultant difference, D(F) = D - D(fr), was plotted against F during the compression phase (Fig. 4b). At higher forces this plot was linear indicating a linearity of the machine deformation with F at these forces. The slope of the linear portion was the machine deformation constant, $K^{-1} = 2.3 \times 10^{-6}$ cm/N.

(3) The initial part of the plot in Fig. 4b was curved due to a change in the displacement as a result of acceleration of the punches from their initial resting position, i.e., due to a time-dependent change

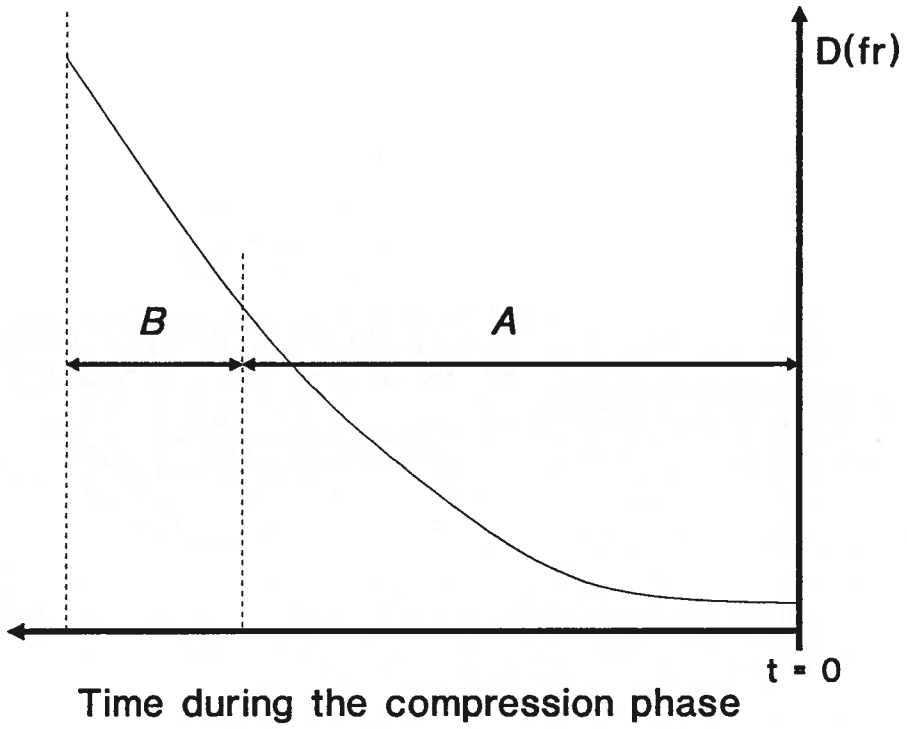

FIG. 4a. Schematic representation of punch displacement at various fractional turret positions, D(fr), as the punches follow the contours of the compression rolls, expressed as a function of time during the compression phase.

D(fr) was obtained by directly measuring the upper and lower punch displacements with an LVDT-slip ring system whilst running the Betapress under speed. A negligible force was applied by filling the die with a high viscosity oil, which was squeezed out during compression. Most solids only partially fill up the die, and, hence, show displacements during the shorter time interval 'A'. Since the die was completely filled with oil, punch displacements were recorded over an additional time interval 'B', during which time the punches also accelerated to full velocity. Therefore, the curve during 'A' corresponds solely to the change in punch displacement with fr, and can be used as the D(fr) curve to calculate punch displacements during compression of the powder bed.

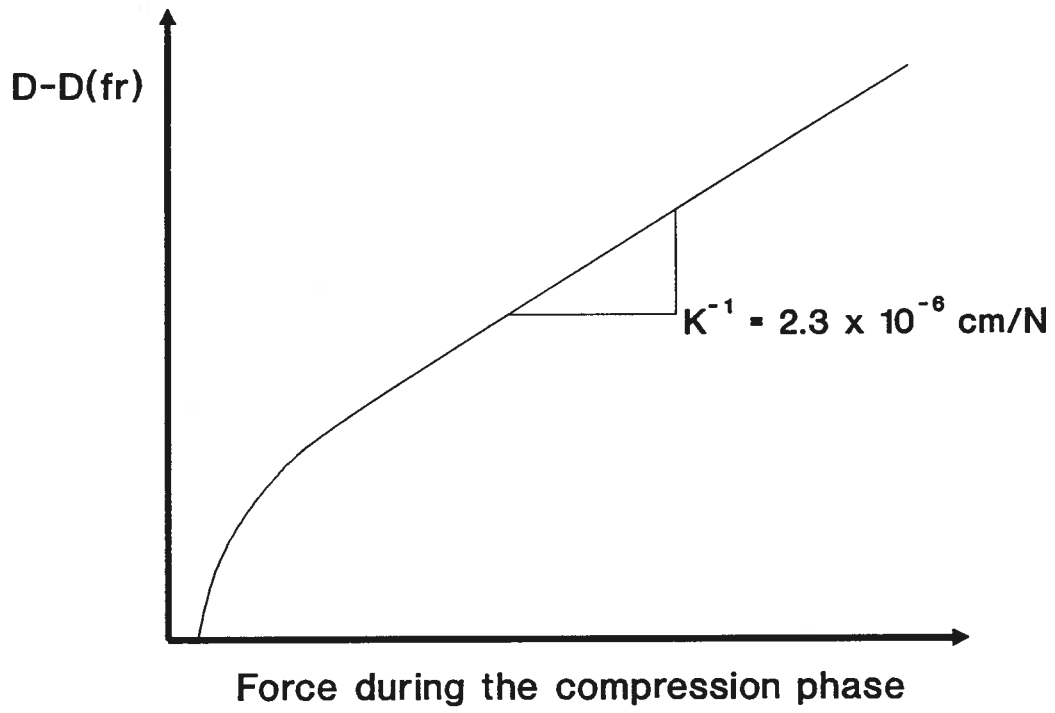

FIG. 4b. Schematic representation of a machine deformation plot obtained by subtracting the D(fr) curve (Fig. 4a) from the measured punch displacement curve, D, during the compression of a solid.

An LVDT-slip ring system was used to measure D. The plot is linear at higher forces indicating that the machine deformation (sum of punch contractions and machine deflections) is linearly related to the punch force during compression. The slope of the linear part is the machine deformation constant, K^{-1}, and was used to calculate the contribution of the machine deformation to the total punch displacement when solids are compressed. The initial curvature in the plot is due to acceleration of the punches to their full velocity from an initial resting position.

in the displacement, D(t), during the initial part of the compression phase. The term D(t) was obtained by extrapolating the linear portion of the plot in Fig. 4b to F = 0 and by subtracting the extrapolated plot from the plot in Fig. 4b. The difference $[D-D(fr)]-K^{-1}.F$ was expressed as a function of time to obtain Fig. 4c. The initial curved part of this figure is ≈10 ms long and contributes ≈0.05 cm to D.

(4) The results from the above experiments were combined to calculate the net punch displacement, D. The calculated displacements for selected solids were verified by measuring the displacement profiles using the LVDT-slip ring system at different peak forces. The calculated displacements for both Manesty and IPT punches agreed with the measured displacements.

(5) The effect of force on machine deformation (the linear portion of the plot in Fig. 4b) was also confirmed by experiments under static conditions in which different thicknesses of feeler gauges were placed between the punch faces at a position at which the punches were aligned with an imaginary line joining the centres of the compression rolls, i.e., at t = 0 in Fig. 4a or 4c. This changed the distance, D, between the punch faces thereby increasing F at a fixed fr. Plotting D against F gave a linear relationship with the slope being almost identical to the K^{-1} value of 2.3×10^{-6} cm/N.

Once the initial experiments to calculate punch displacement and its verification by direct measurements were complete, the LVDT-slip ring system was abandoned and the results from the above experiments were combined in displacement analysis. This analysis requires only an input of

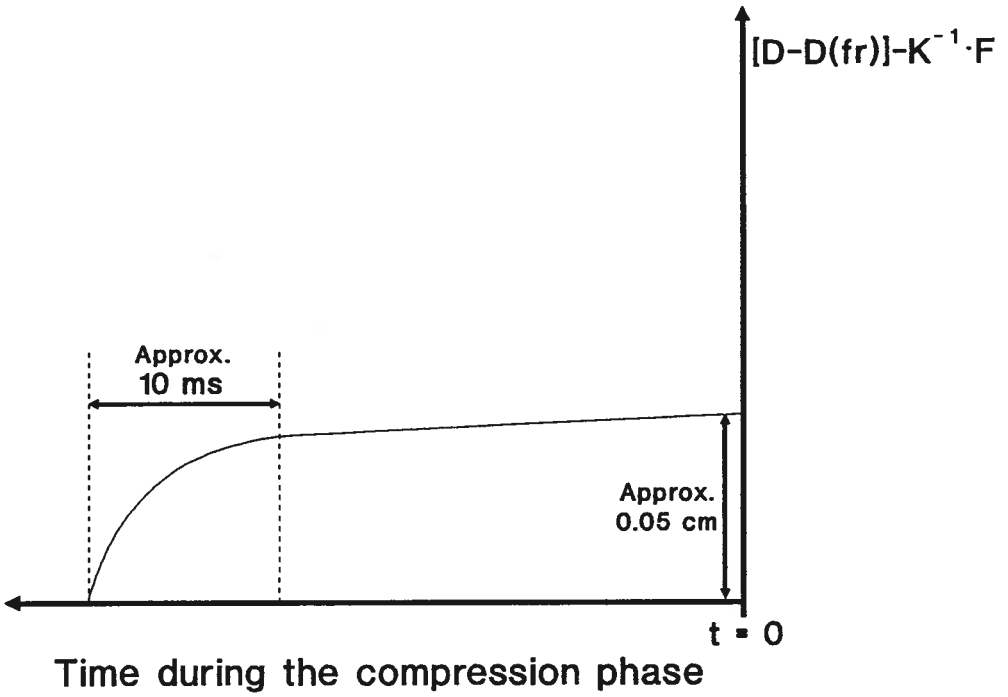

FIG. 4c. Schematic representation of the contribution of acceleration of the punches from an initial resting position to their full velocity during the compression phase.

The linear portion of the plot in Fig. 4b was extrapolated to F = 0 and the extrapolated plot was subtracted from the plot in Fig. 4b. The difference $[D-D(fr)]-K^{-1}\cdot F$ was expressed as a function of time to obtain Fig. 4c. The displacement of ≈0.05 cm is the displacement during the initial time of ≈10 ms. The curve almost levels off after this initial time, indicating that the punches require ≈10 ms to accelerate to their full velocity.

the experimental F versus fr (or F versus time) curves measured using the strain gauges. The computer software automatically calculates the corresponding displacement.

2.3.3. Data collection and analysis

The data collection was triggered by actuating a reed switch by a small bar magnet affixed to the upper flange of the turret. The magnet was positioned on the turret such that the data collection was triggered a few milliseconds before the punches came in contact with the compression rolls. The signals from the strain gauges (or the LVDT) were collected for a period of 0.1s which was a sufficient interval to accommodate the compaction cycle of all materials tested even at the slowest turret speeds used.

Methods used for data collection, analysis and storage have been upgraded since the reports by Oates and Mitchell (1989, 1990). After amplification and filtering, the analogue signals from the strain gauges on the Betapress were converted to digital form using a Metrabyte 12-bit fast A/D converter, and collected by an IBM compatible computer at a rate of 2500 readings per second for each of the two (upper and lower) punch force channels. The raw data were collected using a data acquisition software and were analyzed using a data analysis software with the aid of a math coprocessor fitted in the computer. Separate sets of software were written for the analysis of compression and decompression phases. Each permitted data analysis in two modes: one data file at a time in an individual analysis mode or several data files together in a bulk analysis mode. The total time taken for compression of a tablet and collection, storage and analysis of the corresponding data in the individual analysis mode was

between 2-3 minutes. A number of parameters routinely computed by the software are listed in Table I. The software could produce the results in two formats, (a) the total value of a given parameter during the compression or decompression phase, and (b) the profiles of these parameters as a function of the fractional turret position of the punches during compression or simply the time during compression. The results were saved as ASCII files which could be imported by various commercially available statistics and graphics software.

2.3.4. Preparation of the materials for compression

Tablets were made after mixing each material with the lubricant magnesium stearate previously screened through a fine cloth sieve. The geometric dilution technique was used for obtaining a uniform distribution of the lubricant. In this technique, 0.5% of the sieved lubricant was first mixed with an equal amount of the tableting material on a piece of paper using a spatula. The amount of mixture so produced was doubled in the next step, then quadrupled, and so on, until all of the material was used up. The total amount was finally mixed on a Fisher Kendell Mixer for 5 minutes in closed jars.

The internal lubricant was avoided in the case of materials which possess poor tableting properties, e.g., acetaminophen and ibuprofen. This is because the internal lubricant would compound the poor tableting properties by contaminating the potential bonding sites, if any, thereby inhibiting the bonding. These drugs, and some of their formulations which do not have a previously added lubricant, were tableted after lubricating the die wall and punch faces with a 5% solution of stearic acid in chloroform. The solution was applied to the punch faces and the die wall

TABLE I. Various parameters calculated automatically by the software used to analyse the force versus time data from the Betapress.

Parameter	Absolute[1] Value	Profile[2]
PARAMETERS FROM THE COMPRESSION PHASE		
Force related parameters:		
Upper and lower punch force	Y[a]	Y
Upper and lower punch pressure	Y	Y
Ratio of lower to upper force	Y	-
Displacement related parameters:		
Total punch displacement	Y	Y
Powder bed height at the onset of compression	Y	-
Tablet thickness at peak pressure	Y	-
Maximum and minimum relative density of the tablet	Y	Y
Maximum and minimum value of the Heckel term	Y	Y
Thermodynamic parameters:		
Work done to the powder bed during compression	Y	Y
Power	Y	Y
Maximum power	Y	-
Turret position where maximum power occurs	Y	-
Machine speed related parameters:		
Compression time	Y	-
Decompression time	Y	-
Deformation related parameters:		
Peak offset time (t_{off})	Y	-
Decrease in punch stress during t_{off}	Y	-
Strain rate related parameter:		
Rate of compaction	-	Y
PARAMETERS FROM THE DECOMPRESSION PHASE		
Tablet expansion during decompression	Y	Y
Work of decompression	Y	-
Elastic modulus of tablets	Y	-

1. The absolute values of the various parameters can be used to calculate certain physical constants by either plotting these parameters against pressure during compression or by using them in known equations from the literature.
2. The software also provides the profiles of several parameters with respect to time during compression or fraction of turret revolution during compression

a. Y = yes

in a smooth motion using a small cotton swab wrapped around a thin wooden straw, which produced a uniform layer of stearic acid in a few seconds when the chloroform evaporated. The punch faces and die wall were cleaned and the solution was reapplied before each tablet was made.

2.3.5. Compression protocol

Method I: All materials were compressed over a range of peak pressures by varying the mass of the material in the die keeping the thickness setting on the Betapress fixed. Thus, an increasing amount of material was squeezed in a volume which, in an empty die, would have otherwise stayed constant, and this increased the punch pressure.

Method II: A fixed mass of selected material was subjected to increasing pressures by changing the thickness setting on the Betapress such that the distance between the punch faces decreased.

A series of about 20 tablets, covering a range of peak pressures (P_{max}) between ≈20 MPa to ≈210 MPa, were made with each material. A new aliquot of the material was weighed out for each pressure. Unless otherwise stated, all results correspond to the variation in pressure by Method I.

2.3.6. Machine speed

The machine speed was expressed as 'turret time' which is the time taken for one complete revolution of the turret. All materials were normally compressed at a turret time of 1s. At this speed the machine would manufacture approximately 1000 tablets per minute if all 16 stations of the Betapress were used. Turret times of 1s, 0.88s, 0.75s and 0.65s were used for experiments in which the effect of the machine speed on

tableting parameters was studied. These turret times corresponded with average punch velocities in a vertical direction of about 21 cm/s, 23 cm/s, 29 cm/s and 32 cm/s, respectively, during the initial part of the compression phase.

2.3.7. Relationship between fraction of turret revolution and turret time

The position of the occurrence of various events during the compaction cycle can be described either in terms of time (t) at a given turret time relative to a reference position during the compaction cycle, or in terms of the turret position during its revolution (given as the fraction, fr, of the turret revolution) relative to the same reference position. The compression phase of the compaction cycle begins when the force on the upper and lower punches is first measurable and ends when the punches are vertically aligned with the axes of the two pressure rolls along an imaginary vertical line called the line of dead centre. In terms of time this line was specified as t = 0 (Fig. 5), or as fr = 0 in terms of fraction of turret revolution. The position fr = 0 or t = 0 was the reference position used throughout this work to divide the compaction cycle into the compression and decompression phases, and to obtain the accurate position of various events during compaction. Profiles of various parameters during the compression and decompression phases were obtained relative to this reference position as a function of either t or fr.

A multiplication by the turret time converted fr to t. Thus, at a turret time of 1s, fr = t. Unless otherwise specified all experiments were conducted at a turret time of 1s, hence, the fr-axis on plots showing change in a given parameter with respect to fr can be also be read as a t-axis.

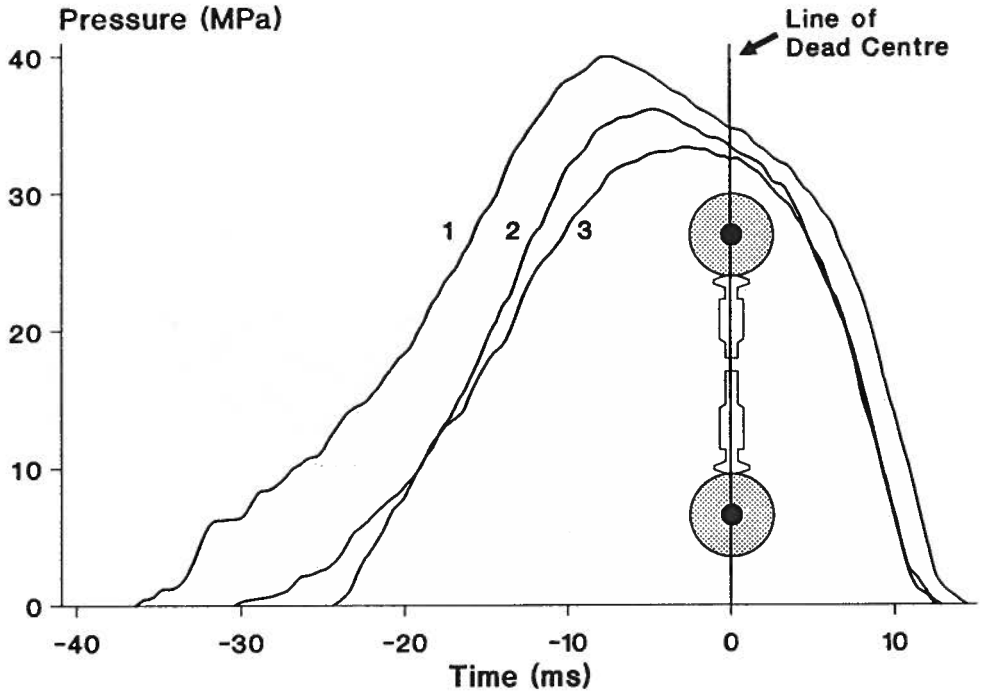

FIG. 5. Pressure-time curves for: (1) Avicel PH102, (2) Spray-dried Lactose, and (3) Emcompress. Turret time = 1s, IPT punches.

At different turret times, the positions of t = 0 after triggering of data collection were different. However, to maintain the uniqueness of the reference position at each machine speed, the position of fr = 0 was kept the same as t = 0. The determination of position of t = 0 (or fr = 0) after the triggering of data collection is given in section 2.4.4.

2.4. ANALYSIS OF THE COMPRESSION PHASE

2.4.1. Calculation of stress, strain and strain rate

Stress was obtained as the punch force given by the strain gauges, divided by the cross sectional area of the powder bed within the die. During the compression phase, strain was defined as a decrease in the height of the powder bed relative to its height at the instant before the decrease. The strain between any two time fractions was calculated as the change in the height of the compact between the two fractions divided by its instantaneous height at the earlier of the two fractions. Dividing by the average height between these two fractions gave the average strain on the powder bed. Using the volume of the powder bed in the calculations instead of its height gave the volumetric strain.

Strain at a given time during compression was calculated using the distance between the upper and lower punch faces. This distance was calculated automatically by the data analysis software using the displacement analysis procedure. Volumetric strain rate was calculated from the volumetric strain according to the above definition.

2.4.2. Determination of tablet porosity (p)

Porosity, p, of a tablet within the die at any time point during the compression phase is given by $p = 1 - \rho_r$, where ρ_r = relative density

calculated as mass per unit volume of the material in the die divided by the true density of the compact material. The data analysis software calculated the volume of material in the die by multiplying the distance between the upper and lower punch faces by the cross-sectional area of the die.

2.4.3. Calculation of yield stress (σ_y)

The yield stress was determined from the equation $\ln (1/p) = K \cdot P + c$ (Heckel, 1961), where $\ln (1/p)$ is the Heckel term and $K = 1/(3\sigma_y)$. A special case of the Heckel plot was used to determine σ_y. The data analysis software gave the maximum value of the Heckel term (H_{max}), at P_{max} during the compression phase. The yield stress for each material was given by $1/(3K)$, where K is the slope of a plot of H_{max} versus P_{max} over a range of P_{max}. These plots were linear with r^2 values ranging between 0.850 for S-ibuprofen and 0.995 for Di-Pac. The r^2 values were generally above 0.95.

2.4.4. Determination of peak offset time

Peak offset time, t_{off}, was defined as the interval between the time to reach P_{max} and t = 0 (Fig. 6). For an accurate determination of t_{off}, it was necessary to know when t = 0 occurred following the triggering of data collection. A prefabricated hardened steel tablet (1.269 cm diameter X 0.3 cm thickness) within the confines of a die was virtually incompressible under the pressures used in this work and showed symmetrical pressure-time profiles with peak pressures, P_{max}, at t = 0 (Oates and Mitchell, 1989). The position of P_{max} was given by the data analysis software as the point where the derivative of pressure with respect to time

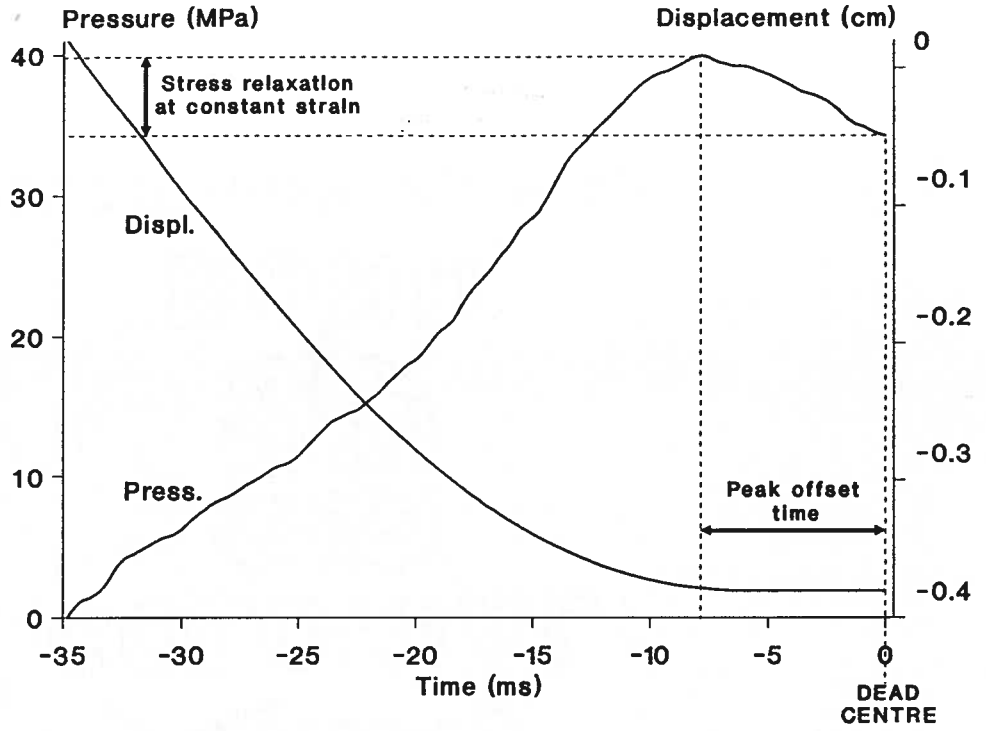

FIG. 6. Pressure and punch displacement-time curves showing stress relaxation at constant strain and peak offset time for Avicel PH102. Turret time = 1s, IPT punches.

was 0. Thus, the position of t = 0, on an experimental pressure-time profile at a given machine speed, could be determined by compressing the steel tablet at that speed and finding the position of P_{max}. However, an alternative and safer procedure was adopted as described below.

When repeatedly compressed without ejection at pressures above 280 MPa, Emcompress showed pressure-time profiles almost identical with those of the steel tablet. Therefore, the position of t = 0 at different speeds was found by determining the positions of P_{max} for Emcompress tablets made by repeated compression, without ejection, at pressures above 280 MPa. The average position of P_{max} for ten tablets at each turret time was used to give the average position of t = 0 at that speed. The coefficient of variation of these averages was less than 0.4% at each turret time indicating high precision in the position of t = 0. When provided with the turret time and the position of t = 0, the data analysis software automatically determined the value of t_{off}.

2.4.5. Factors affecting t_{off}

The following experiments were performed to study various factors likely to affect t_{off}:

Experiment I: Using IPT punches at a turret time of 1 s, tablets were made from Avicel PH102, Emcompress and Spray-dried Lactose over a range of P_{max} by (a) varying the mass of the tablet, with the tablet thickness setting on the machine fixed (Method I, page 41), and (b) fixing the mass of the tablet and varying the thickness setting (Method II, page 41).

Experiment II: Experiment I(a) was repeated at different turret times using Manesty punches in order to study the effect of machine speed on the t_{off} for Avicel PH102 and Emcompress.

Experiment III: To study the effect of different punch types on t_{off}, tablets were made over a range of P_{max} at a turret time of 1 s using both IPT and Manesty punches.

Experiment IV: To study the effect of formulation on t_{off} for drugs with poor compression properties such as acetaminophen and ibuprofen, tablets from crystalline samples and the directly compressible commercial formulations of these drugs were made at a turret time of 1 s using IPT punches. The change in t_{off} with increasing P_{max} was recorded for each sample.

2.4.6. Determination of decrease in pressure during t_{off} (ΔP)

Figure 6 shows that the pressure decreases during t_{off}. The decrease in pressure between the point where t_{off} occurred and t = 0 was termed ΔP. The software automatically calculated ΔP by subtracting the pressure at t = 0 from P_{max}. To compare different materials, the value of ΔP for each material at different pressures was normalised for the corresponding true volume (mass of the tablet divided by the true density of the material) of the materials in the die.

2.4.7. Calculation of work of compression (W_C)

The method of calculating W_C was reported by Oates and Mitchell (1989, 1990). This method determined W_C as a product of force exerted by

the punches to form the compact and the corresponding displacement corrected for the machine deformation during the compression phase. It was shown that ignoring the machine deformation, and calculating the punch displacement solely on the basis of machine geometry, as proposed by previous authors (Rippie and Danielson, 1981; Charlton and Newton, 1984), resulted in errors in W_C of up to 40% (Oates and Mitchell, 1990).

2.6. ANALYSIS OF THE DECOMPRESSION PHASE

The decompression phase begins at fr = 0 and ends when the applied vertical force, F, experienced by the tablet drops to zero, i.e., when the fraction at which F = 0 ($fr_{F=0}$) is reached (Fig. 7). During this phase the machine deformation is recovered and the tablet expands. Thus, the F-fr curve corresponds to the total recovery of the machine and the tablet. To obtain the expansion of the tablet, the machine recovery must be subtracted from the total recovery. This idea was the basis for analysing the decompression phase to obtain tablet expansion and related parameters.

2.6.1. Determination of machine deformation during decompression

The force applied by the press during the compression phase causes the punches and the press to deform. The sum of punch contractions and press deflections is the total machine deformation, D_m, which is totally recovered during decompression. At any given fr during the decompression phase, D_m is directly proportional to F:

$$\Delta D_m = K^{-1} \cdot \Delta F \qquad (4)$$

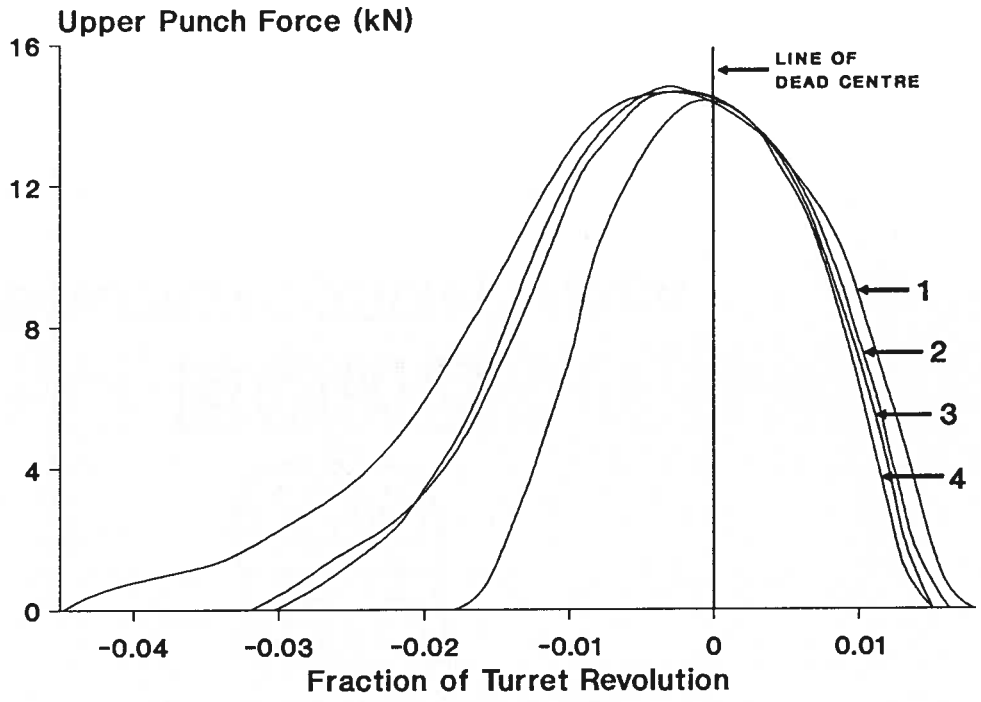

FIG. 7. Upper punch force versus fraction of turret revolution curves for: (1) Avicel PH102, (2) Spray-dried Lactose, (3) Emcompress, and (4) steel+Emcompress tablets. At a turret time of 1s, the x-axis also gives the time for compression and decompression in fractions of a second.

where, ΔD_m = the change in machine deformation, K^{-1} = the machine deformation constant (section 2.3.2) and ΔF = the change in the vertical force.

Throughout the compaction cycle, the upper and lower punch heads are pressed against their respective pressure rolls. The pressure rolls constrain the punches and, during powder compaction, force them together thereby decreasing the distance between the two punch faces. If the powder bed could be replaced by an 'incompressible' solid, the distance between the punch faces would be constant throughout the compaction cycle. Hence, a F-fr curve for an incompressible solid would be proportional to the corresponding D_m-fr curve according to equation 4.

2.6.2. Selection of the incompressible material

The ideal incompressible solid would fill the space between the punch faces, i.e., it would be completely non-porous, and would have a negligible change in dimensions during the compression and decompression phases. Theoretically any liquid would be suitable as an incompressible material, but only if it were not squeezed through the space between the punches and the die wall. After initial experiments with plasticine and silly putty in muslin bags, it was decided to use steel, which could be machined into tablets which fitted the die cavity snugly, and then hardened. However, a series of tablets with varying thicknesses would have been required to vary the punch force at a fixed tablet thickness setting on the press, and there were potential dangers in the impact between the punches and the steel tablets, especially at high forces. Therefore, it was decided to use the hardened steel tablet described in section 2.4.4, which gave almost

negligible punch force when the press was operated at a thickness setting of about 0.3 cm, and to cushion the impact of collision of the punches with the tablet by putting a layer of Emcompress on its top surface. As mentioned earlier (section 2.4.4), repeated compression makes Emcompress behave as an incompressible solid. Thus, 'steel+Emcompress tablets' were used as the incompressible solid for the decompression analysis.

2.6.3. Determination of tablet expansion

A series of F-fr curves was determined by 'compressing' the incompressible solid under running conditions. The ejection cam was removed and the thickness setting was fixed to give a distance of about 0.3 cm between the punch faces at fr = 0 in an empty die. The steel tablet was inserted into the die cavity and various weighed amounts of Emcompress were added to increase the peak force. After each addition, the steel-Emcompress tablet was repeatedly compressed without ejection to minimize any Emcompress recovery. By increasing the mass of Emcompress from 80 to 430 mg in 10 mg increments, about thirty five F-fr curves were recorded with peak forces ranging from 2 to 35 kN. A computer program converted the data from the decompression phase into an array of F-fr curves for evenly spaced values of F at fr = 0 ($F_{fr=0}$) ranging from 0 to 35 kN (Fig. 8). From this array, a F-fr decompression curve could be computed by interpolation for any $F_{fr=0}$ in the range 0 to 35 kN (0 to ≈270 MPa).

A tablet which does not expand axially upon decompression would have a F-fr curve which coincides with the curve computed from the array at a matching $F_{fr=0}$. When a tablet expands axially it would cause additional machine deformation, ΔD_m, which would correspond to the expansion of the tablet and results in a corresponding increase in force, ΔF. To determine

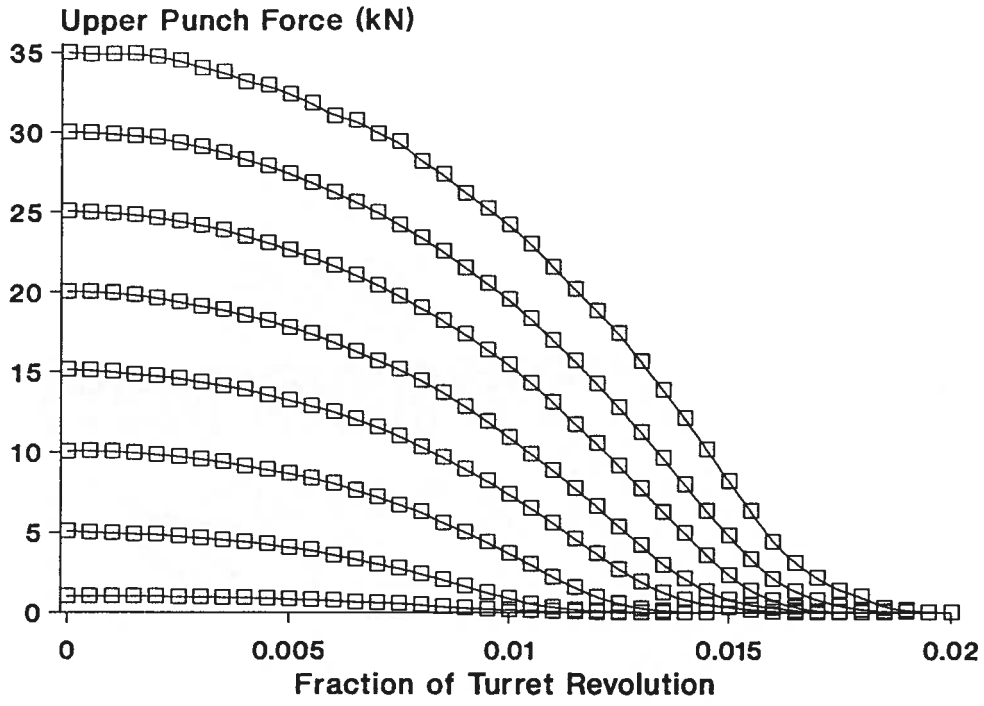

FIG. 8. An array of evenly spaced decompression curves for steel+Emcompress tablets. Decompression curves corresponding to any force at fr = 0 can be calculated by interpolation.

ΔF, the F-fr curve derived from the array was subtracted from the F-fr curve of the test material. A ΔD_m-fr curve was obtained by converting ΔF to ΔD_m using equation 4. The range of turret positions over which ΔD_m was defined began at fr=0 and ended where the force on the array curve dropped to zero. The procedure for deriving ΔD_m from ΔF is illustrated in Fig. 9. Some representative plots of ΔD_m-fr for various materials are shown in Fig. 10.

Any deformation and elastic recovery in the steel tablet would lead to errors in the estimation of ΔD_m. Errors in ΔD_m would increase with increases in compression force and would be greatest for tablets undergoing the least expansion during decompression. Thus, using an elastic modulus for steel of 200 GPa (Popov, 1968), it was found that the maximum error in estimates of ΔD_m would be about 2.4 percent for Avicel PH102, which had a high elastic recovery on decompression, and about 5.0 percent for Emcompress, which had low elastic recovery.

2.6.4. Determination of work of decompression

The F-fr (Fig. 7) and ΔD_m-fr (Fig. 9) plots were combined to obtain plots of F-ΔD_m (Fig. 11). The F-ΔD_m curves were linear, with r^2 values usually above 0.95, and hence could be extrapolated to F = 0 to obtain a quantity called ΔD_m at F = 0 ($\Delta D_{mF=0}$). The area under the curve from ΔD_m = 0 to $\Delta D_{mF=0}$ was the work done by the expanding tablet on the machine during decompression. The work of decompression, W_D, is the negative of this area, where the negative sign indicates that energy is lost by the tablet during expansion.

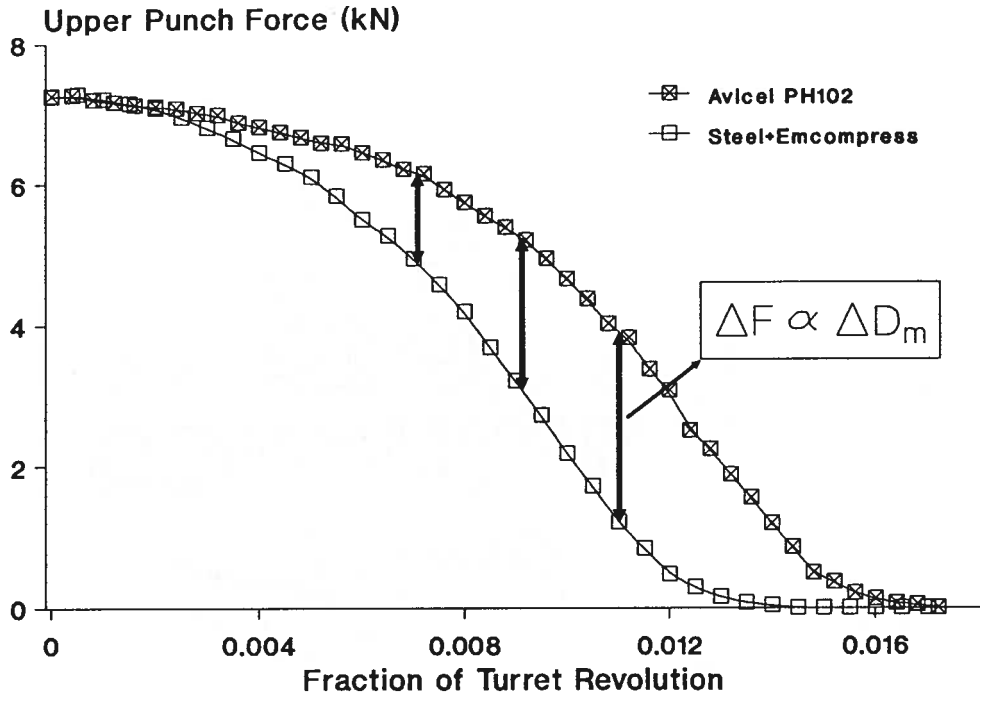

FIG. 9. Diagrammatic representation of calculation of tablet expansion. ΔF is the difference in force between the decompression curve of a test material and an array curve from Fig. 8, and is proportional to ΔD_m, the expansion of the test material.

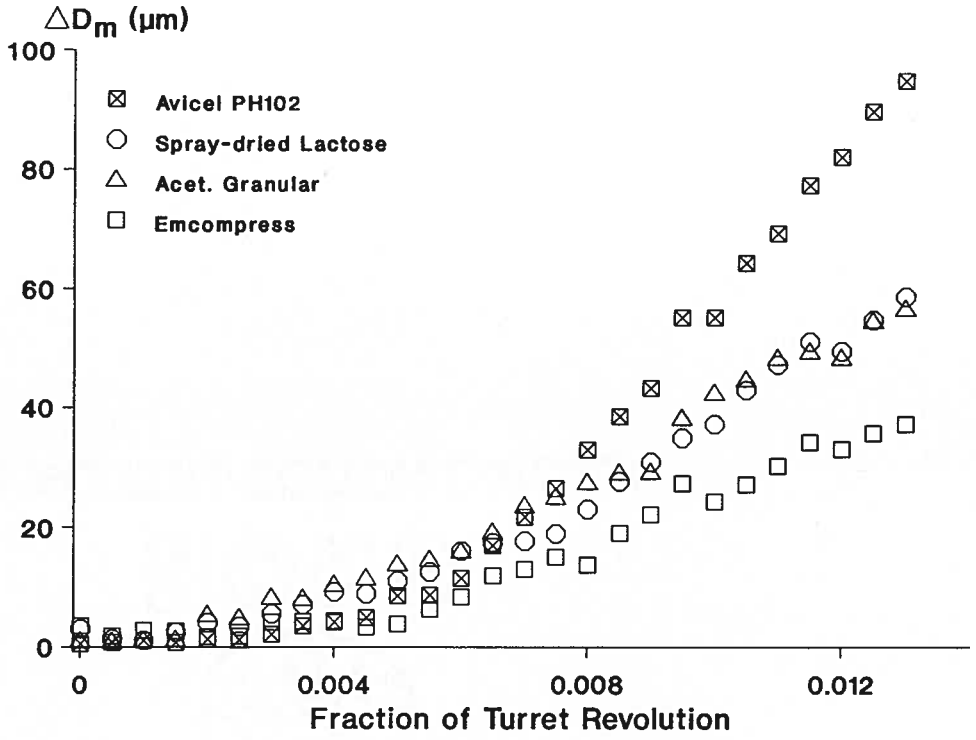

FIG. 10. Tablet expansion for various materials as a function of fraction of turret revolution during decompression.

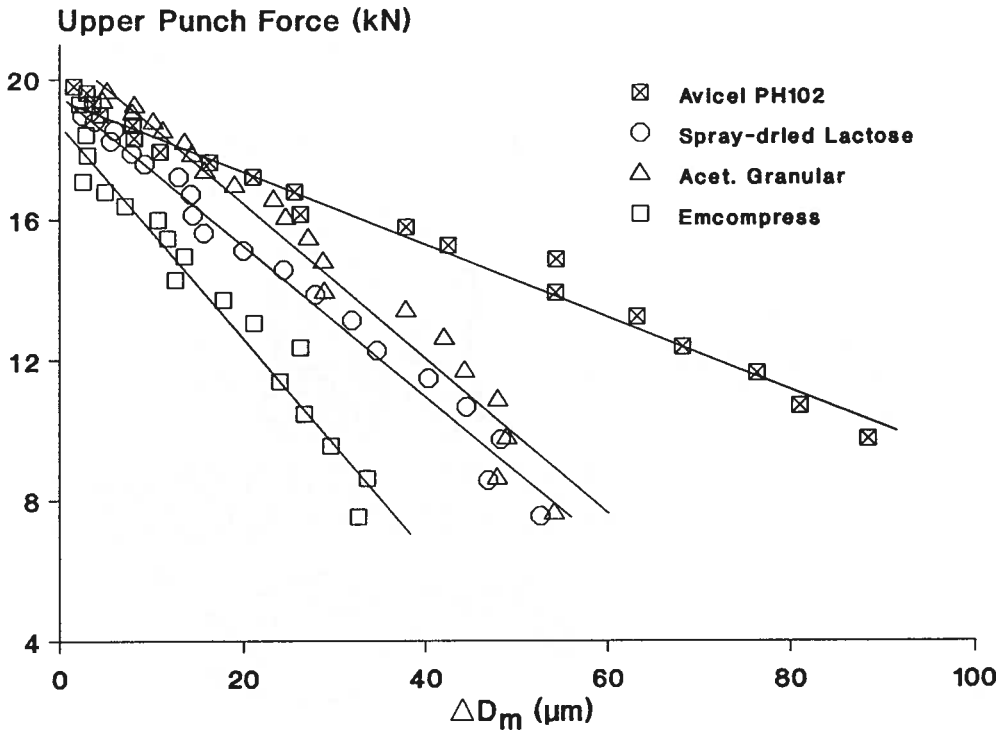

FIG. 11. Decrease in upper punch force during decompression. Each plot represents the expansion of a single tablet and the area from $\Delta D_m = 0$ to $\Delta D_{mF=0}$ gives the work of decompression.

2.6.5. Determination of Young's Modulus

Assuming tablet expansion during decompression was elastic, the force exerted by the expanding tablet on the upper punch was expressed by the following form of Hooke's law:

$$\sigma = E_p \cdot \epsilon \qquad (5)$$

where, σ = the axial stress given by F divided by the cross-sectional area of the punch face, E_p = the modulus of elasticity of a tablet with a certain degree of porosity, and ϵ = axial strain which was obtained as follows:

a. Relative to compact thickness at the end of decompression, $H_{F=0}$ (Fig. 12), the change in the thickness at any fraction during decompression, $\Delta H(fr)$, was given by:

$$\Delta H(fr) = \Delta D_{mF=0} - \Delta D_m(fr) \qquad (6),$$

where the values of $\Delta D_m(fr)$ and $\Delta D_{mF=0}$ were obtained from Figs. 10 and 11, respectively.

b. Tablet thickness at the end of decompression, $H_{F=0}$, was calculated from:

$$H_{F=0} = H_{fr=0} + \Delta D_{mF=0} \qquad (7),$$

where, $H_{fr=0}$, the tablet thickness at fr = 0, was given by,

$$H_{fr=0} = K^{-1} \cdot F_{fr=0} + 0.314 \text{ cm} \qquad (8).$$

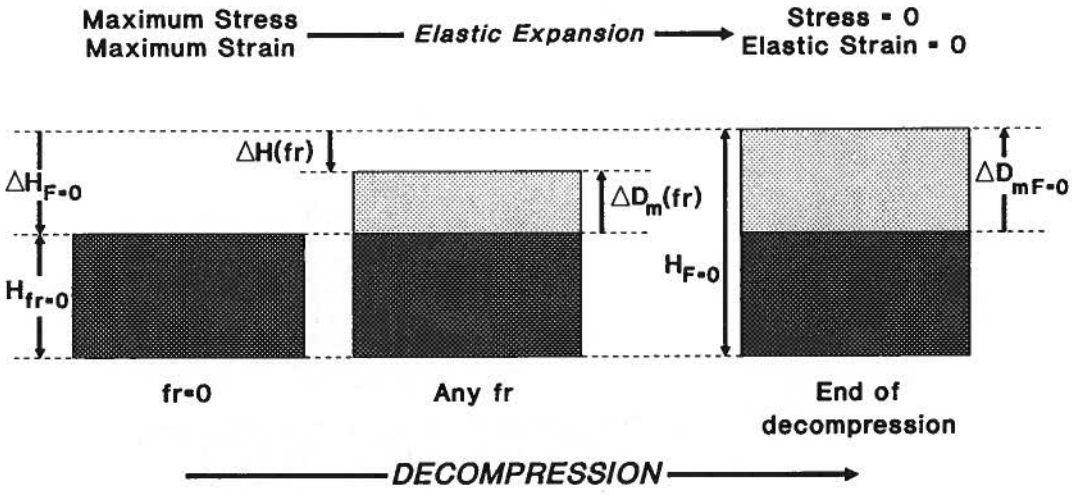

FIG. 12. Schematic representation of tablet expansion at various stages during decompression (drawing not to scale). The quantities shown are used to calculate the modulus E_p of tablets.

The intercept of 0.314 cm is the distance between the punch faces in an empty die at fr = 0 and was close to the machine thickness setting of about 0.3 cm. Equation 5 was derived from an independent experiment in which increasing weights of lead shot (#4, Winchester) were compressed by hand turning the press to give different values of $F_{fr=0}$. The thickness of the ejected lead tablets was measured. Linear regression of this thickness against $F_{fr=0}$ (r^2 = 0.985) gave K^{-1} = 2.2 x 10^{-6} cm/N which was close to the value of 2.3 x 10^{-6} cm/N determined under static conditions using feeler gauges (section 2.3.2). This indicates that the elastic recovery of compacts of lead shot was negligible upon decompression.

c. Combining equations 6 and 7 gave strain as a function of fraction, $\epsilon(fr)$:

$$\epsilon(fr) = \Delta H(fr) / H_{F=0} \qquad (9)$$

Using equation 9, the plots of ΔD_m-fr were converted to plots of ϵ-fr. Dividing F by the cross-sectional area of the punch face converted the plots of F-fr to σ-fr. The σ-fr and ϵ-fr plots were then combined to obtain stress-strain (σ-ϵ) curves, the slopes of which gave E_p for a given tablet according to equation 5. Extrapolation of the plots of E_p versus p (porosity at the end of decompression) to p = 0 gave the values of Young's modulus for the tablet material.

2.6.6. Determination of porosity at the end of decompression

The compact porosity at the end of decompression was calculated from the mass and true density of the material, and the distance between the

punch faces at the end of decompression (hence the in-die volume of the compact at the end of decompression). At the end of decompression the distance between the punch faces equals $H_{F=0}$, where $H_{F=0}$ was calculated from equations 7 and 8. The porosity at the end of decompression was within 95% confidence intervals of the minimum porosity during the compression phase. Hence, the minimum porosities during the compression phase were used to construct the plots of E_p versus p.

2.7. DETERMINATION OF TABLET STRENGTH

The strength of the tablets was determined in a diametral compression test using a CT-40 tablet strength tester (Systems Engineering). On this tester a tablet is placed vertically on a small round platform, an upper cross-beam with a platen moves down onto the tablet and applies force across its diameter. The platform is connected to a strain gauged load cell the analog signals from which were recorded via an analog to digital converter on an Apple II+ computer and analysed to obtain a force-time curve up to tablet failure. All tablets were stored at about 21°C under a relative humidity of 30-40% for 24 h before the determination of the force of failure.

3. RESULTS AND DISCUSSION

3.1. MATERIAL PROPERTIES

The true and bulk densities of various solids are given in Table II. These values were verified by comparing with other, independent measurements, or by comparison with the values in the literature. The values of true densities obtained from the helium pycnometry were verified by using suspension density measurements on selected solids (Dwivedi, 1988). The bulk densities for most excipients are close to those reported in the Handbook of Pharmaceutical Excipients (1986).

The melting points of several solids are given in Table II. In most cases these correspond to the melting of crystalline samples of each solid. With certain formulations (e.g., for some Compaps), multiple peaks were obtained on the DSC curves, and the temperature on the leading edge of the final endotherm was taken as the melting point. The melting points of some other solids (e.g., sucrose, lactose) correspond to melting with decomposition. The melting points for celluloses are decomposition temperatures. The melting points of samples containing α-lactose monohydrate (e.g. α-Lactose monohydrate, Fast-Flo Lactose and Spray-dried Lactose) correspond to the melting of the sample after dehydration. The dehydration causes a small degree of anomeric conversion from the α-anomer to β-anomer in open pans (Dwivedi, 1988).

The melting points were used to calculate the homologous temperature of each solid where the homologous temperature is the ratio of absolute room temperature (293 K during tableting on the rotary press) to the absolute melting temperature of the solid (Table II). The homologous temperature indicates the proximity of room temperature to melting

TABLE II. Physical constants of the solids compressed on Betapress.

Material	True Density[1] (g/cm^3)	Bulk Density[2] (g/cm^3)	Melting[3] Temperature (K)	Homologous[4] Temperature
A-Tab	2.774	0.68	-	-
Acetaminophen Fine Powder	1.301	0.26	443	0.661
Acetaminophen Granular	1.294	0.64	443	0.661
Acetaminophen Powder	1.296	0.35	443	0.661
Acetylsalicylic Acid	1.350	-	432	0.678
Anhydrous Emcompress	2.780	0.74	-	-
Anhydrous Lactose	1.564	0.51	508	0.577
Asagran	1.385	0.59	432	0.678
Avicel Large	1.555	0.32	538	0.545
Avicel PH101	1.556	0.28	538	0.545
Avicel PH102	1.549	0.33	538	0.545
Avicel PH105	1.556	0.25	538	0.545
Caffeine	1.458	0.29	511	0.573
Cal-Star	2.316	0.86	-	-
Cellactose	1.542	0.37	471	0.622
Compap CG	1.300	0.43	441	0.664
Compap Coarse 73 L	1.395	0.56	439	0.667
Compap Coarse L	1.290	0.54	439	0.667
Compap L	1.306	0.44	441	0.664
DCI-63	1.233	0.57	342	0.857
Di-Pac	1.543	0.66	460	0.638
Di-Tab	2.330	0.83	-	-
Elcema G250	1.525	0.34	538	0.545
Emcocel	1.539	0.31	538	0.545
Emcompress	2.353	0.81	-	-
Emdex	1.504	0.64	421	0.697
Fast-Flo Lactose	1.533	(0.69)	488	0.600
Lactose DCL 21	1.561	0.59	508	0.577
Mannitol (Crystalline)	1.490	0.52	431	0.680
Mannitol M.G.	1.482	0.66	428	0.685
Neosorb (Sorbitol)	1.487	0.59	369	0.795
α-Lactose monohydrate	1.538	0.43	488	0.600
Potassium Chloride	1.980	-	-	-
Racemic ibuprofen	1.120	0.38	348	0.842
Rhodapap DC-P3	1.295	0.39	441	0.664
S-Ibuprofen	1.096	0.45	323	0.907
Sodium Chloride	2.170	(0.93)	-	-
Spray-dried Lactose	1.538	0.64	489	0.599
STA-Rx-1500	1.480	0.65	-	-
Sucrose (crystalline)	1.584	0.78	453	0.647
Sugartab	1.560	0.61	443	0.661
Tri-Tab	2.883	0.78	-	-
Xylitol (Crystalline)	1.533	0.71	364	0.805

1. Determined by helium pycnometry (coefficient of variation < 0.15%, n = 8); 2. Determined using a procedure adopted from the Handbook of Pharmaceutical Excipients (1986). The values in parenthesis are taken from this Handbook; 3. Determined using DSC (see text in section 3.1 for comments on these values); 4. Ratio of room temperature (293 K) to the absolute melting temperature.

temperature, and is an useful parameter in explaining the deformation behaviour of the solids (section 3.6.2).

3.2. THE SOLID STATE OF IBUPROFEN

Currently, there is great interest in the significance of drug chirality in pharmaceutical development and regulation (Hutt, 1991) and increasing emphasis is being placed on the use of single enantiomers, rather than the racemic drug, in dosage forms. Ibuprofen is a chiral drug. The chemical structure of ibuprofen in Fig. 13 shows that the molecule has one chiral center. Hence, there are two enantiomers. Racemic ibuprofen contains equal amounts of these enantiomeric molecules. Both S-ibuprofen and racemic ibuprofen are commercially available for use in tableting. These samples were characterized to establish the differences in the nature of their solid state.

Racemic drugs may be classified into three types based on a melting point phase diagram. The most common type is the racemic compound which contains an equal number of molecules of each enantiomer in the unit cell of the crystal. The solid therefore is a one phase crystalline addition compound, and the binary phase diagram of the two enantiomers shows two eutectic points. The melting point of a racemic compound may be either below or above the melting point of the pure enantiomers.

The second less common type of racemic drug is the racemic mixture or conglomerate in which the two enantiomers crystallize separately. The solid therefore is a two phase physical mixture. In the binary phase diagram there is only one eutectic point which corresponds to the melting point of the racemic mixture.

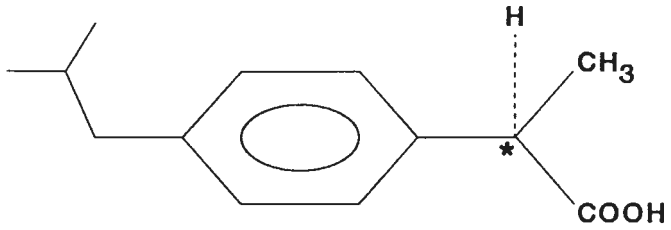

(R)-(-)-ibuprofen

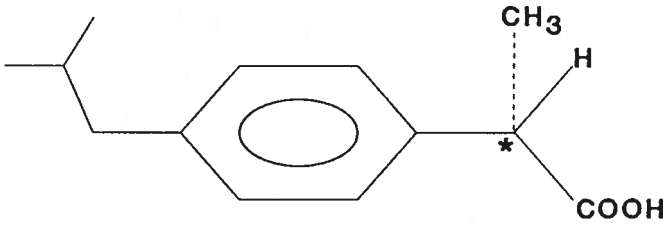

(S)-(+)-ibuprofen

FIG. 13. Chemical structure of ibuprofen.

The third type of racemic drug is obtained when the two enantiomers form a continuous series of solid solutions (mixed crystals). A solid solution of the two enantiomers with equimolar enantiomeric composition is designated a racemic solid solution or pseudoracemate.

The literature sometimes refers to racemic ibuprofen as a racemic compound and sometimes as a racemic mixture. The USP describes ibuprofen as a '(±) mixture' which is misleading. To identify the racemic modification of ibuprofen, DSC and powder X-ray diffraction were used and the two component phase diagram between R and S-ibuprofen was constructed based on the DSC results.

3.2.1. DSC and powder X-ray diffraction of ibuprofen samples

DSC scans indicate that the melting points of R-ibuprofen and S-ibuprofen are nearly identical. Some representative DSC curves of various samples of ibuprofen are given in Fig. 14. The melting point of S-ibuprofen is much lower than that of racemic ibuprofen and samples of intermediate composition show a clearly defined eutectic melting endotherm. This suggests that racemic ibuprofen is a racemic compound. The final melting of DCI-63, the formulation containing 63% ibuprofen, occurred at a temperature close to the melting point of racemic ibuprofen which indicates that racemic ibuprofen was used to prepare this formulation.

The powder X-ray diffraction patterns (Fig. 15) of the two enantiomers were identical, but different from the pattern of racemic ibuprofen. This confirms that racemic ibuprofen is a racemic compound capable of existing as a separate phase in the solid state independent of its constituent enantiomers. The diffraction pattern of a racemic mixture would be identical with that of its enantiomers, while that of a racemic

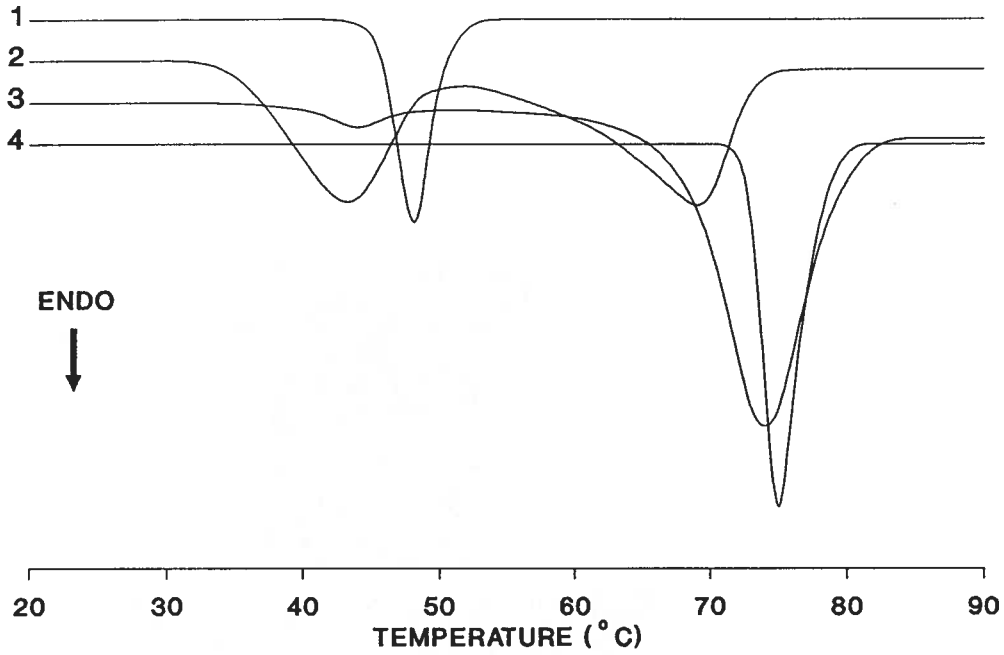

FIG. 14. Representative DSC curves of various compositions of ibuprofen: (1) 96% S-ibuprofen, (2) 27.6 % S-ibuprofen, (3) 46 % S-ibuprofen, (4) racemic ibuprofen.

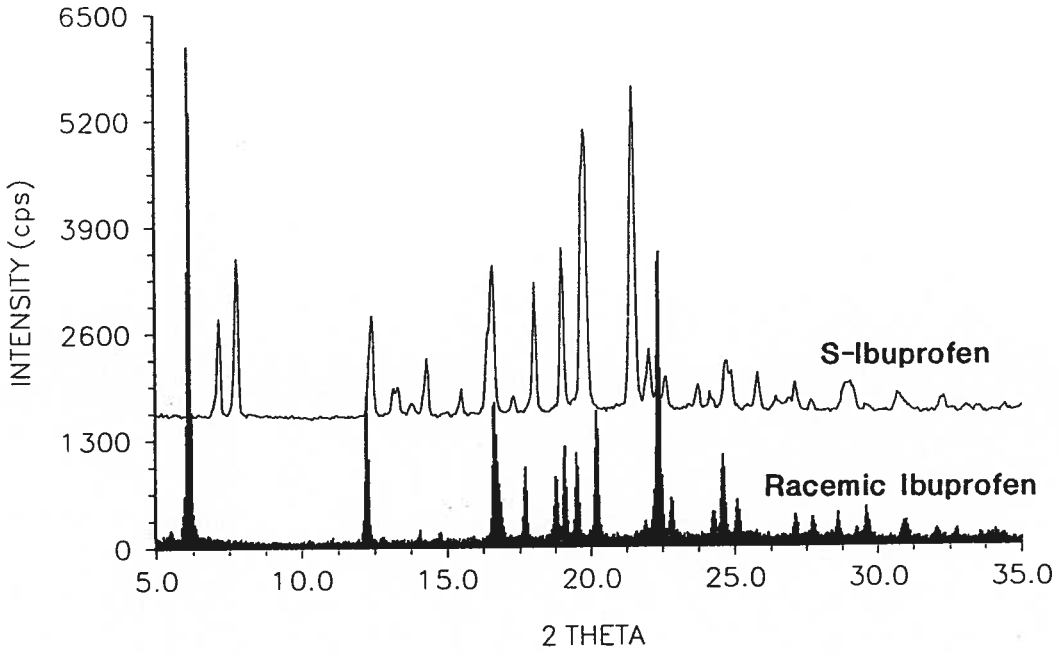

FIG. 15. Powder X-ray diffraction patterns of S-ibuprofen and racemic ibuprofen. The pattern of R-ibuprofen was identical to that of S-ibuprofen. The pattern of S-ibuprofen is shown with a baseline offset.

solid solution would show slight shifts in the peak positions depending upon the nature of the solid solution (whether it is a substitutional or an interstitial solid solution). The term racemic mixture, often used in the literature to describe crystalline racemic ibuprofen, is therefore incorrect and misleading.

3.2.2. The binary phase diagram of ibuprofen

Fundamental confirmation that racemic ibuprofen is a racemic compound, and not a racemic mixture, was provided by the binary phase diagram (Fig. 16). The phase diagram is characteristic of a eutectic system with a binary addition compound formation. The melting points, T_m, determined by extrapolating the leading edge of the melting endotherm to the baseline, were 46°C, 46.5°C and 71°C for R-ibuprofen, S-ibuprofen and racemic ibuprofen, respectively. The eutectic temperature was 37°C and the eutectic points occurred at approximately 0.18 and 0.82 mole fractions of S-ibuprofen. The extrapolation method gives accurate values of T_m for single phases such as R-ibuprofen, S-ibuprofen and racemic ibuprofen but becomes unreliable for mixtures of intermediate composition due to broadening in the eutectic and melting endotherms (Fig. 14). Hence, for constructing the phase diagram the temperatures at the peaks of the eutectic and melting endotherms (i.e., the end of fusion) were used. The peak temperatures are a function of mass of the sample, but the approximately constant sample mass (5 mg) reduces the possibility of mass-related effects when comparing results from different experiments. The eutectic melting peaks could not be observed for samples with compositions below about 0.18 mole fraction S-ibuprofen and above about 0.82 mole fraction S-ibuprofen due to their close proximity to the terminal

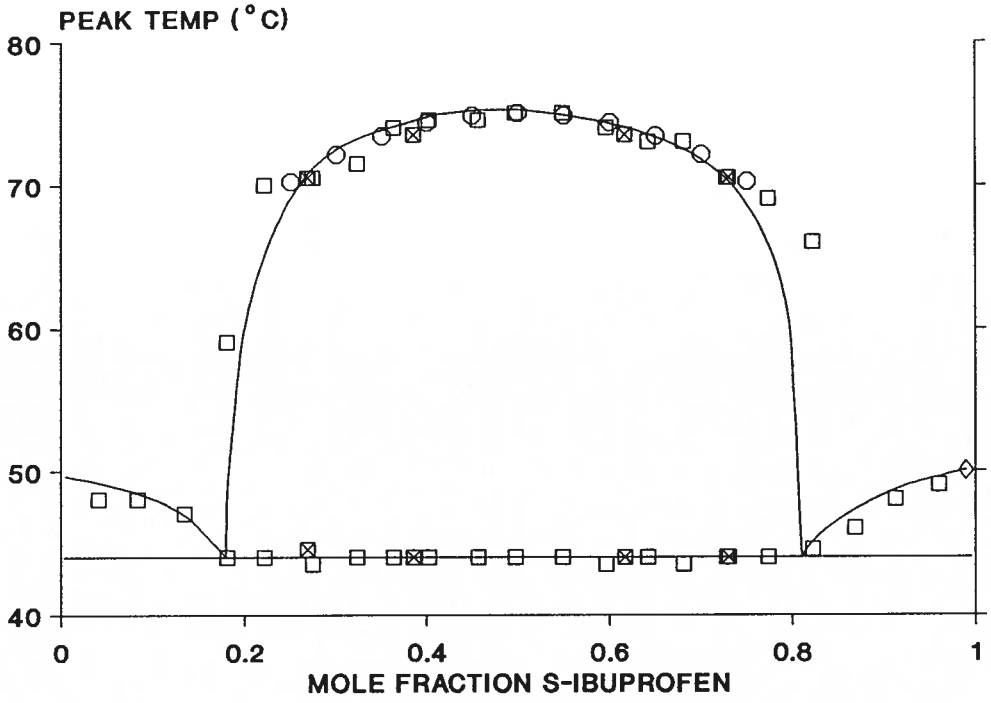

FIG. 16. Isobaric binary phase diagram of ibuprofen enantiomers showing a racemic compound formation between S and R-ibuprofen. Open squares: fused, recrystallized, and annealed mixtures of R-ibuprofen and S-ibuprofen; Crossed squares: fused, recrystallized and annealed mixtures of R-ibuprofen and S-ibuprofen with racemic ibuprofen; Circles: points calculated using equation 11; Diamond: 99.7% S-ibuprofen from Ethyl Corporation.

enantiomeric melting peaks. The melting point of a 1:1 fused mixture of R-ibuprofen and S-ibuprofen coincided with the melting point of racemic ibuprofen. Additional points on the phase diagram were obtained by plotting the melting points of fused samples containing various proportions of racemic ibuprofen with either R-ibuprofen or S-ibuprofen (Fig. 16). These points were in accordance with the fact that admixture of a racemic compound with either of its component enantiomers will depress its melting point. The melting point of a racemic mixture would be the minimum temperature on a binary phase diagram, i.e., the eutectic point, and admixture with either pure enantiomer would elevate it to higher temperatures.

In the phase diagram of a racemic compound, the absolute temperatures, T^f, on the liquidus curve, under which the racemic compound exists as a stable phase, can be predicted as a function of mole fraction enantiomeric composition, x, from its heat of fusion (ΔH^f_R) and absolute melting point (T^f_R, end of fusion) by using these quantities in the equation:

$$\ln 4x(1-x) = \frac{2\,\Delta H^f_R}{R} \cdot \left(\frac{1}{T^f_R} - \frac{1}{T^f} \right) \qquad (11)$$

where ΔH^f_R is assumed to be constant over the range of compositions for which T^f is predicted. This equation can be derived from that of Prigogine and Defay (1954). Figure 16 shows that the experimental liquidus curve determined from the DSC observations on ibuprofen was in good agreement with the liquidus curve predicted using equation 11. The prediction, however, is accurate only in the region of the congruent melting point

(dystectic or indifferent point), but fails outside this region because the assumption of constancy of ΔH^f_R fails. The Prigogine-Defay equation was used by Bettinetti *et al.* (1990) and Pitre and Stradi (1990) to predict the binary phase diagrams of sobrerol and dropropizine, respectively.

A test of equation 11 is to plot ln x(1-x) against $1/T^f$, where T^f is determined experimentally. A linear plot should be obtained the slope of which should give ΔH^f_R after division by 2/R. For ibuprofen the plot was linear (Fig. 17) and the slope gave a ΔH^f_R value of 26.4 ± 1.8 kJ/mol which agreed with the value of 26.9 ± 1.0 kJ/mol obtained directly from the area under the DSC melting endotherm of racemic ibuprofen.

The phase diagram and X-ray analysis indicate that ibuprofen USP is a racemic compound and that the USP XXII (1990) monograph description of ibuprofen as a '(±) mixture' is ambiguous.

The mechanical properties of S-ibuprofen and racemic ibuprofen are, in fact, very similar (section 3.8.1). Hence the question whether or not S-ibuprofen should be used instead of racemic ibuprofen in tablet formulations would have to be based primarily on the differences in their solid state, in particular differences in their solubilities, and also on the basis of previously reported pharmacokinetic differences (e.g., Jamali *et al.*, 1988; Ahn *et al.*, 1991, Beck *et al.*, 1991).

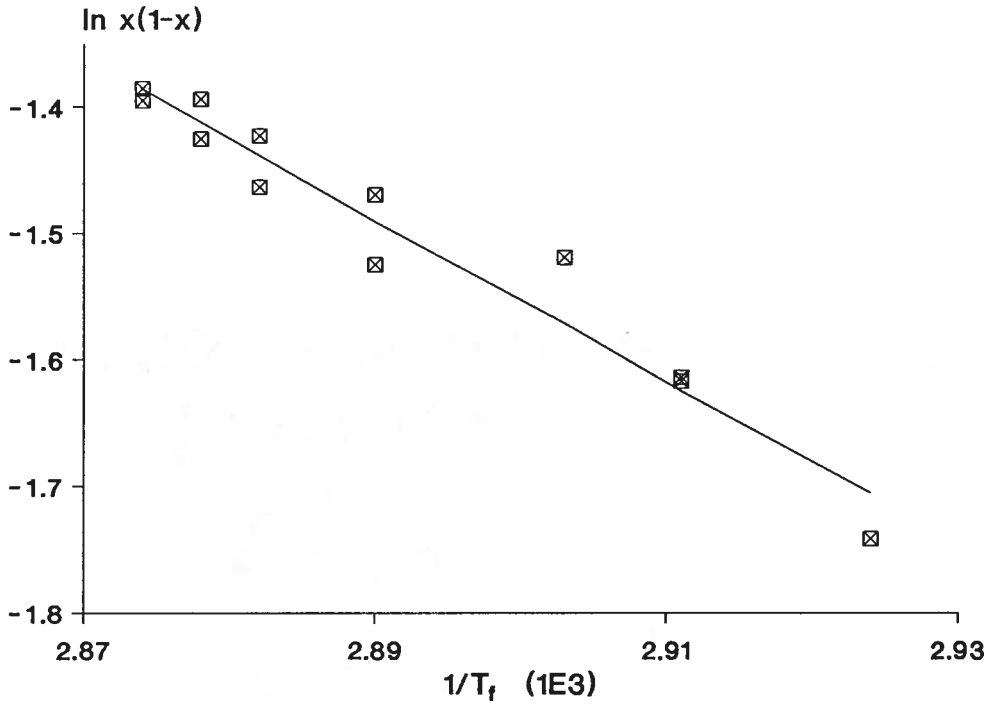

FIG. 17. Test of Prigogine Defay equation. The T_f values were experimentally determined from DSC. The slope affords the value of $\Delta H_f{}^r$.

3.3. ANALYSIS OF POWDER COMPACTION

The tableting process is divisible into a compression and a decompression phase. The overall (punch or die) stress during the compression phase increases mainly due to a build up of elastic stresses in the powder bed. These stresses arise as the particles are progressively confined into a rapidly decreasing volume between the two punches and the die wall. Any permanent deformation of the particles by flow, or by fracture of some kind, will relieve these stresses. At a certain stage during the compression phase the stresses within the powder bed rise to a maximum corresponding to a punch pressure P_{max}. The stresses then decrease as the punches are separated during the decompression phase.

The magnitude of the stress during tableting depends on the strain within the powder bed. This strain can be defined as a change in the dimension of any given particle under stress relative to its original dimensions.

The rate of strain during tableting is also important since it may influence both the mode of deformation and the stress required to cause deformation. To understand the deformation of particles by flow during compression, changes in microscopic strain rates at the points of interparticulate contact should be studied. Mathematical modeling of the microscopic strain rate changes is possible, but would be very complex on a rotary press. Modeling these changes would include factors such as indentation hardness and elastic modulus derived from single crystal microindentation, initial particle shape and changes in shape during compression, the number of particles surrounding each individual particle (the coordination number) and changes in this number, and particle

reorientation due to angular momentum induced by unequal stresses on each particle (Duncan-Hewitt, 1988; Duncan-Hewitt and Weatherly, 1990a, 1990b). The changes in the microscopic areas of inter-particulate contact, changes in the porosity of the powder bed and a non-uniform distribution of this porosity, and work hardening of particles if the deformation is predominantly due to dislocation induced crystallographic slip will complicate the model further.

For simplicity, strain on a powder bed can be approximated by calculating strain as the decrease in the height of the powder bed relative to its original height. The height of the powder bed at any instant during compression can be obtained from an accurate knowledge of the punch displacement. When data are collected at several small fractions of the total compression time, the strain between any two time intervals can be calculated as the fractional change in the height of the compact. Dividing by the average height between these two intervals (i.e., the instantaneous average powder bed height) gives the average strain on the powder bed. Using the instantaneous volume of the powder bed in the calculations instead of height gives the instantaneous volumetric strain.

Similarly, the strain rate calculated from an accurate knowledge of punch displacement can be used as an approximation of the microscopic strain rates. To include both the movement of the particles and changes in the pore space, the calculated strain rate should be based on the volume of the powder bed and not just the height.

It is shown in the following sections that the characterization of deformation behaviour of pharmaceutical materials during tableting can be accomplished by using punch pressure and macroscopic volumetric strain rate as approximations of stress and strain rate respectively at the points of

interparticulate contact. Supporting information from the compression phase such as the porosity of the compact (p), the yield value of the solids (σ_y), the work of compression (W_C), t_{off} and the decrease in the P_{max} during t_{off} (ΔP), as well as information from the decompression phase such as Young's modulus (E) and the work of decompression (W_D) can be used in such a characterization.

3.3.1. Machine deformation during powder compaction

The design of the Manesty Betapress is such that it deforms along with the powder particles during compaction. Both the upper and lower compression rolls are mounted on bearings, and the lower beam carrying the lower compression roll is supported by a spring. Under pressure, the bearings allow an upward displacement of the upper roll and a downward displacement of the lower roll. The spring supporting the lower cross-beam allows a downward deflection of the cross-beam which further displaces the lower compression roll in a downward direction. The punches contract under pressure. The machine deflections constitute up to 80% of the total machine deformation, while the remaining 20% is due to the contraction of the punches. The downward deflection of the lower roll constitutes about 65% of the total machine deflections, the remaining 35% resulting due to the upward deflection of the upper roll (Oates and Mitchell, 1989).

The Betapress can therefore be considered as a large elastic body in which the punch contractions and roll deflections constitute the total machine deformation under load. Machine deformation has usually been ignored in the tableting literature. Oates and Mitchell (1989, 1990) established that the machine deformation is significant and cannot be overlooked when analysing the overall punch displacement. The use of the

relationship between machine deformation and punch force in calculating the punch displacement was demonstrated in section 2.3.2. The discussion of the compression and decompression phases in the following sections shows how this relationship can be further used to analyse the compaction cycle by obtaining only the force versus time data on a Manesty Betapress. This analysis results in parameters related to particle deformation during compression, compact expansion during decompression, and energy consumption during compression, which are useful in interpreting the deformation behaviour of solids under pressure.

3.3.2. Particle deformation during powder compaction

The possible mechanisms by which powder particles can deform under pressure during compaction are described in section 1.3. Whether or not a particle will deform by one of these mechanisms, and the relative amounts of the deformation by a given mechanism during compaction, will depend primarily on the conditions of stress, strain and strain rate. The permanent deformation may occur by only one of the mechanisms 2-5 (section 1.3), or by a mixture of these mechanisms depending on the conditions of stress, strain and strain rate.

The stress on the particles at which permanent deformation by flow is initiated is the yield stress, σ_y. If the particles continue to deform by a flow process, the stress required to sustain the flow after its initiation is the flow stress (Courtney, 1990).

3.3.3. Stress, strain and strain rate during compaction

The particle deformation during compaction occurs at the points of interparticulate contact or in the regions in the immediate vicinity of

these contact points. The 'stress' during compaction is the stress at the points of the interparticulate contact, or the true stress (σ_T) as defined earlier. The strain is the amount of deformation of the particles under this stress relative to their original dimensions, and the strain rate is the rate of such deformation. The terms stress, strain, and strain rate, therefore, apply strictly to the deformation at the microscopic level, and, throughout this discussion, are used to describe events at the microscopic level.

3.3.4. Influence of strain rate on particle deformation

For materials showing viscous/viscoplastic flow, the flow stress increases directly with strain rate at the points of contact. Thus the amount of viscous/viscoplastic flow during compaction will vary directly with the strain rate. The strain rate has a negligible influence if the particles deform by plastic flow or if they undergo fracture since these processes are not strain-rate dependent. Plastic flow and fracture are strain-rate dependent only when loading is of the impact type, i.e., when the rate of loading is much more rapid than the speed of dislocation induced crystallographic slip in the case of plastic flow, or of crack initiation and propagation in the case of fracture. During tableting, the compaction occurs over a period of time which, although very short, is longer than the instantaneous impact phenomenon. Hence, during compaction, plastic deformation and fracture can be considered to be independent of strain-rate.

Duncan-Hewitt and Weatherly (1989a) indicated the importance of strain rate in understanding the deformation phenomenon in single crystal microindentation experiments. In an earlier study, Roberts and Rowe (1985)

reported the influence of the variation in punch speed to obtain varying strain rates (or rates of compaction) on tableting parameters of pharmaceutical solids during powder compaction on a compaction simulator.

3.3.5. Approximation of stress, strain and strain rate during compaction

There is an inhomogeneous distribution of the stress and strain in different parts of the powder bed during compaction. In reality, it is almost impossible to determine the stress, strain and strain rate during the compaction of a powder bed. Nevertheless, an approximation of average values of these parameters by using similar parameters determined at a macroscopic level would be useful in understanding the particle deformation behaviour during powder compaction. The punch pressure, P, during the compaction cycle (both the compression and decompression phases) can be used to approximate the stress. The punch pressure is the punch force divided by the cross-sectional area of the punch face, where the punch force is recorded by strain gauges affixed to some remote part of the press. The decrease in powder bed height during the compression phase relative to instantaneous bed height, or an increase in the compact height during the decompression phase relative to the instantaneous compact height, can be used to approximate the strain. Hence, the rate of compaction calculated from an accurate knowledge of punch movement during the compression phase can be used as an approximation of the microscopic strain rates during this phase. To include both the movement of the particles and changes in the pore space, the calculated rate of compaction should be based on the volume of the powder bed and not just the height. The above approximations will be in error during initial part of the

compression phase when the reduction in the powder bed volume is rearrangement dominated.

A discussion of the compression and decompression phases, and a description of the various parameters obtained from their analysis, is given in the following sections. These parameters, and the above mentioned general concepts relating deformation, stress and strain rates, were used to ascertain the deformation behaviour of particles during compaction. A discussion of the deformation behaviour of a number of general categories of solids is presented at the end of the discussion.

3.4. PARAMETERS FROM THE COMPRESSION PHASE

The compression phase of the compaction cycle begins when the strain gauges first record an increase in pressure above a certain baseline value. This phase ends when the punches are vertically aligned with the centres of the compression rolls (Fig. 5, page 43).

3.4.1. A general view of the events during the compression phase

At the beginning of the compression phase, the areas of contact between the particles in the powder bed are usually microscopic in size. The stress at these 'points' of contact, i.e., the true stress (σ_T), will be much higher than the punch pressure (P). Even if P is relatively small, σ_T may be high enough to overcome σ_y and the particles will yield and deform by some type of flow. After yielding, particle deformation by flow will continue if σ_T is higher than the flow stress.

The flow will cause the area of interparticulate contact to gradually increase. Hence P gradually increases because the structure formed due to increased interparticulate contact increasingly resists the punch movement.

The particulate material in the die is able to influence the punch movement to a significant degree because, as mentioned above, the machine itself behaves as an elastic body. Thus, punch movement is defined partially by the machine geometry, and partially by the nature of the material in the die. The increase in P tends to increase σ_T, while the increase in the area of interparticulate contact tends to decrease σ_T. Thus, the actual value of σ_T is governed by the relative rates of increase in the value of P and the degree of interparticulate contact. The σ_T will nevertheless be higher than P throughout the compression phase because the compacts invariably have a certain degree of pore space. The values of σ_T and P will converge to equality as the area of interparticulate contact becomes very large. There will be an unequal distribution of σ_T within the compacts due to differences in the nature of interparticulate contacts and the density gradients within the compact.

After a certain degree of flow the particles will fracture if and when a σ_T value equal to fracture stress is achieved. Fracture stress is the stress required to cause the initiation and propagation of a crack in the particles. For materials having high σ_y, which, at room temperature, is normally true for materials with high melting temperature, fracture may occur even before the particles have yielded. This is because, in the process of building up the σ_T to a value equal to σ_y, the particles may develop regions of very high stress concentrations, e.g., at microscopic flaws in their structure, or develop triaxial stresses on the particles. Under such conditions it will be energetically preferable for the particles to fracture without any prior permanent deformation. Therefore, solids with high σ_y may behave as intrinsically brittle materials at room temperature under normal conditions of powder compaction.

3.4.2. The rate of compaction profiles

On a rotary press, the rate of compaction is the rate at which the upper and lower punches are brought together. Between any two time fractions during compression the rate of compaction can be calculated by dividing the decrease in the powder bed height or volume by the time interval between the two fractions. This rate is expected to be highest at the beginning of the compression phase. It will decrease as the stresses in the powder bed offer increasing resistance to the punch movement, and will be negligible when the flat top of the punch heads comes in contact with the compression rolls.

As the compression phase progresses, the initially high rate of compaction, and hence the high flow stress (assuming that the rate of compaction is an approximation of the strain rate), will decrease as the punches slow down due to an increase in the resistance offered by the compact. If σ_y has been exceeded and if σ_T is higher than the flow stress, flow will continue as long as enough voids are available to accommodate the flow. As the P_{max} approaches, the rate of compaction and the flow stresses will reach a minimum, and the particles will flow with even greater ease, provided sufficient pores are still available. The flow, and the consequent stress relief, will continue during the dwell time, if any. If the particles fracture, the fracture will continue to occur if σ_T is higher than the fracture stress, and the change in the rate of compaction would have a negligible effect on this process.

The volumetric rate of compaction profiles during the compression phase for various materials, when compressed to the same P_{max}, are shown in Fig. 18. Although the initial magnitude of the rate of compaction is different for different materials, the shape of the plots is similar. This

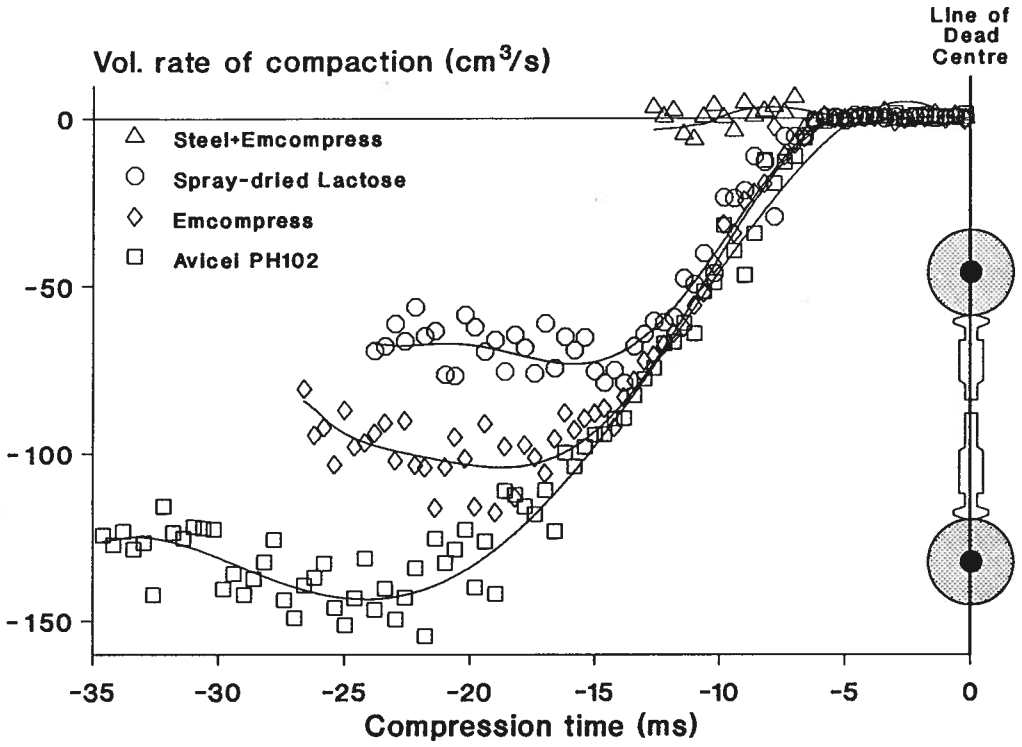

FIG. 18. Volumetric rate of compaction profiles during the compression phase. Each profile shows an initial acceleratory phase, an intermediate deceleratory phase and the final phase of constant powder bed volume where punch head flats are in contact with the compression rolls of the press. Each material was compressed to nearly the same P_{max} using IPT type punches at a turret time of 1 s.

suggests that while the magnitude of the initial rate of compaction is governed by the material, the pattern of change in the rate of compaction is a machine characteristic.

The rate of compaction profiles of all materials show an initial acceleratory phase, a deceleratory phase and a phase of zero rate of compaction. The latter phase can be described as the dwell phase of the compression time during which the flat heads of the punches are in contact with the compression rolls and the distance between the punch faces is constant. According to geometric calculations, and at a turret speed of 1 revolution per second, the IPT punch head flats should have a dwell time of ≈6 ms. The duration of ≈7 ms of the constant strain phase agrees with this time.

The initial differences in the rate of compaction can be related to differences in the bulk density of the different materials. Those with smaller bulk density (e.g., Avicel PH102, ≈0.3 g/cm^3) have a much higher initial rate of compaction than materials with higher bulk density (e.g., Emcompress, ≈0.8 g/cm^3). This follows from the fact that the rate of compaction is another way of expressing the punch velocity. At the beginning of the compression phase, materials with a low bulk density offer less resistance to the punches, hence the initial punch velocity or the rate of compaction is much higher than when a material with a higher bulk density is compressed. The lowest initial rates of compaction occur when a prefabricated steel tablet, with a thin cushioning layer of Emcompress on its top, is compressed. Since the steel+Emcompress tablet is an almost non-porous body, the punches decelerate almost instantaneously, and the rates of compaction decrease very rapidly to a nearly negligible level.

For all materials the initial rate of compaction increases as the punches accelerate into the powder bed, which initially offers little resistance to the punch movement. As the powder bed begins to resist the punch movement more firmly, a few milliseconds into the compression time, this acceleratory phase ends and the rate of compaction decreases. The duration of the acceleratory phase appears to be characteristic of the material compressed (Fig. 19). Materials with highest initial rate of compaction, e.g. Avicel PH102, have the longest acceleratory phase. This again reflects the differences between the bulk densities of the various materials. A material with a low bulk density allows little initial resistance and takes longer to become sufficiently dense to decelerate the punch movement than a material with a higher bulk density (Fig. 19).

As mentioned in section 3.3.5, the rate of compaction during the compression phase can be used as an approximation of strain rate at the microscopic points of contact. Whether or not this approximation is valid during the initial acceleratory phase of the rate of compaction change is questionable. During this initial phase, when the particles undergo predominantly a rearrangement phenomenon and when they just begin to be deformed at their contacts, the strain at these contacts is small relative to the size of the individual particles. On these grounds, the strain rate is expected to be intrinsically low at the start of compression. The rate of compaction, on the other hand, is high because of the low powder bed density and due to the acceleration of the punches from their initial resting positions. The initial part of the compression phase is therefore a very dynamic stage of compaction, and it will be difficult to state clearly whether the strain rate at the particulate level is high, or, if in fact, it is low while the rate of compaction is high. This dilemma is

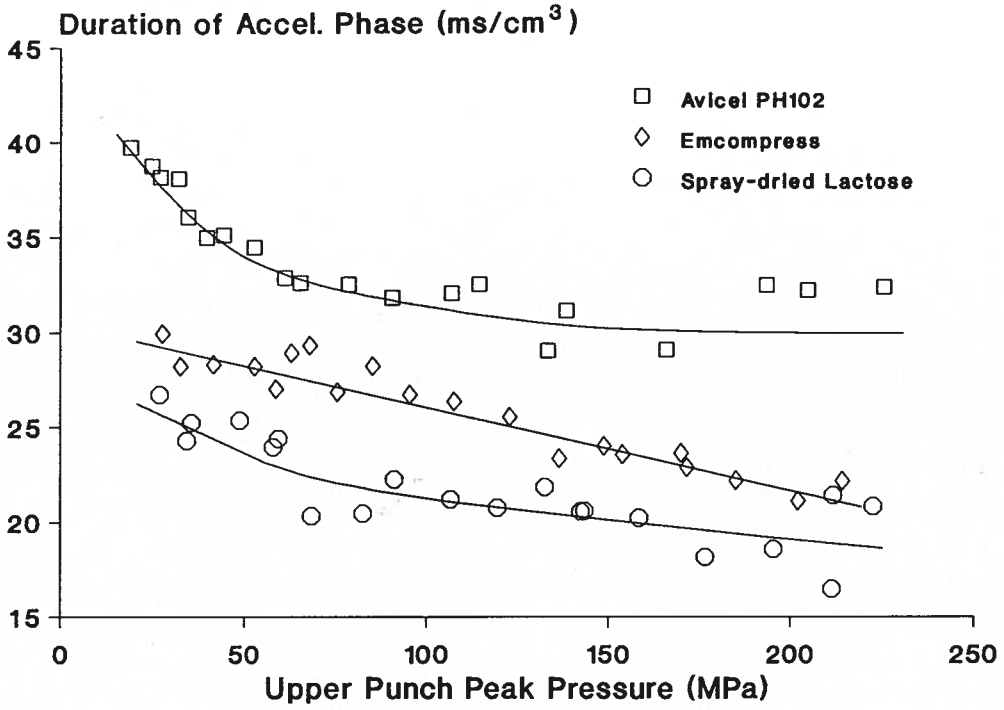

FIG. 19. Change in duration of the acceleratory phase of volumetric rate of compaction profiles with P_{max} for three direct compression excipients. The duration of the acceleratory phase has been normalised for true volume of the three materials at each P_{max}.

further emphasised by the rate of compaction profiles of the 'steel+Emcompress' tablets. Since a 'steel+Emcompress' tablet is an almost non-porous body, the rate of compaction is very low. But, due to the same non-porous nature, there must actually be a very high rate of elastic straining of this tablet at the start of the compression phase.

The above arguments indicate that it may not be correct to approximate the strain rate in a powder bed during the initial part of the compression phase by using the rate of compaction. The rate of compaction may be a valid approximation once the initial rearrangement dominated phase of compaction is over, and once the powder bed has entered into a deformation dominated phase. The latter phase would probably start at the end of the initial acceleratory phase of the rate of compaction change.

The profiles of rate of compaction with respect to time during the compression phase, when superimposed on the profiles of P (Fig. 20a-20d), are helpful in a mechanistic interpretation of events during the compression phase. The initial parts of the P versus t profiles in Fig. 20a-20d show an inflection point between approximately 7 and 14 MPa. This point occurs during the acceleratory phase of punch movement, and the rates of increase in P before and after this point are evidently different. The rate of increase in P for Avicel PH102 is higher before this point due to a sudden build up of σ_T mainly in response to friction at the points of interparticulate contact during the initial particle rearrangement phenomenon. The friction may cause a certain degree of bonding, and some deformation and, possibly even fracture, of the particles at their contacts. These phenomena would make the powder bed somewhat resistant to collapsing in the initial part of the compression phase. After a certain level of σ_T is built up, which will depend on a complex interplay of the

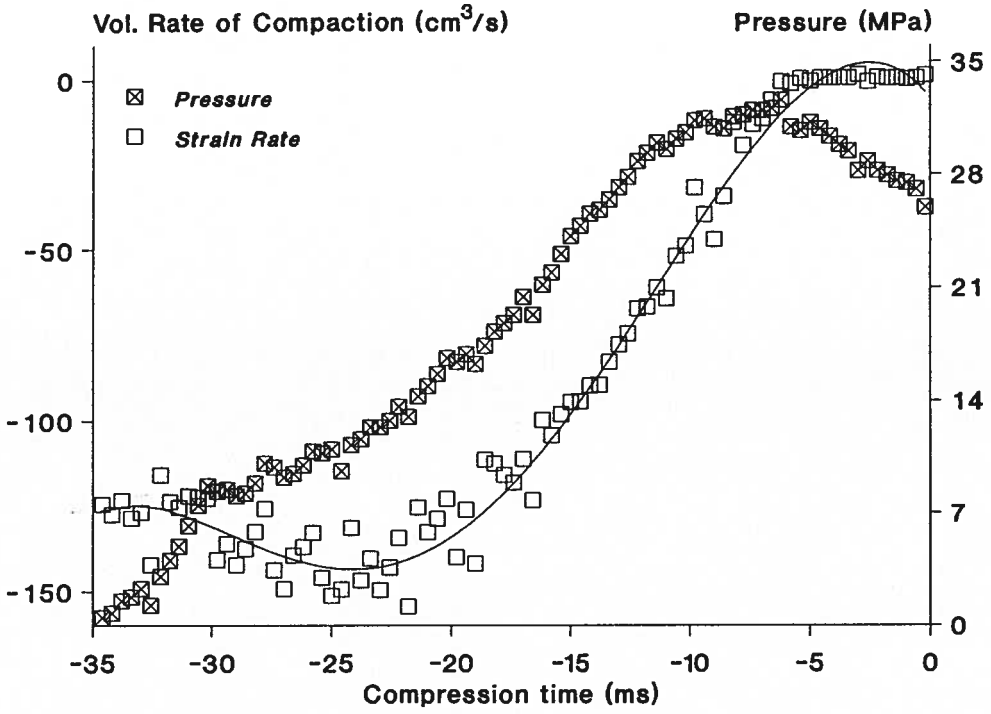

FIG. 20a. Volumetric rate of compaction profiles superimposed on the corresponding stress profiles during the compression phase for Avicel PH102. Turret time = 1 s, IPT punches.

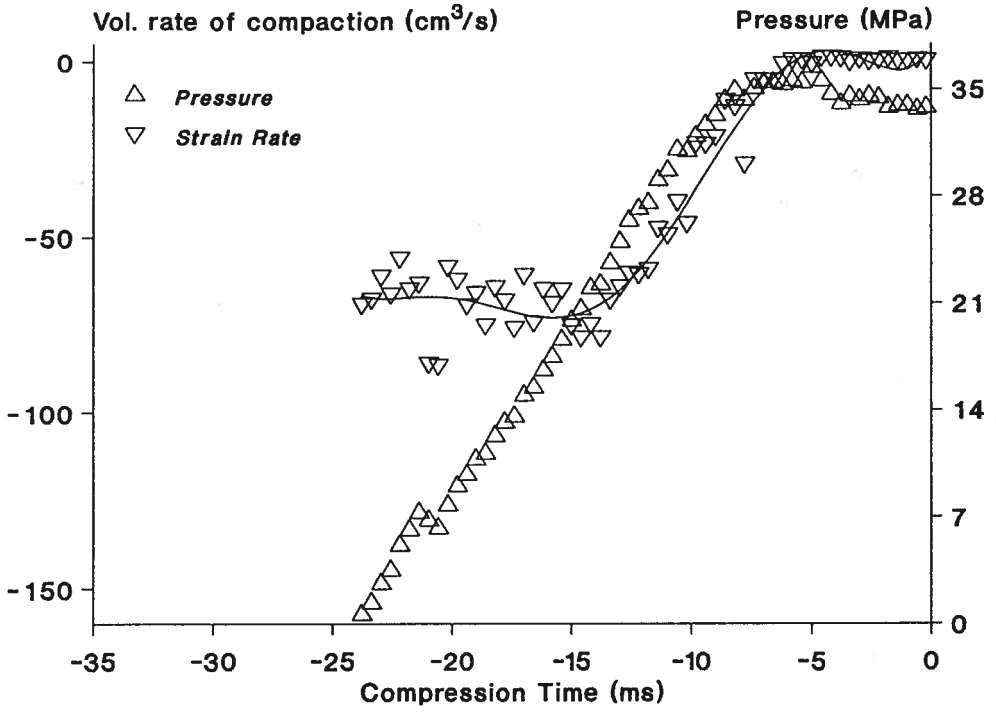

FIG. 20b. Volumetric rate of compaction profiles superimposed on the corresponding stress profiles during the compression phase for Fast-Flo Lactose. Turret time = 1 s, IPT punches.

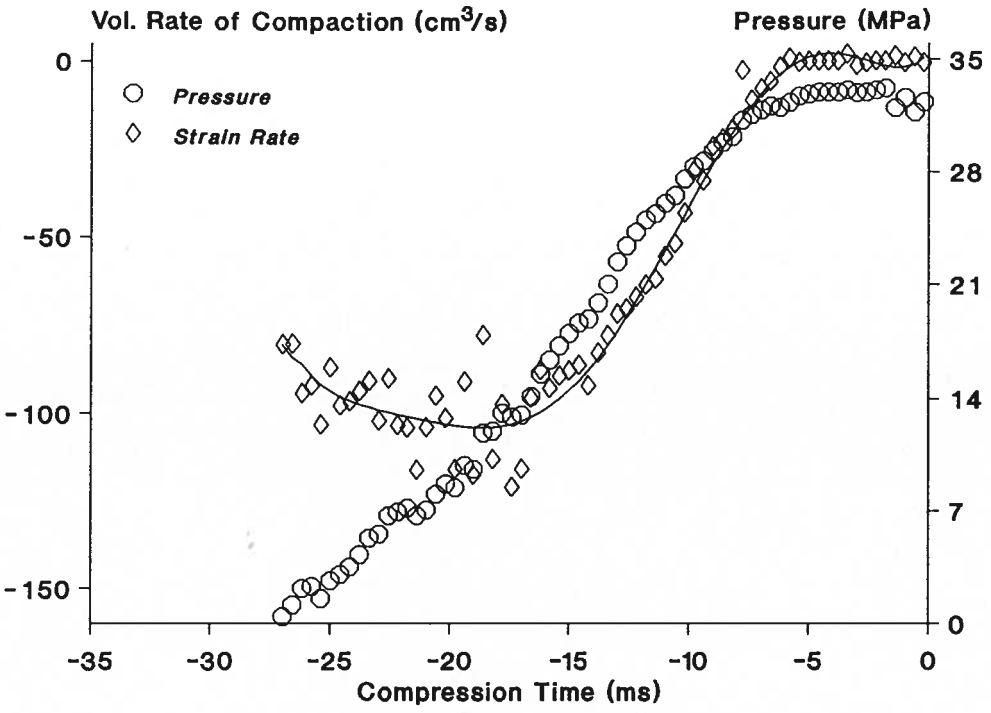

FIG. 20c. Volumetric rate of compaction profiles superimposed on the corresponding stress profiles during the compression phase for Emcompress. Turret time = 1 s, IPT punches.

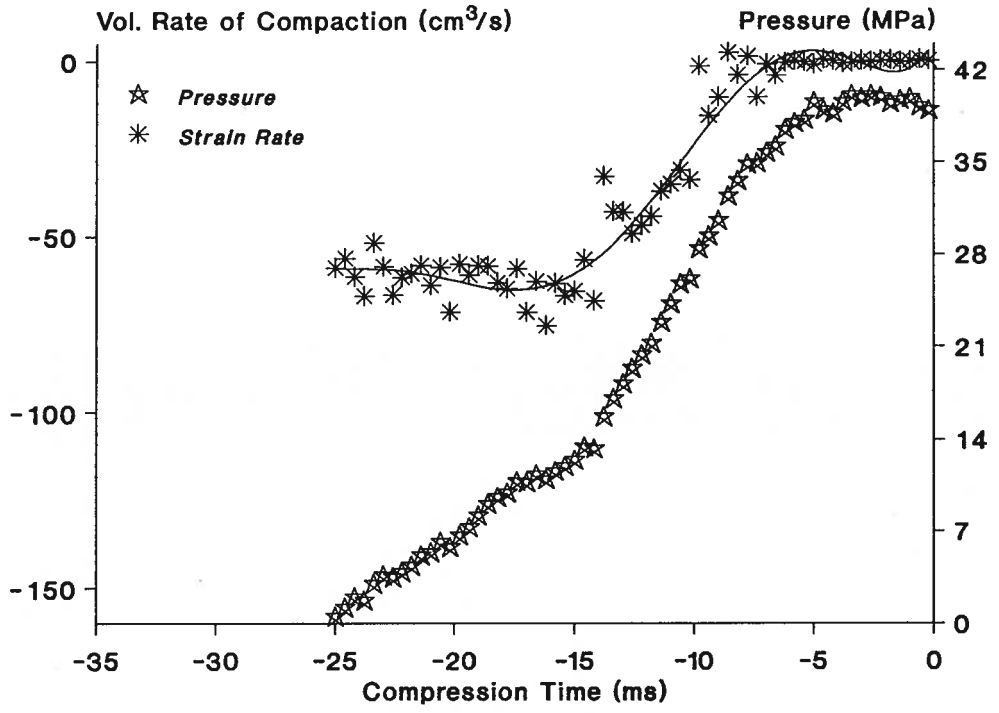

FIG. 20d. Volumetric rate of compaction profiles superimposed on the corresponding stress profiles during the compression phase for acetylsalicylic acid. Turret time = 1 s, IPT punches.

rearrangement and friction related phenomena, a failure of the initially resilient structure of the powder bed takes place. This appears as the inflection point, after which, the rates of compaction enter the deceleratory phase, and the increase in stress is more gradual because the particles continue to deform by flow during this phase.

Thus, the inflection point can be considered to be a transition point between a phase of rearrangement dominated compaction and a phase of particle deformation dominated compaction. Once the deformation dominated phase has begun, the punch pressure and the rate of compaction can be assumed to be estimates respectively of the stress and strain rate at the particulate level.

Fast-Flo Lactose has apparently a lower ability to flow than Avicel and therefore has a smaller difference between the rates of increase in stress before and after the inflection point (Fig. 20b). The P versus t profile of Emcompress (Fig. 20c) shows no change in the rates of increase in P before and after this point which indicates that Emcompress particles do not deform by a flow process during the deceleratory phase. Acetylsalicylic acid has the opposite pattern of increase in P (Fig. 20d) to Avicel. The rate of increase in P is slower before the inflection point, because acetylsalicylic acid is a very easily deformed substance and its particles fill up the voids at low pressures. As the inflection point is approached the powder bed becomes very dense (i.e., the porosity becomes very low), and the compact becomes resistant to the punch movement, hence P increases more rapidly.

3.4.3. Porosity-stress relationship

A material with a high propensity to fracture will have negligible deformational flow, thus maintaining a large porosity throughout the acceleratory, the deceleratory and the constant rate phases of the rate of compaction profile. On the other hand a material with a certain degree of flow becomes compacted to relatively lower porosity and reaches constant porosity only during the latter phase of the rate of compaction profile when the powder bed volume (or strain) is almost constant.

Even among those materials that show particle flow, one would expect a varying degree of change in compact porosity depending upon the actual type of flow. It should therefore be possible to ascertain the mechanism of deformation of the particles of various materials during compression with a reasonable degree of confidence by using some type of porosity-stress relationship. Several equations correlating the powder bed volume, and hence porosity, with applied stress are available (MacLeod, 1983). A commonly employed relationship of this type is given by the Heckel plots of $\ln(1/p)$ against overall stress during compression (Heckel, 1961). Based on changes in Heckel plots due to changes in particle size, Hersey and Rees (1971) classified solids into two categories: Type 1 materials, which deform mainly by plastic deformation, and Type 2 materials which deform mainly by fragmentation. These plots alone have been used to characterize the compaction mechanisms on a single punch press (Duberg and Nystrom, 1986). Yield values are estimated from the slope of the Heckel plots, but difficulties arise where the plots are not linear (Jones, 1978; Marshall, 1989). York (1979) reported differences in the estimated σ_y values when Heckel plots were constructed using different methods under different experimental conditions. An alternative method of obtaining σ_y was used in

this work. The values of $\ln(1/p)$ at P_{max} (H_{max}) were plotted against P_{max}. Values of σ_y were obtained from the slopes of these plots which, as shown in Fig. 21 for a representative selection of materials, are linear. The values of σ_y of various materials are listed in Table III. The different materials shown on this plot demonstrate the wide range of changes in porosity among the various pharmaceutical materials. Materials such as the calcium phosphates show little change in H_{max}, whereas drugs such as ibuprofen and acetylsalicylic acid show a much larger change over a similar range of P_{max}. The σ_y values listed in Table III reflect these differences and indicate the ease with which a given material is compacted to a given porosity. These σ_y values are useful in comparing the different materials on a relative scale, and in ascertaining the deformation mechanisms of these solids (section 3.8).

3.4.4. Position of the peak punch pressure: Peak offset time

If the powder bed were replaced by a nearly nonporous, and hence an almost incompressible substance, e.g. the steel tablet, the stress recorded via the strain gauges will correspond mainly to the machine deformation, and, to a very small extent, to the deformation of the steel tablet. Since the machine deformation is completely recoverable, the compression and decompression phases will be mirror images of each other, and the stress profiles will be symmetrical about the position of vertical alignment of the punches with the centres of the compression rolls. The peak punch pressure, P_{max}, for an incompressible solid will therefore occur at the dead centre position.

When a porous powder bed is compressed, the P_{max} does not necessarily coincide with this dead centre position. The position of P_{max} relative to

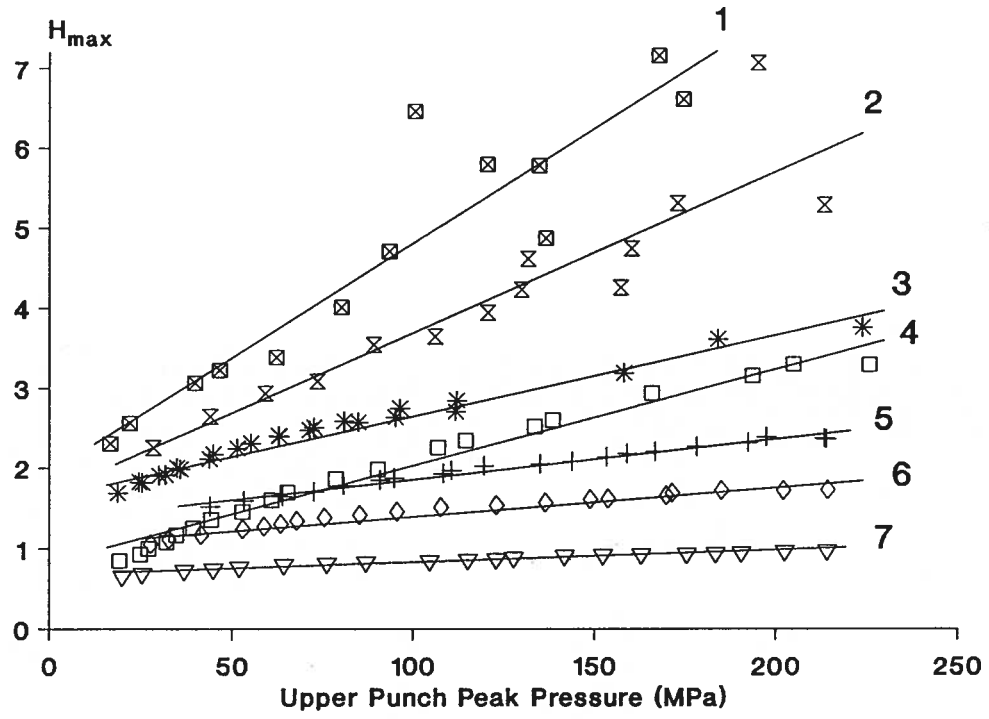

FIG. 21. Plots of the maximum value of Heckel term (H_{max}) at P_{max} during the compression phase against the corresponding P_{max} for different materials. Each data point corresponds to one tablet. Slopes obtained by linear regression of these plots give the yield strength (σ_y) of each material. (1) Acetylsalicylic acid, (2) S-Ibuprofen, (3) Acetaminophen Granular, (4) Avicel PH102, (5) α-Lactose monohydrate, (6) Emcompress, (7) Tri-Tab.

TABLE III. The σ_y values determined from Heckel Plots of the various solids.

Material	σ_y[1] (MPa)
A-Tab	165 (23)
Acetaminophen Fine Powder	40.3 (4.9)
Acetaminophen Granular	33.1 (3.6)
Acetaminophen Powder	39.3 (3.9)
Acetylsalicylic Acid	11.5 (4.1)
Anhydrous Emcompress	162 (23)
Anhydrous Lactose	58.7 (3.6
Asagran	13.8 (3.2)
Avicel Large	30.5 (3.3)
Avicel PH101	25.8 (1.9)
Avicel PH102	26.7 (2.8)
Avicel PH105	28.2 (3.0)
Caffeine	44.3 (4.6)
Cal-Star	89.3 (16)
Cellactose	43.7 (3.8)
Compap CG	36.3 (3.0)
Compap Coarse 73 L	36.0 (2.8)
Compap Coarse L	29.6 (2.0)
Compap L	38.3 (3.5)
DCI-63	12.5 (2.5)
Di-Pac	49.3 (2.5)
Di-Tab	92.3 (15)
Elcema G250	32.2 (1.7)
Emcocel	25.4 (1.6)
Emcompress	95.0 (16)
Emdex	34.7 (2.6)
Fast-Flo Lactose	49.0 (3.6)
Lactose DCL 21	55.0 (4.2)
Mannitol (Crystalline)	54.7 (3.8)
Mannitol M.G.	45.3 (4.2)
Neosorb (Sorbitol)	38.0 (3.2)
α-Lactose monohydrate	69.0 (5.1)
Potassium Chloride	20.0 (4.1)
Racemic ibuprofen	11.2 (3.2)
Rhodapap DC-P3	42.7 (3.0)
S-Ibuprofen	16.2 (5.9)
Sodium Chloride	35.3 (3.9)
Spray-dried Lactose	53.7 (4.9)
STA-Rx-1500	18.1 (1.6)
Sucrose (crystalline)	55.3 (16)
Sugartab	35.7 (3.2)
Tri-Tab	221 (35)
Xylitol (Crystalline)	52.0 (7.5)

1. Values (standard error): determined from the slope of H_{max} versus P_{max} plots.

the dead centre position will depend on the rate at which the material deforms in response to the rate of compaction under a given set of machine conditions which are defined by the punch type and machine speed. Hence, any change in the material which affects its ability to deform will be reflected in the position of P_{max}. Both too much or too little flow will bring the position of P_{max} closer to the dead centre position. This is because a material which readily flows becomes compacted to very low porosities earlier on in the compression phase and will behave almost as an incompressible solid when the P_{max} is reached, while a material which does not deform by flow will have no strain rate dependency. Both of these conditions will cause the P_{max} to occur relatively close to the dead centre position. For materials with a degree of flow somewhere in between these two extremes the P_{max} will precede the dead centre position of the punches.

Some representative pressure-time profiles for Avicel PH102, Spray-dried Lactose, and Emcompress are shown in Fig. 5 (page 43). All three materials show an offset of P_{max} with respect to the vertical alignment of the punches with the pressure rolls at $t = 0$. The interval between the position where P_{max} occurs and the position where the dead centre occurs is defined as the peak offset time, t_{off}. The duration of t_{off} is different for each material. The net punch displacement profile (Fig. 6, page 46) shows that the displacement and therefore the distance between the upper and lower punch faces is approximately constant during t_{off}. Assuming that the distance between punch faces, especially in the region where P_{max} occurs, is an indication of strain in the particles, and that the punch pressure is an indication of stress at the particles, it can be seen that the stress decreases during t_{off} while the strain remains essentially

constant. Hence t_{off} is indicative of stress relaxation since the stress is decaying at constant strain albeit for a very short time.

Factors that can affect the degree of deformational flow during tableting are likely to affect the magnitude of t_{off}. At least three such machine-related factors can be readily identified, namely, P_{max}, turret time and punch type. A fourth factor is the addition of one or more components which impart an increased degree of flow to the formulation. Each of these factors is discussed below.

3.4.4a. Effect of P_{max} on t_{off}

Figure 22 shows the changes in t_{off} for Avicel PH102, Spray-dried Lactose and Emcompress with changes in the P_{max} using IPT punches at a turret time of 1 s. Each of these excipients has excellent tableting properties, and the differences in t_{off} reflect differences in their deformation mechanisms. Table IV gives the range of t_{off} values for several solids when these solids were compressed over a range of P_{max}.

Avicel PH102 has the longest t_{off} with values up to about 8 ms at the lowest P_{max} studied, suggesting that stress relief during the compression phase is achieved by some type of flow into the voids of the tablet. Emcompress has much shorter t_{off} values than Avicel PH102 and Spray-dried Lactose, suggesting that it does not flow during compression. Spray-dried Lactose is manufactured from a suspension of lactose crystals and consists of aggregates of amorphous lactose with loose or embedded lactose crystals (Kussendrager *et al.*, 1981). Amorphous lactose deforms by flow while crystalline lactose undergoes particle fracture (Morita *et al.*, 1984; Vromans *et al.*, 1986). Thus, Spray-dried Lactose exhibits deformation

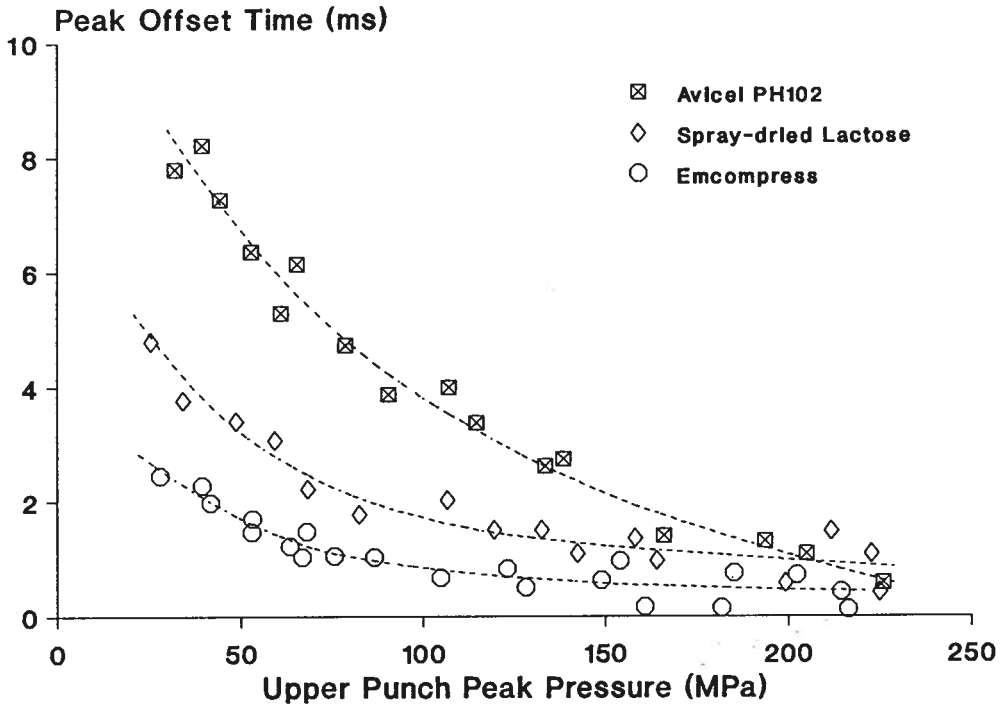

FIG. 22. Variation in peak offset times with peak pressure for three direct compression excipients. Turret time = 1s, IPT punches.

TABLE IV. Range of t_{off}, and $\Delta P/V_T$ values* corresponding to a range of P_{max}.

Material	P_{max} (MPa)	t_{off} (ms)	$\Delta P/V_{T_3}$ (MPa/cm^3)
A-Tab	28.3-214	3.2-0.9	6.0-1.1
Acetaminophen Fine Powder	26.9-213	3.1-0.4	3.6-0.23
Acetaminophen Granular	18.7-224	2.6-0	5.0-0
Acetaminophen Powder	17.8-220	3.5-0.6	2.7-2.1
Acetylsalicylic Acid	16.6-211	3.0-0.1	3.0-0.88
Anhydrous Emcompress	28.3-213	3.0-1.0	6.4-0.31
Anhydrous Lactose	33.5-215	3.0-1.5	6.8-0
Asagran	31.5-212	1.5-0	1.0-0
Avicel Large	20.9-225	7.2-0.4	12 -0.51
Avicel PH101	18.7-211	7.7-0.8	12 -0.52
Avicel PH102	18.9-226	8.2-0.6	20 -0.11
Avicel PH105	16.5-228	7.1-0.1	12 -0.47
Caffeine	17.8-203	7.1-0.7	8.5-0.46
Cal-Star	25.3-215	4.3-0.3	5.5-0
Cellactose	19.5-227	6.9-1.0	4.5-1.0
Compap CG	23.4-210	6.9-0.5	6.5-0.26
Compap Coarse 73 L	22.8-214	5.0-1.0	6.3-0.47
Compap Coarse L	26.9-211	3.7-0.7	4.3-0.27
Compap L	23.1-216	4.3-0.8	5.0-0.44
DCI-63	27.9-212	4.0-0.1	3.5-0
Di-Pac	39.1-222	5.0-1.3	9.6-1.8
Di-Tab	27.6-215	3.1-0.3	3.3-0.09
Elcema G250	29.4-212	6.4-0.9	10 - 0.79
Emcocel	37.8-215	6.4-1.2	12 - 1.1
Emcompress	27.6-214	6.4-0.4	8.0-0.21
Emdex	15.2-221	6.4-1.1	12 - 0.41
Fast-Flo Lactose	32.1-221	4.5-0.4	7.1-0
Lactose DCL 21	26.9-210	4.5-0.8	7.2-0
Mannitol (Crystalline)	39.3-218	4.5-1.5	9.9-2.6
Mannitol M.G.	24.5-218	6.0-0.8	8.1-0.71
Neosorb (Sorbitol)	32.8-223	6.0-1.2	17 -1.7
α-Lactose monohydrate	43.9-214	3.4-1.3	6.9-1.4
Potassium Chloride	38.5-208	3.4-0.2	6.2-0
Racemic Ibuprofen	29.2-224	2.0-0	3.5-0
Rhodapap DC-P3	32.1-219	3.0-0.9	5.2-0.12
S-Ibuprofen	28.3-214	3.0-0.0	1.4-0
Sodium Chloride	39.7-215	3.0-0.6	5.4-0.37
Spray-dried lactose	26.8-223	3.0-1.1	8.2-1.4
STA-Rx-1500	38.8-221	4.8-0.3	11 -0.12
Sucrose (Crystalline)	27.7-219	4.8-1.3	5.2-0.68
Sugartab	25.8-211	6.5-1.2	11 -1.8
Tri-Tab	19.9-214	4.4-0.8	6.2-0.61
Xylitol (Crystalline)	18.8-220	5.9-0.3	7.8-0.1

* IPT Punches; turret time 1s

characteristics that are intermediate between those of Avicel PH102 and Emcompress, with t_{off} of up to about 5 ms at the lowest P_{max} studied.

The ability of particles to relieve stress within the confines of a die cavity will become increasingly restricted as the porosity of a powder bed decreases with increase in the punch pressure. This is illustrated by the results in Fig. 22 which, for each material, show that the duration of t_{off} decreases asymptotically towards a lower limit as P_{max} is increased.

The P_{max} on a rotary tablet press can be increased either by increasing the mass of the material in the die at a fixed thickness setting on the press (Method I, page 41), or by changing the thickness setting to reduce tablet thickness keeping the mass constant (Method II, page 41). Figure 23 shows that the duration of t_{off} is independent of the method of increasing P_{max}. It was easier to change the mass of the material in the die at a fixed thickness setting, and this procedure for changing P_{max} was used in all further experiments.

3.4.4b. Effect of machine speed on t_{off}

The t_{off} for Avicel PH102 at different turret times are shown in Fig. 24a. Decreasing the turret time reduces t_{off} showing that at faster machine speeds, i.e., at faster rates of compaction or faster strain rates, Avicel PH102 has less time to relieve stress by deforming by flow than at slower speeds. Situations can sometimes occur where a formulation produces good tablets on slow machines but fails when transferred to higher speed machines. One reason may be a decrease in the extent of deformation of the material by flow as indicated by a decrease in t_{off} at faster machine speeds. For Emcompress, t_{off} is independent of turret time (Fig. 24b) indicating that the rate of stress relief for Emcompress does not depend on

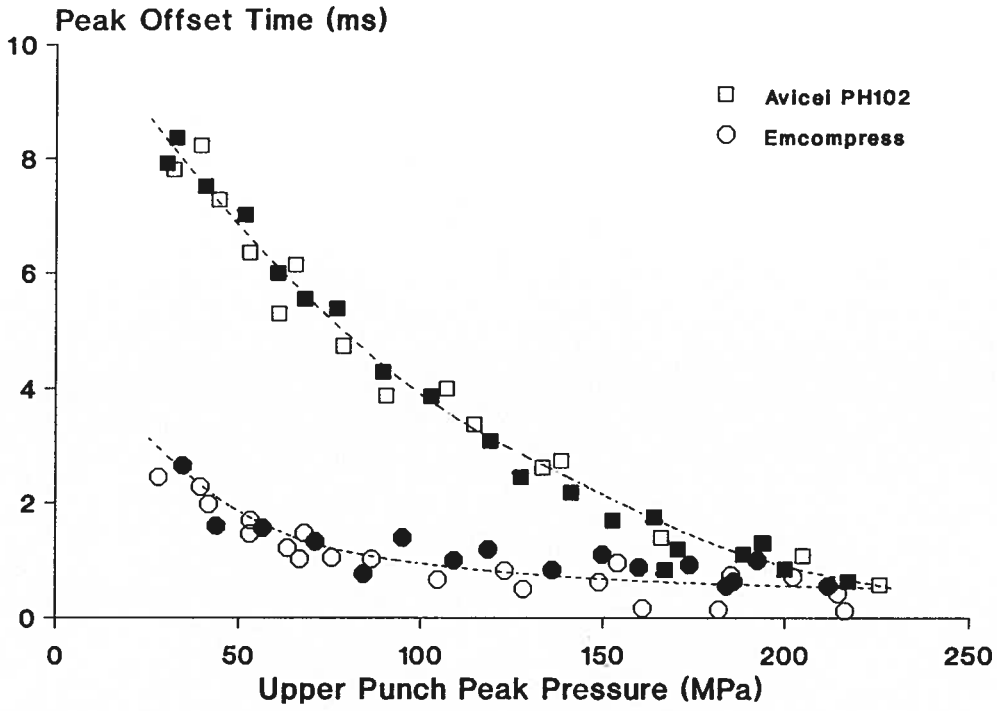

FIG. 23. Variation in peak offset time with peak pressure. Turret time = 1s, IPT punches. Open symbols, peak pressure varied by changing the mass at fixed thickness setting; closed symbols, peak pressure varied by changing the thickness setting keeping the mass constant.

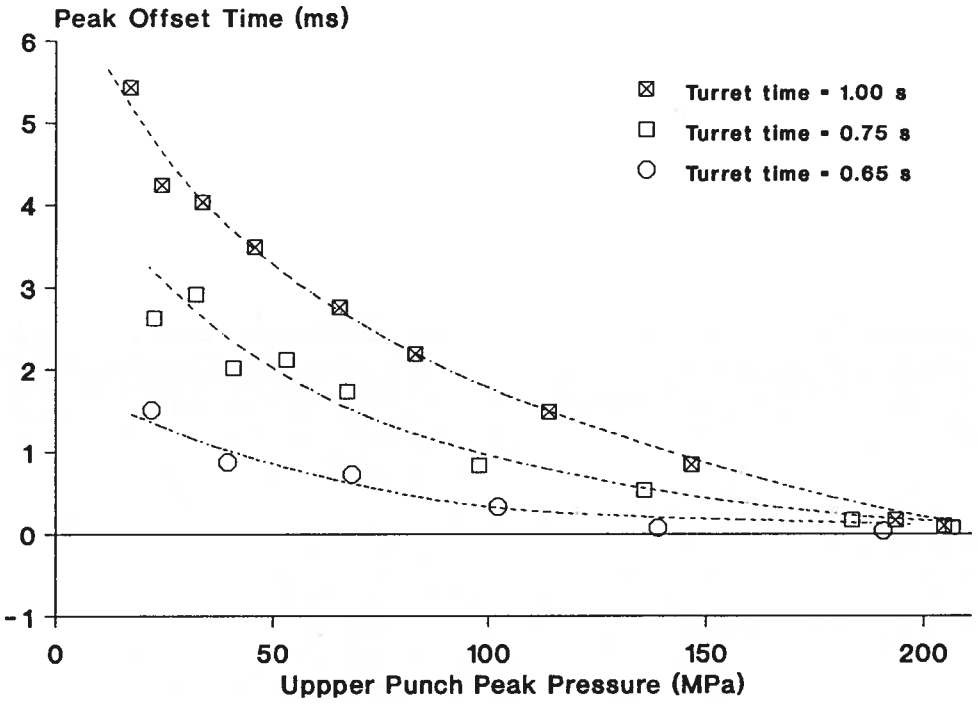

FIG. 24a. Effect of turret time on peak offset times for Avicel PH102. Manesty punches.

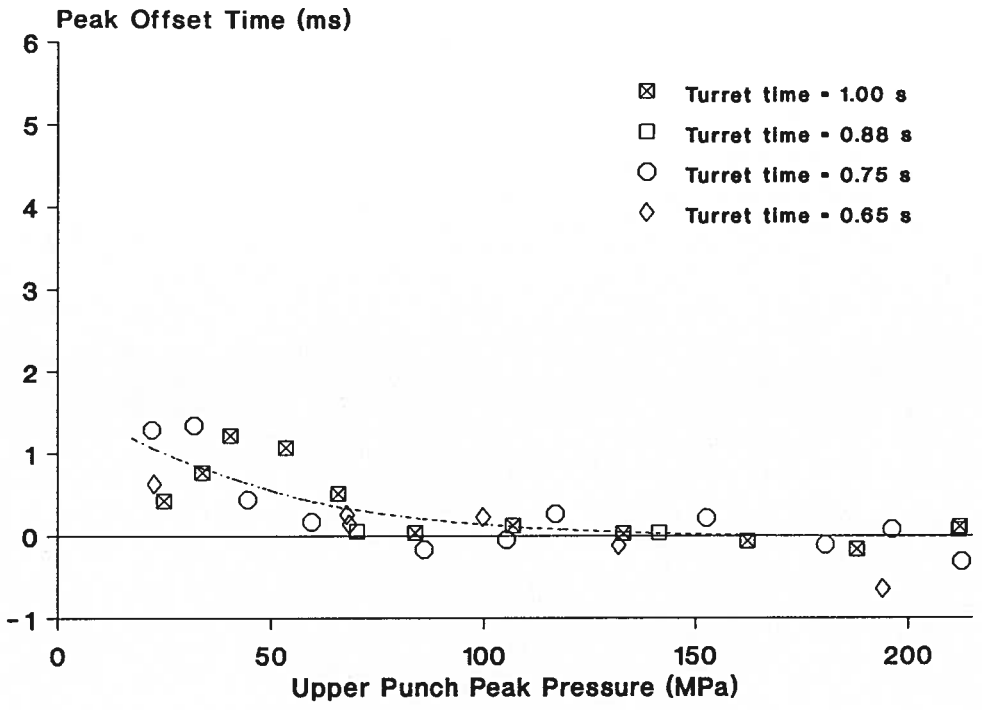

FIG. 24b. Effect of turret time on peak offset times for Emcompress. Manesty punches.

the rate of at which it is compressed. In other words, Emcompress probably has a deformation mechanism which is independent of the rate of compaction.

3.4.4c. Effect of punch type on t_{off}

The IPT punches have a flatter punch head profile than the Manesty punches (Fig. 1, page 28) thereby providing a longer dwell time for stress relaxation. Figure 25 shows the t_{off} for Avicel PH102 and Emcompress when compressed using the two punch types. At P_{max} below 110 MPa, the t_{off} for Avicel PH102 becomes progressively longer when compressed using IPT punches than with Manesty punches. For Emcompress, differences in t_{off} due to punch type were not significant. These observations suggest that the tableting behaviour of materials deforming by a strain rate dependent process is more likely to be affected than that of materials with non-strain rate dependent deformation when the tooling is changed from IPT to Manesty type. Above about 110 MPa, equivalent to about 1.5 tons, there is little difference in t_{off} for Avicel PH102 between the two punch types suggesting that differences in dwell time are less significant than the decrease in porosity above this pressure.

3.4.4d. Effect of formulation variables on t_{off}

Drugs such as acetaminophen and ibuprofen which cap or laminate during or after decompression are modified commercially by formulating them with polymeric substances which, at a given temperature, are more likely deform by flow under stress than crystalline materials. An examination of Rhodapap DC-P3 (97% acetaminophen + 3% polyvinylpyrrolidone, PVP) under a scanning electron microscope indicated that it is made by spray drying a slurry of acetaminophen crystals in a solution of the polymer. Compap CG

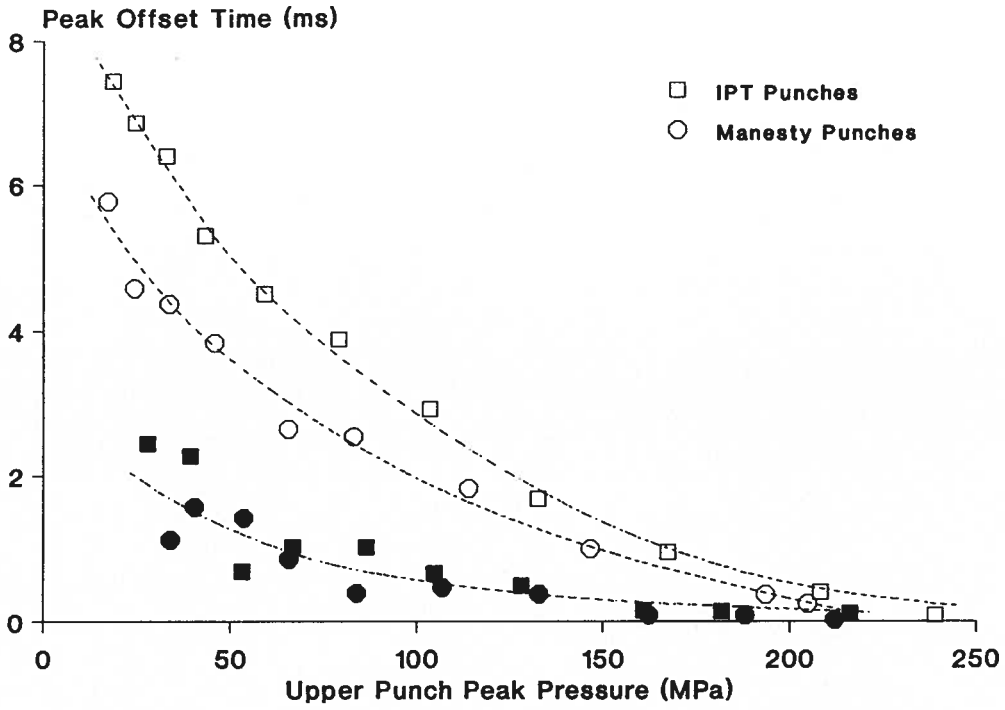

FIG. 25. Effect of punch type on peak offset times. Turret time = 1s. Open symbols, Avicel PH102; closed symbols, Emcompress.

(90% acetaminophen + 10% excipients) appears to be made by a similar process.

Figure 26a shows the relationship between t_{off} and P_{max} for three samples of crystalline acetaminophen. The t_{off} values for the three samples are highly variable and are indistinguishable from one another despite major differences in their particle size distributions. The short t_{off} values indicate that crystalline acetaminophen undergoes only a small amount of deformational flow during compression.

It is evident from Fig. 26b that the addition of a small amount of PVP as in Rhodapap DC-P3 increases flow sufficiently to prolong t_{off} by about 2 ms for P_{max} up to about 90 MPa. Rhodapap DC-P3 forms strong tablets below this pressure but shows lamination at higher pressures where its t_{off} approaches that of crystalline acetaminophen. Compap CG contains a greater amount of excipients and forms intact tablets up to P_{max} of about 210 MPa. These excipients presumably deform by flow, and t_{off} is increased. The tablet strengths of Compap CG are comparable to those of the tablets of Rhodapap DC-P3 (Fig. 27).

Similar results were obtained for ibuprofen (Fig. 28). The directly compressible ibuprofen, DCI-63, has longer t_{off} relative to crystalline ibuprofen at P_{max} up to about 90 MPa. There are no differences in t_{off} above this pressure. Like the direct compression forms of acetaminophen, DCI-63 forms tablets only below about 90 MPa, whereas above this pressure lamination occurs. Crystalline ibuprofen, on the other hand, does not form tablets at any pressure.

The increase in t_{off} for the direct compression formulations of acetaminophen and ibuprofen suggests that these formulations permit a degree of deformation by flow which leads to interparticulate bonding.

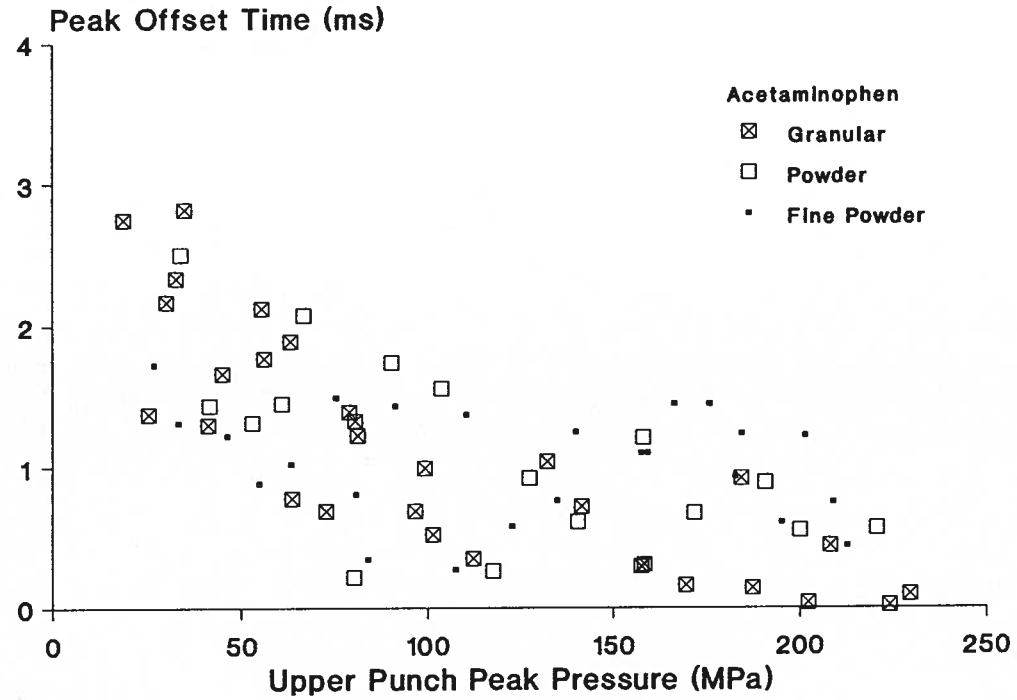

FIG. 26a. Variation in peak offset times with peak pressure for various particle sizes of acetaminophen. Turret time = 1s, IPT punches.

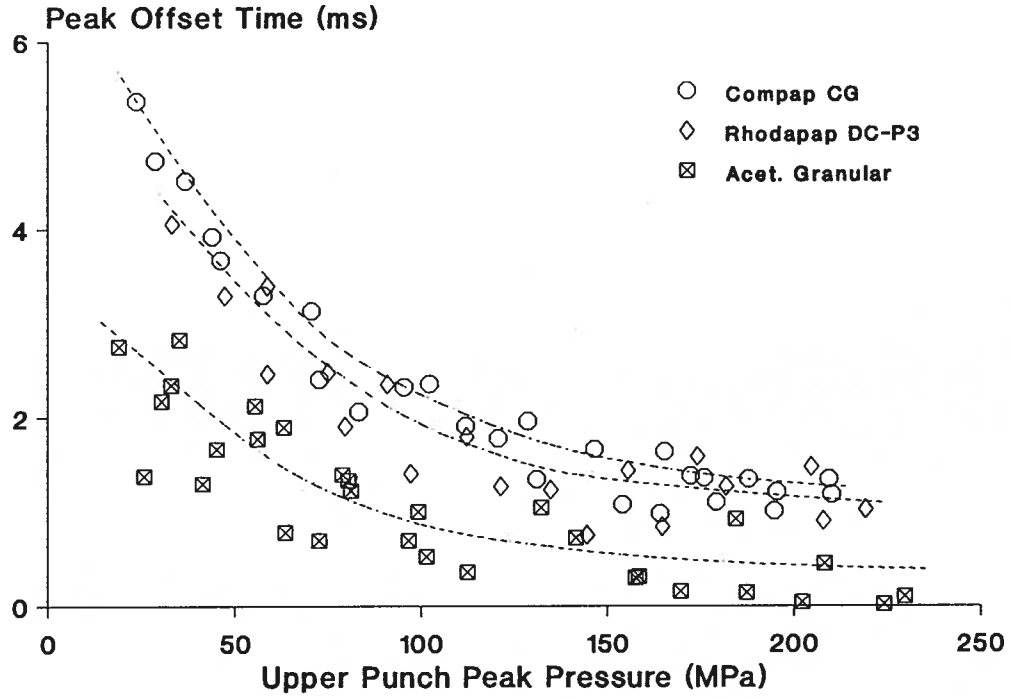

FIG. 26b. Variation in peak offset times with peak pressure for acetaminophen and its selected formulations. Turret time = 1s, IPT punches.

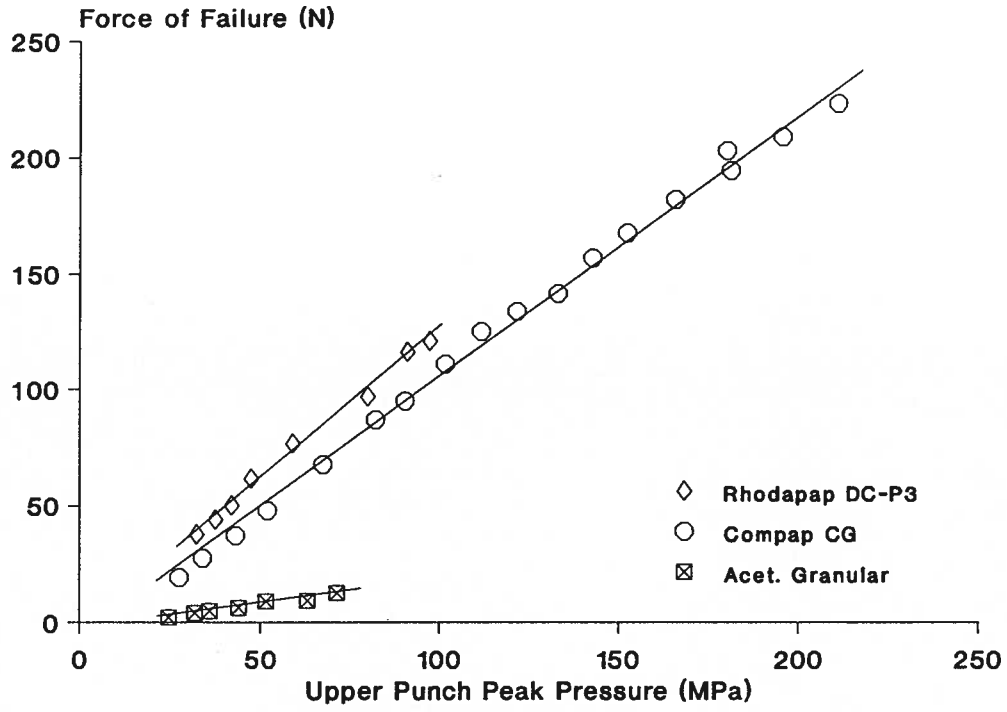

FIG. 27. Variation in force of failure with peak pressure for crystalline and direct compression forms of acetaminophen. Turret time = 1s, IPT punches.

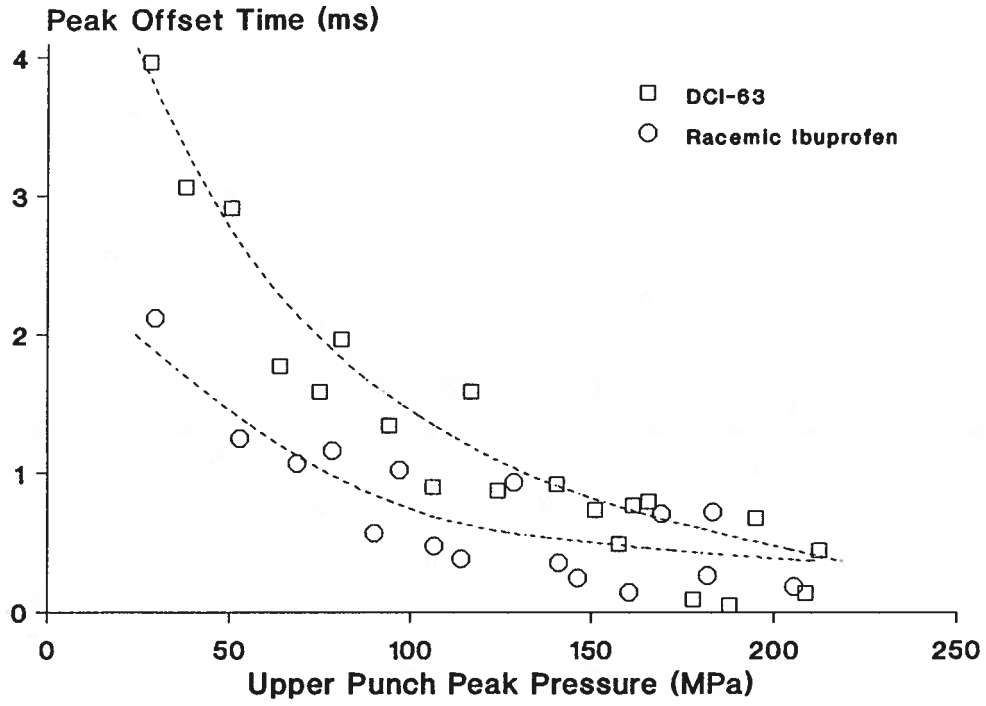

FIG. 28. Comparison of peak offset times for crystalline ibuprofen and a direct compression formulation. Turret time = 1s, IPT punches.

Thus, it appears that the strength of tablets is, at least in part, dependent on the degree of deformational flow under pressure.

3.4.5. Decrease in punch pressure during the phase of constant strain

When the rate of compaction achieves a minimum value towards the end of the compression phase, then the powder bed is under a state of almost constant strain. Since the rate of compaction is close to zero, the flow stresses achieve a minimum value and σ_T will be readily relieved by particle flow into the pores, if any pores still exist at this stage. This is when t_{off} also occurs and, as mentioned earlier, any pressure drop (ΔP) during t_{off} due to the relief of σ_T comprises the phenomenon of stress relaxation at constant strain. The values of ΔP normalized for true volume ($\Delta P/V_T$) for some materials when compressed over a range of P_{max} are given in Fig. 29. The differences in the slopes of these plots indicate the different rate of stress relief for each material, and, also, to a certain extent, suggest the mechanism of deformation. A material showing a small change in $\Delta P/V_T$ over the range of P_{max} used (e.g. Emcompress) has a mechanism of deformation with little strain-rate dependency (i.e., fracture or plastic flow). On the other hand, a material with large change in $\Delta P/V_T$ over a similar pressure range (e.g. Avicel PH102) has a mechanism of deformation which is strain-rate dependent (i.e., viscous or viscoplastic flow).

The range of $\Delta P/V_T$ corresponding to the range of P_{max} for the solids compressed on the Betapress is given in Table IV. The $\Delta P/V_T$ is a measure of the ability of various materials to deform by a viscous/viscoplastic flow mechanism. It appears therefore that t_{off} and $\Delta P/V_T$ can be used to ascertain the deformation mechanisms during compression. These parameters

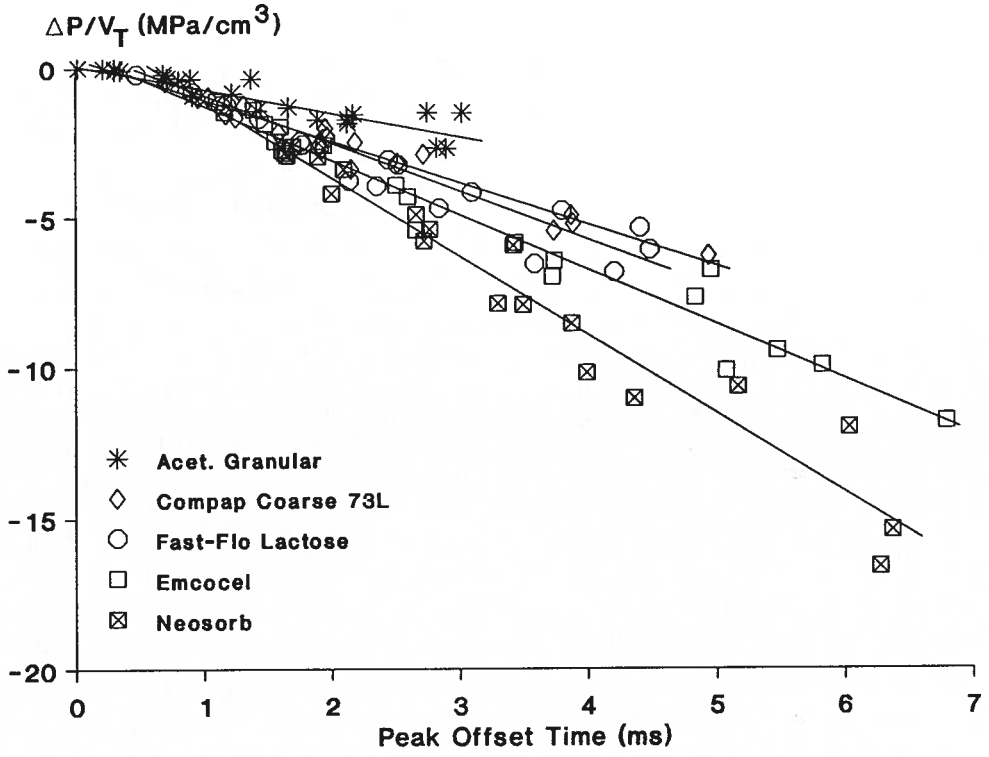

FIG. 29. Decrease in punch stress during t_{off} normalised for true volume ($\Delta P/V_T$) of different materials as a function of t_{off}. The difference in the slopes of these plots indicate a difference in the rate of stress relief during t_{off} of the different materials.

were used in conjunction with other parameters from the compression and decompression phases to analyse the deformation behaviour of various solids during compaction on the Betapress (section 3.8).

3.4.6. Work of compression

A large amount of energy is imparted to the powder bed by the press during the compression phase. This energy can be expressed as the work of compression, W_C. The range of values of W_C corresponding to a range of P_{max} during the compression phase is given in Table V. These values are corrected for the work of machine deformation as described by Oates and Mitchell (1990) and are normalised for tablet mass to account for differences in the tablet masses between the different materials. The work of compression is a useful parameter in analysing the energetics of particle rearrangement and deformation during compaction. Along with the work of decompression (section 3.5.1), it can be used in understanding the particle deformation behaviour during powder compaction (section 3.6).

3.5. PARAMETERS FROM THE DECOMPRESSION PHASE

The decompression phase begins at the end of the constant rate of compaction part of the compression phase when the punches are at the dead centre position. For all powders, the punch pressure decreases more rapidly during decompression than the rate at which it increases during compression. This suggests that only a part of the energy expended during compression is recovered during decompression. The recovered energy corresponds to the recovery of the machine and also to the recovery (axial expansion) of the compact formed during compression. The pressure-time

TABLE V. Range of W_C and W_D values* corresponding to a range of P_{max}.

Material	P_{max} (MPa)	W_C (J/g)	W_D (J/g)
A-Tab	28.3-214	3.80-22.2	0.11-2.4
Acetaminophen Fine Powder	26.9-213	2.60-19.4	0.09-2.5
Acetaminophen Granular	18.7-224	1.50-14.4	0.10-2.1
Acetaminophen Powder	17.8-220	1.20-17.1	0.12-2.2
Acetylsalicylic Acid	16.6-211	1.80-8.00	0.06-2.2
Anhydrous Emcompress	28.3-213	3.90-22.2	0.09-2.4
Anhydrous Lactose	33.5-215	3.10-23.0	0.10-2.9
Asagran	31.5-212	3.50-12.5	0.16-4.2
Avicel Large	20.9-225	9.40-44.8	0.19-4.5
Avicel PH101	18.7-211	7.70-40.8	0.12-3.7
Avicel PH102	18.9-226	3.30-30.9	0.07-3.4
Avicel PH105	16.5-228	5.60-36.8	0.12-4.8
Caffeine	17.8-203	2.10-21.1	0.15-1.5
Cal-Star	25.3-215	3.37-15.7	0.05-2.8
Cellactose	19.5-227	5.80-36.0	0.10-4.4
Compap CG	23.4-210	6.00-31.5	0.11-2.6
Compap Coarse 73 L	22.8-214	3.70-25.4	0.08-2.9
Compap Coarse L	26.9-211	5.20-26.1	0.12-3.2
Compap L	23.1-216	6.60-31.9	0.12-3.4
DCI-63	27.9-212	5.90-19.6	0.11-3.0
Di-Pac	39.1-222	5.80-23.5	0.08-2.8
Di-Tab	27.6-215	3.30-15.2	0.04-2.1
Elcema G250	29.4-212	5.40-26.6	0.15-2.8
Emcocel	37.8-215	14.3- 41.6	0.32-3.1
Emcompress	27.6-214	3.40-15.0	0.08-1.5
Emdex	15.2-221	2.20-29.3	0.06-2.0
Fast-Flo Lactose	32.1-221	5.30-27.0	0.18-3.9
Lactose DCL 21	26.9-210	1.90-21.3	0.09-3.0
Mannitol (Crystalline)	39.3-218	5.70-25.8	0.14-2.0
Mannitol M.G.	24.5-218	3.44-21.2	0.08-4.7
Neosorb (Sorbitol)	32.8-223	5.88-25.5	0.16-3.6
α-Lactose monohydrate	43.9-214	3.70-18.4	0.15-2.2
Potassium Chloride	38.5-208	5.20-15.5	0.07-0.9
Racemic Ibuprofen	29.2-224	4.70-15.8	0.11-3.3
Rhodapap DC-P3	32.1-219	7.70-31.3	0.15-4.0
S-Ibuprofen	28.3-214	2.80-11.5	0.06-3.7
Sodium Chloride	39.7-215	3.40-15.4	0.05-1.3
Spray-dried lactose	26.8-223	4.10-23.2	0.07-2.6
STA-Rx-1500	38.8-221	3.80-24.6	0.28-3.4
Sucrose (Crystalline)	27.7-219	3.30-16.9	0.09-1.7
Sugartab	25.8-211	3.40-18.7	0.04-1.4
Tri-Tab	19.9-214	1.70-15.4	0.07-3.0
Xylitol (Crystalline)	18.8-220	2.07-14.6	0.22-3.6

* IPT Punches; turret time 1s

curve for a given material during the decompression therefore corresponds to the recovery of the machine plus the compact expansion. To isolate the compact expansion from the total recovery during decompression, it is necessary to subtract the machine recovery from the total recovery. Using this idea, the tablet expansion, work of decompression, and the Young's modulus were determined from the decompression phase (section 2.6).

3.5.1. Elastic expansion and work of decompression (W_D)

Figure 11 (page 57) shows F-ΔD_m plots for a number of pharmaceutical materials. The linearity of these plots for all materials tested is strong evidence in support of the hypothesis that in-die tablet expansion during decompression is elastic. During decompression, force is registered only for as long as the expanding tablet is in contact with the receding upper punch face. Since tablet expansion may continue both during and after ejection from the die (Aulton *et al.*, 1973; York and Baily, 1977), $\Delta D_{mF=0}$ obtained from Fig. 11 may not represent the total tablet expansion.

Representative ΔD_m-fr plots shown in Fig. 10 give a direct indication of tablet expansion during decompression. Such plots are useful for showing differences in the expansion of various materials, or formulations, after compression to the same peak force. Microcrystalline celluloses showed the greatest expansion during the decompression phase of the compaction cycle, while brittle substances such as Emcompress and sucrose showed the least. A similar rank order was found in plots of W_D as a function of peak force, in which the greatest amount of work during decompression is done by the microcrystalline celluloses (e.g., Avicel PH102, Fig. 30). The range of W_D values corresponding to a range of P_{max} are given in Table V for the various materials compressed on the Betapress.

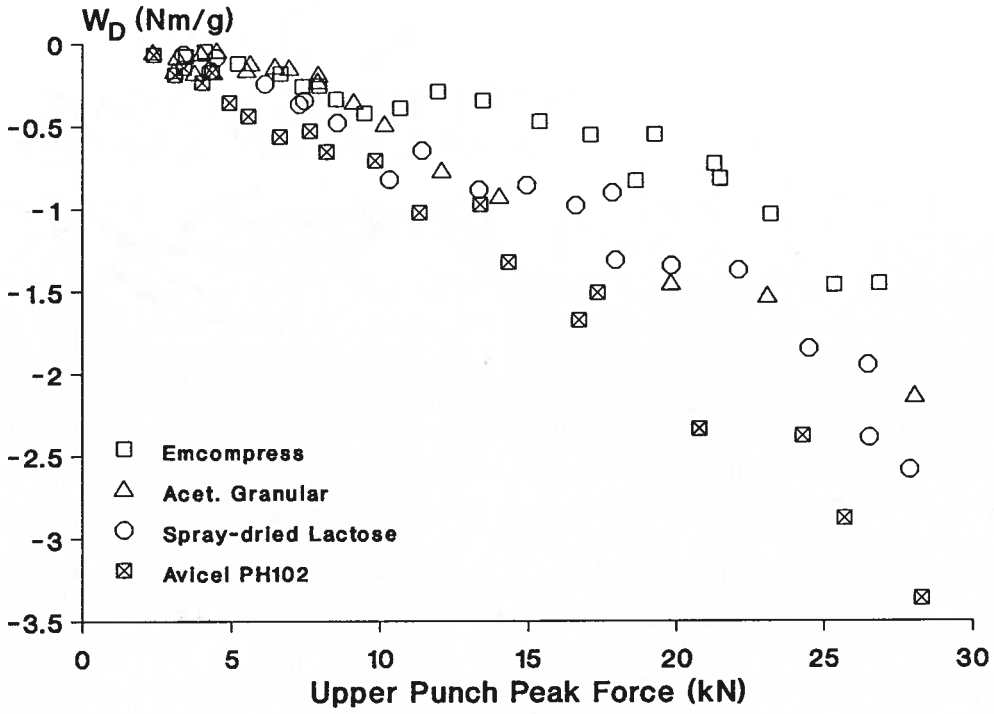

FIG. 30. Change in work of decompression with upper punch peak force. Each data point is obtained from the decompression analysis of a single tablet.

3.5.2. Determination of Young's Modulus

The modulus of elasticity of a tablet with a certain porosity was determined from the stress-strain plots during decompression. The stress and strain used on such plots were determined using the punch pressure and the change in the compact height respectively, and are therefore only approximations of the stress and strain at the particulate level. This approximation is however quite reliable since the compact during decompression, unlike the powder bed during compression, is a well defined object and changes in its dimensions during decompression are very small.

With increasing peak force, tablet porosity, p, decreases and as it approaches 0, the modulus of elasticity of compacts, E_p, will approach the Young's modulus, E, of the fully dense material. Some representative plots of E_p against p are shown in Fig. 31. Extrapolation of these plots to p = 0 provides an estimate of E.

For low p values, E can be estimated from the least squares solution of the following linear equation (Wachtman, 1969):

$$E_p = E + b \cdot p \qquad (12)$$

Estimates of E are commonly obtained by least squares solutions of equation 13 which is based on an exponential relationship between E_p and p (Spriggs, 1961):

$$\ln E_p = \ln E + b \cdot p \qquad (13)$$

The application of least squares solutions to nontransformed data requires the values of E_p corresponding to each p value to be normally distributed and randomly selected from such distributions. In addition,

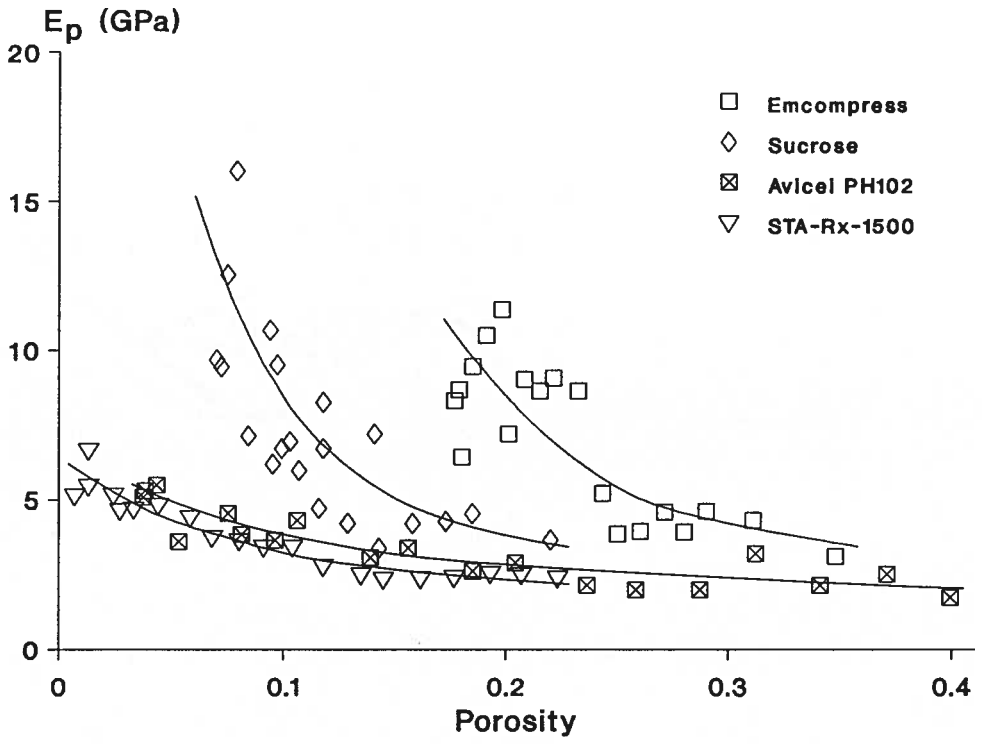

FIG. 31. Variation in modulus of elasticity of tablets with tablet porosity. Extrapolation to zero porosity gives the Young's modulus.

the distributions of E_p at each p value must have equal variances, i.e. the variances must be homoscedastic. While the least squares analysis is quite robust with respect to deviations from the requirements of normality and randomness, the variances must meet the requirement of homoscedasticity (Zar, 1984). The latter requirement can be tested by plotting the residuals of a linear least squares model, e.g. equation 12, against p (Draper and Smith, 1966; Zar, 1984). A plot showing nearly the same value of residuals at all p values indicates homoscedasticity, and a simple linear relationship can be used. If the value of residuals increases with increasing values of p, the variances are heteroscedastic such that a logarithmic transformation in the form of equation 13 can be applied to make them homoscedastic (Carroll and Ruppert, 1988). Residual plots for all materials tested in the present study were curved implying a curvilinear relationship between E_p and p. Linear regression on nontransformed or log-transformed data was therefore invalid. Since neither equation 12 nor 13 could be used, the E_p versus p plots were curve-fitted using polynomial regression. The degree of polynomial was selected on the basis of a t-test at a critical probability level of 0.05. For most materials a quadratic expression yielded a satisfactory fit.

The values of slope, b, obtained from linear regression are "measures of the rate of change in the modulus relative to the change in porosity" and were related by Spriggs (1961) to the "proportions of closed and open pores, or the proportions of continuous solid-phase structure and continuous pore-phase structure". The need for polynomial regression in our work suggests that factors other than those mentioned by Spriggs (1961), are responsible for changes in E_p with p. These factors may

include the effect of increasing load leading to differences in the preferred orientation of certain crystal faces during consolidation.

For easily deformed substances such as Avicel PH102 and STA-Rx-1500, the extrapolation to zero porosity using polynomial regression is short producing reliable E values. Compacts made from substances such as Emcompress and sucrose were much more porous than compacts made from Avicel PH102 and STA-Rx-1500, even after compression at high pressures, and showed a sharp inflection in E_p values. Therefore, the extrapolated estimates of E are less reliable. Nevertheless, Table VI shows that the E values obtained from the Betapress are, in most cases, reasonably close to the range of published values given in Table VII. This is encouraging for the following reasons:

a. All tablets contained 0.5 percent magnesium stearate as lubricant and are not therefore a single component. Measurements of E_p using nonlubricated materials in a die previously lubricated with a 5 percent solution of stearic acid in chloroform showed increased scatter.

b. Compressive and flexure tests are made on preformed, unconfined compacts. In contrast, the tableting process can be likened to the formation of a spring (or rather an assembly of springs with an associated viscous component) where the spring is formed during compaction and confined within the die cavity during the decompression analysis of elastic recovery.

c. An elastic modulus implies that an equilibrium exists. Compressive and flexure tests are normally performed at low rates of deformation of pre-equilibrated compacts whereas on the Betapress, the modulus is determined under high rate of expansion on a non-equilibrated tablet.

TABLE VI. E values of determined from the decompression analysis.

Material	E* (GPa)
A-Tab	8.1 (2.4)
Acetaminophen Fine Powder	11 (1.9)
Acetaminophen Granular	9.7 (2.7)
Acetaminophen Powder	10 (3.4)
Acetylsalicylic Acid	7.2 (1.9)
Anhydrous Emcompress	10 (1.4)
Anhydrous Lactose	8.1 (3.0)
Asagran	4.6 (1.2)
Avicel Large	4.1 (0.7)
Avicel PH101	4.5 (0.5)
Avicel PH102	5.8 (1.1)
Avicel PH105	4.4 (0.5)
Caffeine	15 (7.2)
Cal-Star	9.0 (2.2)
Cellactose	4.6 (0.5)
Compap CG	8.5 (1.3)
Compap Coarse 73 L	7.5 (0.9)
Compap Coarse L	7.2 (1.5)
Compap L	8.0 (1.3)
DCI-63	6.0 (1.7)
Di-Pac	8.2 (1.8)
Di-Tab	8.1 (1.5)
Elcema G250	7.4 (0.4)
Emcocel	6.1 (1.0)
Emcompress	27 (5.4)
Emdex	9.7 (3.7)
Fast-Flo Lactose	6.0 (0.7)
Lactose DCL 21	8.5 (1.1)
Mannitol (Crystalline)	25 (4.7)
Mannitol M.G.	5.0 (1.8)
Neosorb (Sorbitol)	5.2 (1.4)
α-Lactose monohydrate	36 (3.9)
Potassium Chloride	14 (6.9)
Racemic ibuprofen	5.9 (1.7)
Rhodapap DC-P3	6.8 (2.6)
S-Ibuprofen	5.4 (1.3)
Sodium Chloride	18 (6.9)
Spray-dried Lactose	17 (3.4)
STA-Rx-1500	6.6 (0.8)
Sucrose (crystalline)	54 (6.1)
Sugartab	20 (3.4)
Tri-Tab	16 (4.1)
Xylitol (Crystalline)	7.2 (2.5)

* Values (95% confidence intervals of the estimate of E).

TABLE VII. Literature values of E*.

Material	E (GPa)	Reference#
Acetaminophen	8.4	5
Acetylsalicylic Acid	8.8	9
Avicel PH101	0.01-9.0	3,4b,8
Avicel PH102	4.7, 8.5	2,6
Avicel PH105	10	2
Elcema	5.4-8.6	4b, 10a, 10b
Emcocel	9.0-9.4	2
Emcompress	7.0-182	4b, 10, 10a, 10b
Mannitol (Crystalline)	24	10
Microcrystalline cellulose (unspecified type)	8.3-16	1, 10, 10a, 10b
α-Lactose monohydrate	0.84-53	12
Potassium Chloride	9.2-26	6, 11
Rhodapap DC-P3 (Acetaminophen DC)	5.7	10
Sodium Chloride	7.8-186	4, 7, 9, 11
Spray-dried Lactose	5.3-14	4b, 10, 10a
STA-Rx-1500	1.4-6.1	4b, 10a, 10b
Sucrose (crystalline)	19 -73	5

* These values correspond to different methods of determining E. These methods include four-point flexure testing of large rectangular compacts, compressive testing of single crystals, single crystal microindentation, compressive testing of large cylindrical compacts, and the calculation of E using tablet indentation hardness and yield value from Heckel plots. Please see the references for individual methods corresponding to each value.

References are numbered as follows:
1. Atkins and Mai 1985; 2. Bassam *et al.*, 1988; 3. Church and Kennerley 1982; 4. Church and Kennerley 1983; 5. Duncan-Hewitt 1988; 6. Kerridge and Newton 1986; 7. Lawn and Wilshaw 1975; 8. Mashadi and Newton 1987; 9. Ridgway *et al.*, 1969; 10. Roberts and Rowe 1987a; 11. Simmons and Wang 1971; 12. Wong and Aulton 1989.

a. Values reported by Church (1984) extrapolated to zero porosity using Spriggs' equation (Spriggs 1961).
b. Values reported by Church (1984) extrapolated to zero porosity using Wachtman's equation (Wachtman 1969).

d. Total tablet recovery during unloading and postcompression includes both elastic and time-dependent viscoelastic components (Rippie and Danielson, 1981). Although viscoelastic expansion can be a significant part of the total recovery (Celik and Travers, 1985), its contribution will be negligible on the Betapress where the decompression time was always less than 20 ms at a turret revolution time of 1 s. As stated above, the linearity of the F-ΔD_m plots (Fig. 11, page 57) also indicates that expansion in this time period is purely elastic.

Errors in the calculation of ΔD_m values due to expansion of the steel tablet leads to corresponding error in the estimation of E. Thus the maximum error in E_p was about 4.5 percent for Avicel PH102 and about 3 percent for Emcompress. Extrapolation of E_p values, corrected for the expansion of the steel tablet, to p = 0 gave E values which were within the 95 percent confidence intervals of the E values in Table VI.

For a given material compacted to a specific porosity, some of the scatter in the values of E_p can be attributed to the interrelated effects of crystal anisotropy and variation in powder orientation when filling the die cavity. This is reflected in the 95 percent confidence intervals reported in Table VI. The E values reported in this table are 'average' Young's moduli for the various materials tested. The actual moduli for individual faces of the single crystals of these materials will differ due to crystal anisotropy. For instance, the E value of 54 GPa for sucrose is between the values of 19 GPa for the (100) surface and 73 GPa for the (001) surface found by single crystal microindentation work (Duncan-Hewitt, 1988). It is also within the range of 48 to 97 GPa calculated from the initial linear portion of the stress-strain data for different

crystallographic axes of a sucrose crystal obtained by a hydrostatic compression procedure (Bridgman, 1949).

3.5.3. Effect of formulation and processing on Young's modulus

The E values of the processed forms of various excipients such as Di-Pac/Sugartab, microcrystalline celluloses, and Anhydrous Lactose/Fast-Flo Lactose/Lactose DCL 21 are lower than sucrose, powdered cellulose (Elcema G250) and α-lactose monohydrate, respectively (Table VI). A lower E value means greater recovery during decompression on the Betapress. This suggests that tablets made from formulated or processed materials might be expected to possess a greater tendency to laminate or cap. In general, however, the tablets are stronger. Thus, tablets of Di-Pac (Fig. 32a), microcrystalline celluloses (Avicel PH102 and Emcocel, Fig. 32b), and Anhydrous Lactose/Fast-Flo Lactose/Lactose DCL 21 (Fig. 32c) were much stronger than sucrose, powdered cellulose, and α-lactose monohydrate, respectively. Similarly, the direct compression forms of acetaminophen gave much stronger tablets than crystalline acetaminophen (Fig. 27, page 110), even though the E values are lower (Table VI).

The apparent paradox arising from the ability of the direct compression forms to produce stronger tablets, despite their greater elasticity, is explained by the tendency of these forms to deform by viscoplastic flow during compression, which leads to more extensive bond formation. An indication of the degree of viscoplastic deformation during compression is given by peak offset time, t_{off}, described earlier. Thus, E values should be used in conjunction with t_{off} to characterise the behaviour of materials during high speed compression. An interesting situation is presented by crystalline ibuprofen and its direct compression

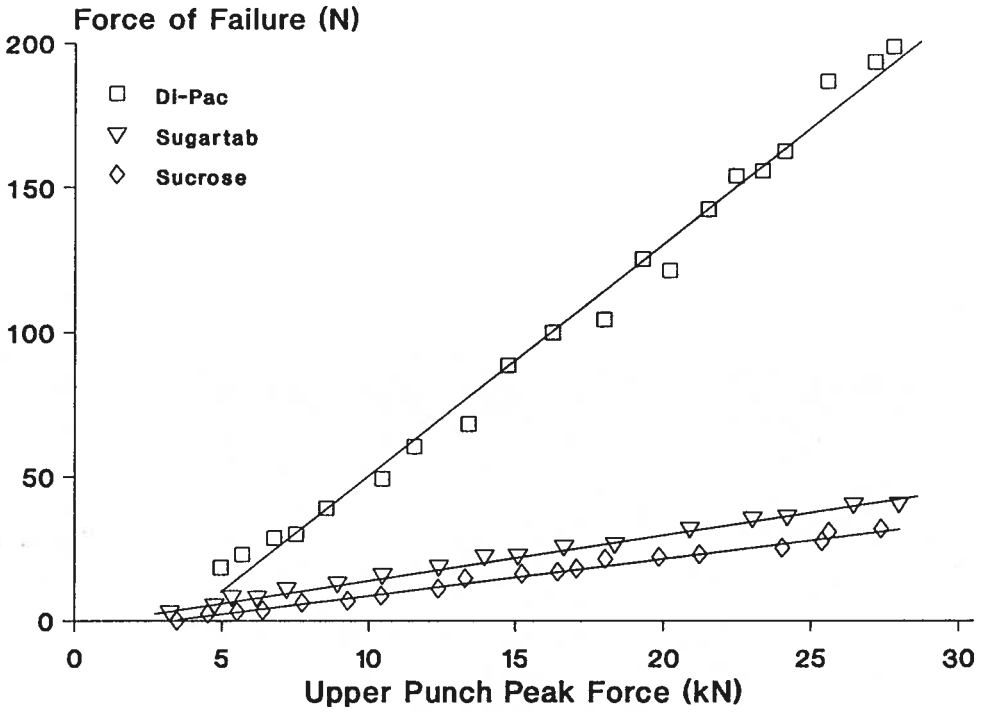

FIG. 32a. Variation in force of failure of tablets with upper punch peak force for sucrose and its direct compression forms.

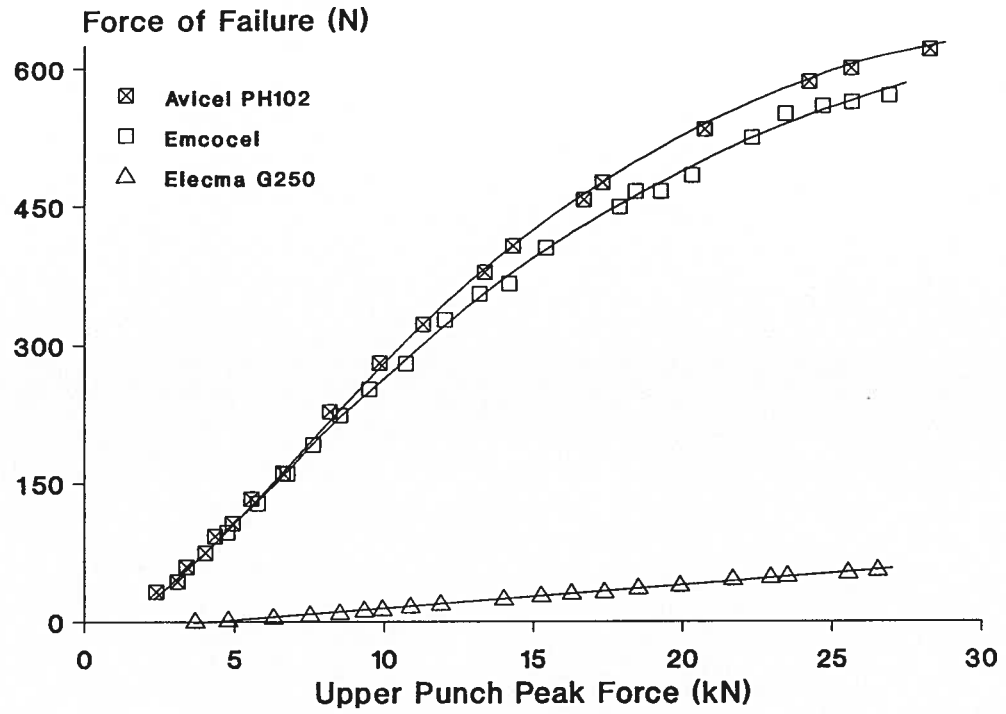

FIG. 32b. Variation in force of failure of tablets with upper punch peak force for various celluloses.

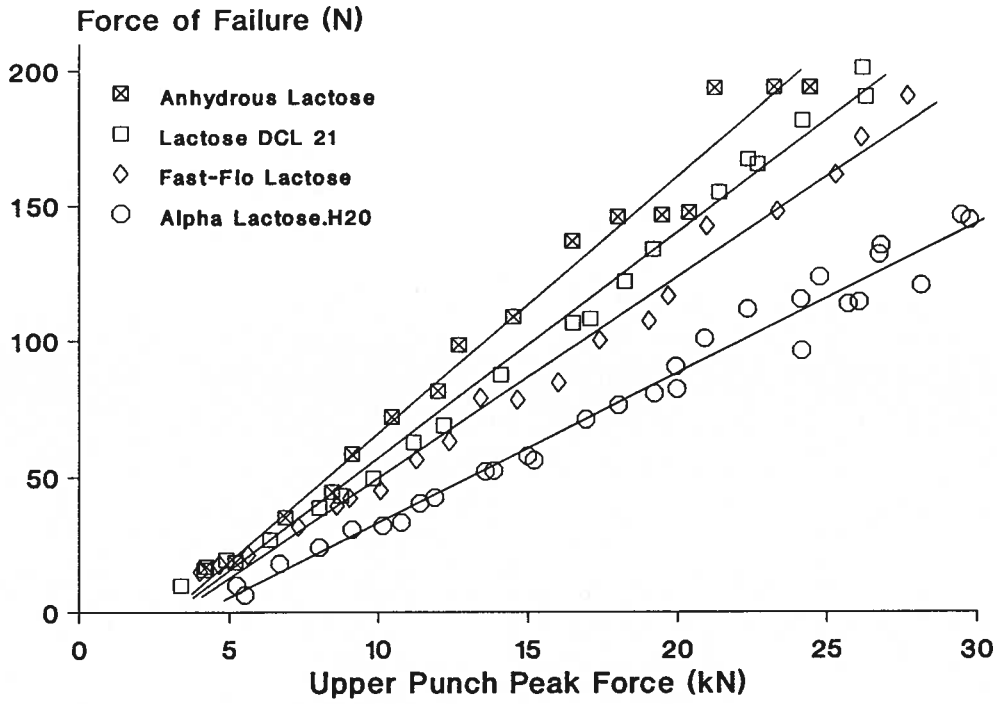

FIG. 32c. Variation in force of failure of tablets with upper punch peak force for various lactoses.

formulation, DCI-63. The expansion of both materials is identical and as great as Avicel PH102. DCI-63 contains 63 percent ibuprofen, lubricant and other USP/NF grade excipients suggesting that the major component(s) of the excipients have similar elastic properties to ibuprofen. Compared with crystalline ibuprofen which cannot be compacted into tablets, DCI-63 shows an increase in the t_{off} (Fig. 28, page 111) indicating that the excipients impart viscoplastic flow to the formulation and facilitate interparticulate bonding.

3.5.4. The use of decompression analysis and of Young's modulus

The analysis of machine recovery during decompression using the relationship between punch force and machine deformation provides a reliable estimate of the in-die tablet expansion and E_p. Together with the measurement of t_{off} and work of compression (Oates and Mitchell, 1989), the calculation of tablet expansion, work of decompression and E_p, using the decompression analysis, could be useful in preformulation studies on new drugs and excipients, in the quality control of in-coming tableting materials, and for in-process validation of compaction.

The E values of pharmaceutical materials determined by compressive or flexure testing of compacts, tablet indentation, and single crystal microindentation require specialized equipment. The present method is a novel application of a high speed rotary press in that the Young's modulus, a fundamental material constant, is readily obtained under normal tableting conditions without the use of specialized equipment.

The Young's modulus is an indicator of the stiffness of a material and can be used on its own to describe the deformability of a solid under load in the elastic regime of deformation. A material with a low E value

would tend to deform more easily than a material with a high E value. Young's modulus alone is of little significance in identifying the flow or fracture characteristics of particles during compaction, but can be of use in this respect in conjunction with W_D and other parameters, such as σ_y, t_{off}, $\Delta P/V_T$ and W_C derived from the compression phase.

3.6. ENERGY CHANGES DURING COMPACTION

The following section refers to the energy changes during compaction in terms of the W_C and the W_D values. The W_C and W_D values (both normalized for tablet mass) corresponding to the range of P_{max} over which each material was compressed, are given in Table V (page 115). The correlation between possible mechanisms of deformation, the homologous temperature of various materials, and the energy changes during the compaction of these materials, are discussed below.

3.6.1. Consumption of energy during the compression phase

The increases in stress at the points of interparticulate contact involve an increase in the energy of the powder bed as the machine does work on the powder bed. The process of permanent deformation of particles tends to decrease this energy and the excess energy thus released increases the temperature of the powder bed, as well as that of the punches and the die. Other processes such as friction also contribute to this energy change. These events are accompanied by bond formation during the compression phase. During decompression the converse is true since the expanding tablet does work on the machine. Thus, the difference W_C-W_D is an approximation of the work lost in particle deformation and bond formation during the compression phase. A material with low W_C-W_D values

would deform more readily and require very little energy from the machine, or alternatively will have a strain-rate independent deformation mechanism and thus would not require a continuous input of energy by the machine until the P_{max} is reached during the compression phase. The range of W_C-W_D values, corresponding to the range of P_{max} values given in Table V, are presented in Table VIII.

3.6.2 Temperature dependence of the mechanisms of deformation and its correlation with the energy changes during compaction

The deformation mechanism of any given material may be temperature dependent. A material which fractures at room temperature may flow at a higher temperature closer to its melting point. This concept can be expanded to compare different materials in the sense that a material with a low melting point would probably have a greater tendency to flow at room temperature, and hence deform with greater ease, than a material with a higher melting point. A plot of W_C-W_D for various organic materials against their homologous temperature, i.e. the ratio of absolute room temperature (293 K) to their absolute melting temperature, seems to agree reasonably well with this contention (Fig. 33). The scatter of W_C-W_D on this plot is probably due to differences between particle size, particle shape, crystal system, type and strength of bonds within and in between the particles, and true and bulk densities of the various materials. Also the melting points of certain materials on this plot (e.g. the celluloses and sucroses) do not really correspond to melting, but to decomposition or melting with decomposition. Nonetheless, a more or less general trend on Fig. 33 indicates that the energy of deformation (reflected by W_C-W_D) is, in general, related to the inherent energy of bonding within the particles

TABLE VIII. Range of W_C-W_D, porosity and F_f values* corresponding to the P_{max} range given in Table IV.

Material	W_C-W_D (J/g)	Porosity	F_f (N)
A-Tab	3.69-19.8	0.516-0.348	8.88-145
Acetaminophen Fine Powder	2.51-16.9	0.225-0.041	b
Acetaminophen Granular	1.40-12.3	0.184-0.024	2.10-12.4[c]
Acetaminophen Powder	1.08-14.9	0.220-0.040	b
Acetylsalicylic Acid	1.74- 5.79	0.101--0.007[a]	11.0-21.9
Anhydrous Emcompress	3.81-19.8	0.518-0.349	9.33-147
Anhydrous Lactose	3.00-20.1	0.292-0.098	16.5-194
Asagran	3.34- 8.35	0.110--0.001[a]	29.3-128
Avicel Large	9.21-40.3	0.447-0.049	6.14-223[c]
Avicel PH101	7.58-37.1	0.443-0.034	30.4->500[d]
Avicel PH102	3.23-40.2	0.430-0.038	32.0->500
Avicel PH105	5.48-32.0	0.439-0.038	50.0->500[d]
Caffeine	1.95-19.6	0.334-0.098	62.4-100[c]
Cal-Star	3.32-12.9	0.352-0.167	13.2-174
Cellactose	5.70-31.6	0.401-0.083	0.73-289
Compap CG	5.89-28.9	0.315-0.054	19.1-192[c]
Compap Coarse 73 L	3.62-22.5	0.305-0.047	4.61-158
Compap Coarse L	5.08-22.9	0.268-0.031	6.29-137
Compap L	6.48-28.5	0.296-0.060	20.4-170[c]
DCI-63	5.79-16.6	0.149--0.002[a]	29.4-91.2[c]
Di-Pac	5.72-20.7	0.248-0.068	18.3-198
Di-Tab	3.26-13.1	0.341-0.170	11.7-140
Elcema G250	5.25-23.8	0.341-0.040	0-55.8
Emcocel	14.0- 38.5	0.281-0.028	96.8->500
Emcompress	3.32-13.5	0.281-0.177	9.60-135
Emdex	2.14-27.3	0.378-0.047	5.81-380
Fast-Flo Lactose	5.12-23.1	0.294-0.080	14.8-190
Lactose DCL 21	1.81-18.3	0.310-0.092	9.60-190
Mannitol (Crystalline)	5.56-23.8	0.257-0.088	10.0-131[c]
Mannitol M.G.	3.36-16.5	0.257-0.062	7.92-148
Neosorb (Sorbitol)	5.72-21.9	0.263-0.052	29.4-353
α-Lactose monohydrate	3.55-16.2	0.218-0.094	6.07-135
Potassium Chloride	5.13-14.6	0.158-0.009	6.73-61.7
Racemic Ibuprofen	4.59-12.5	0.106--0.011[a]	b
Rhodapap DC-P3	7.55-27.3	0.279-0.064	34.9-121[c]
S-Ibuprofen	2.74- 7.76	0.105--0.001[a]	b
Sodium Chloride	3.35-14.1	0.211-0.045	14.0-32.5[e]
Spray-dried Lactose	4.03-20.6	0.287-0.079	6.00-108
STA-Rx-1500	3.52-21.2	0.223-0.007	3.00-8.80[e]
Sucrose (crystalline)	3.21-15.2	0.220-0.070	0-31.7
Sugartab	3.36-17.3	0.211-0.036	2.80-41.0
Tri-Tab	1.63-12.4	0.527-0.384	4.99-107
Xylitol (Crystalline)	1.85-11.0	0.226-0.054	2.86-55.9

* (IPT Punches; turret time 1s). a. Compacts fully dense at high pressures and transmit the stress radially; b. No tablets at any pressure; c. Tablets laminate at high pressures; d. Tablets at high pressures overload the CT-40 load cell; e. No tablet at low pressures.

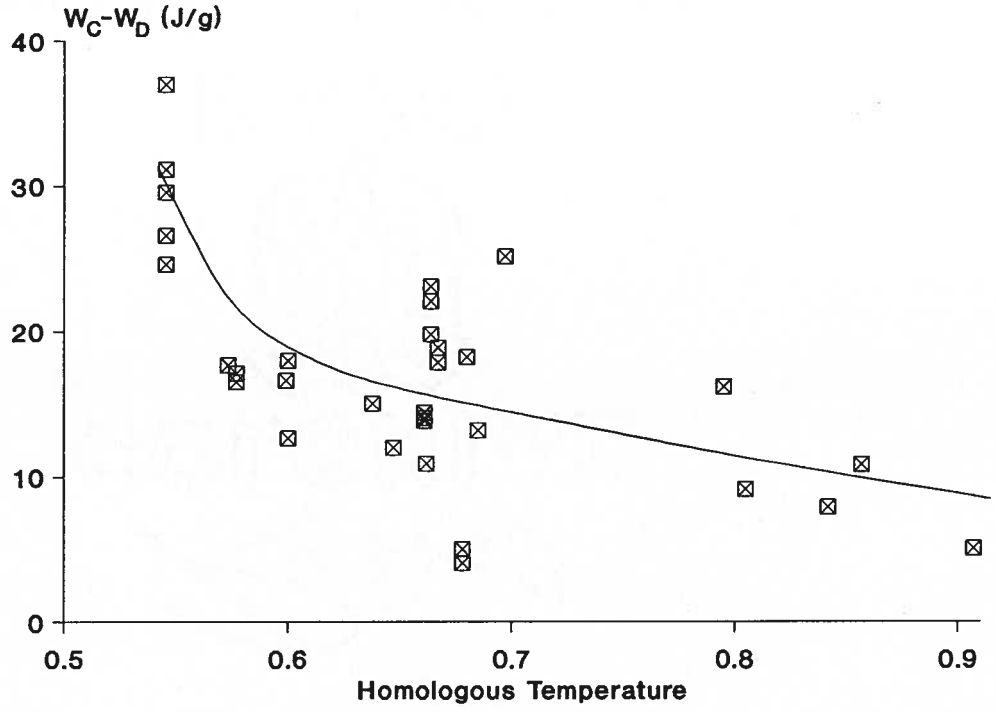

FIG. 33. A plot of the difference in the lost work (W_C-W_D) at highest and lowest P_{max} (≈215 MPa and ≈20 MPa respectively) for several organic substances against their homologous temperatures (the ratio of absolute room temperature, 293 K, to the absolute melting temperature), when each material was compressed over a similar P_{max} range. Each point represents one material.

(reflected by the homologous temperature). This plot does not establish the actual deformation mechanism, but can be used for this purpose in conjunction with other properties obtained from the compaction cycle.

3.6.3. Relationship between tablet strength and W_C-W_D

The lost energy represented by W_C-W_D is also an indication of the energy stored in the tablets partly in the form of bonds between the particles and partly in the form of stressed but unyielded particles. After decompression the stress on these unyielded particles will be relieved by a slow stress-relaxation phenomenon, thereby releasing the excess energy in the form of heat. The energy stored in the form of bonds within the tablets can be approximated by various tablet strength tests, e.g., tensile fracture test by diametral compression (Fell and Newton, 1968, 1970), impact test (Hiestand *et al.*, 1971), flexure test (David and Augsburger, 1974), tablet indentation hardness test (Jetzer *et al.*, 1983), or the more recently proposed impact fracture wear test (Duncan-Hewitt and Grant, 1987b).

All materials were tableted over a similar range of P_{max} and the force of failure, F_f, was measured using a diametral compression test. A plot of F_f of the strongest intact tablet of each material against the corresponding W_C-W_D shows a rough correlation between tablet strength and W_C-W_D (Fig. 34). Various formulations and processed materials which form intact and/or much stronger tablets relative to their parent compounds have much higher W_C-W_D, e.g. various Compaps compared with crystalline acetaminophen, Di-Pac compared with sucrose, Fast-Flo Lactose compared with α-lactose monohydrate, and DCI-63 compared with racemic ibuprofen. Thus, W_C-W_D is also an indication of the tablet strength of various materials

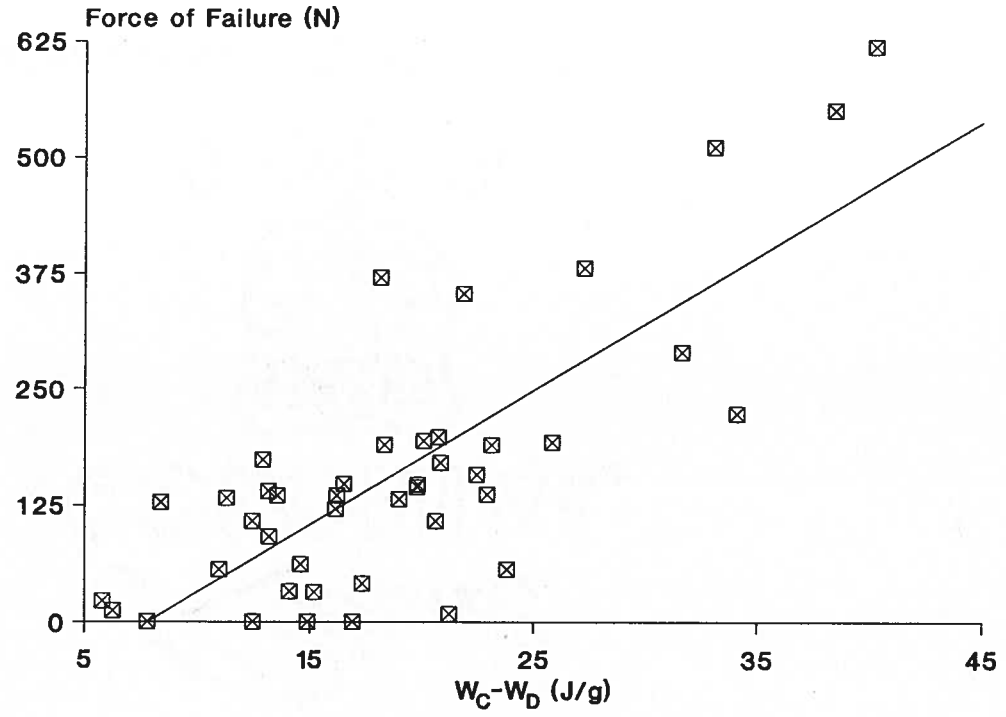

FIG. 34. A plot of F_f of the strongest intact tablet produced when a material was compressed over a range of P_{max}, against the corresponding lost work (W_C-W_D). Each point represents one material.

regardless of the mechanism of deformation of their particles during the compression phase. A similar quantity called net work was used by Ragnarsson (1985) to characterize materials, and was shown to be sensitive to friction and bonding.

3.6.4. Relationship between W_C-W_D and porosity changes

The aim of compaction is to decrease the porosity of a powder bed by compression, thereby increasing the probability of the particles forming a cohesive, compact structure. The larger the change in porosity, the larger is the amount of work consumed during compression. A plot of the difference between W_C-W_D at P_{max} ≈215 MPa and at P_{max} ≈20 MPa against the corresponding porosity change for the materials listed in Table VIII is linear (Fig. 35) indicating a direct relationship between the amount of energy consumed and the reduction in porosity. A bulky solid (high bulk volume, e.g. Avicels) has a greater reduction in porosity, relative to a less bulky solid (low bulk volume, e.g. Emcompress, Tri-Tab). Hence the amount of energy consumed per unit mass is higher. The probability of this energy being stored as bonds is also likely to be higher, and the tablets should be stronger. This seems to be true as indicated by the general trend in Fig. 34.

It follows from Figs. 34 and 35 that, to increase the tablet strength of a particular solid, it is necessary to increase the bulk volume of the solid either by mixing it with a more bulky substance, or by processing it in a manner that increases the bulk volume. More often than not, this will be accompanied by a change in the mechanism of particle deformation, which will be reflected by a change in the various parameters obtained from the compression and the decompression phases. Examples of this can be seen in

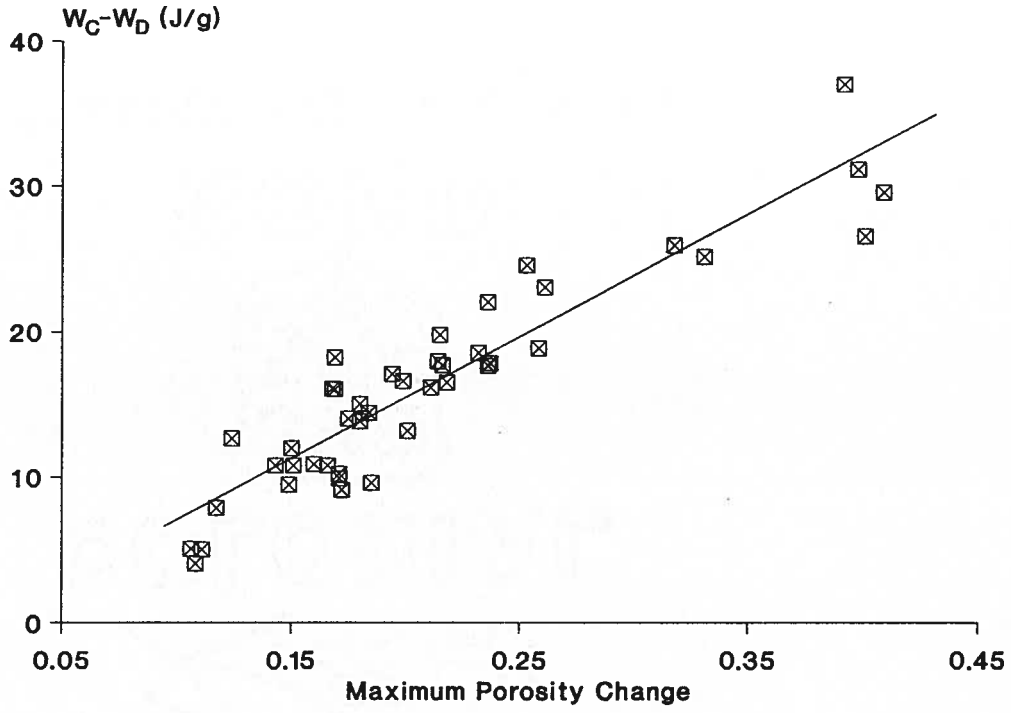

FIG. 35. A plot of the difference in the lost work (W_C-W_D) at highest and lowest P_{max} (≈215 MPa and ≈20 MPa respectively) for several substances, against the corresponding change in compact porosity, when each material was compressed over a similar P_{max} range. Each point represents one material.

Table VIII. Cellactose and microcrystalline celluloses form much stronger tablets than lactose and powdered cellulose respectively.

3.7. POSSIBLE MECHANISMS OF PARTICLE DEFORMATION

Hypothetically, if a given material could have different deformation mechanisms, then the ease of deformation at the room temperature would have the following order: viscous > viscoplastic among the strain-rate dependent mechanisms, and plastic > fracture (if σ_y is low) and fracture > plastic (if σ_y is high) among the non-strain-rate dependent mechanisms.

Materials which deform by viscous flow, especially those having low coefficients of viscosity, may sustain a large amount of strain without fracturing. Such behaviour is observed in ductile metals. Pharmaceutical materials may not exhibit a truely ductile behaviour because most of these materials are organic compounds with more complex crystal lattices than the ductile metals. Nevertheless, those pharmaceutical materials that readily deform at low stresses can be termed 'ductile' for the lack of a better term. Such materials will deform much more at a given strain rate and under a given stress than viscoplastic materials. Both ductile and viscoplastic materials will have relatively low σ_y values, but the values of ductile materials will be much lower than those of viscoplastic materials. Both will compact to very low porosities, and will have low E values indicating that they are very easily deformable even under low stresses. The primary difference between them will be in their strain-rate dependency, which will be reflected in the values of t_{off} and $\Delta P/V_T$ obtained from the compression phase (sections 3.4.4 and 3.4.5). Ductile materials will be compacted to very low porosities at lower pressures than a viscoplastic material and, in effect, will behave as almost

incompressible solids with a very short t_{off} and almost no $\Delta P/V_T$. On the other hand, viscoplastic materials, being slightly stiffer, will have longer t_{off} values which will decrease with increase in P_{max}, and have a much higher $\Delta P/V_T$. Due to differences in the ease of their deformability there will also be differences in the energy consumed during compression, i.e., W_C-W_D for ductile materials will be much lower than for viscoplastic materials.

The σ_y of plastic materials will be greater than ductile or viscoplastic materials but smaller than intrinsically brittle materials. Both plastic and intrinsically brittle materials will have low t_{off} values with small $\Delta P/V_T$, but for different reasons. A plastic material would flow during compression phase to fill the voids which would result in low porosities, whereas a brittle material would fracture without filling up the voids thereby leaving a porous compact at the end of the compression phase with a structure capable of resisting flow. The E values of both plastic and brittle materials would tend to be higher than those of the ductile or viscoplastic materials indicating their greater stiffness under similar conditions of compression. Since the element of strain-rate dependency is absent in plastic flow/fracture mechanisms, the energy consumption by these materials (W_C-W_D) during compression will be much lower than in the case of viscoplastic materials because the machine does not have to work continuously during the compression phase.

The above discussion provides a general background by which one can attempt to identify the principal particle deformation mechanisms of various materials. The materials listed in Tables II-VI have been

categorised on the basis of their stress and strain rate behaviour and on the properties derived from the compaction cycle.

3.8. DEFORMATION MECHANISMS OF THE VARIOUS CATEGORIES OF SOLIDS

3.8.1. Deformation mechanism of acetylsalicylic acid, ibuprofen and their formulations

Drugs such as acetylsalicylic acid, racemic ibuprofen, S-ibuprofen, and formulations such as Asagran and DCI-63, all have very short t_{off} and very low $\Delta P/V_T$ preliminarily suggesting that their deformation is not strain-rate dependent. The very low values of σ_y and E indicate that the particles of these materials are easily deformed. The low values of W_C-W_D show that only a small amount of energy is consumed in deforming these materials. At high P_{max}, the porosity becomes less than zero indicating that the compacts become fully dense and undergo a hydrostatic compression, which causes significant radial expansion of the die wall. Thus, the volume between the punch faces, if not corrected for radial expansion, becomes lower than the true volume of the powder resulting in a negative porosity.

The low values of E, σ_y and W_C-W_D suggest that these materials are readily deformed and can be classified as low yield-strength ductile solids. Due to their viscous nature they become almost nonporous at very low stresses, and then behave as almost incompressible solids. This results in low t_{off} and correspondingly low $\Delta P/V_T$, and can give rise to the erroneous impression that the deformation of these materials is independent of rate of compaction.

The low melting temperatures of acetylsalicylic acid, racemic ibuprofen and S-ibuprofen are consistent with a viscous deformation

mechanism. At room temperature (293 K) their homologous temperatures are 0.68, 0.84 and 0.91 respectively. The ease of their deformation becomes obvious considering that almost all materials tend to show some degree of flow above a homologous temperature of about 0.5. Any rise in temperature during tableting will further increase the degree of the viscous flow of these drugs and formulations.

3.8.2. Deformation mechanism of calcium phosphates

Three types of calcium phosphate are available commercially: dicalcium phosphate dihydrate (Cal-Star, Di-Tab, Emcompress), anhydrous dicalcium phosphate (Anhydrous Emcompress, A-Tab) and tricalcium phosphate (Tri-Tab). All have short t_{off} values, low $\Delta P/V_T$, high to very high σ_y, and higher E compared with other materials. The higher σ_y and E values suggest that these materials are very stiff and not easily deformed. The compacts remain very porous at the end of the compression phase. At high P_{max}, the residual porosity values of ≈0.17 for the dihydrates, ≈0.35 for the anhydrous samples and ≈0.38 for tricalcium phosphate suggest an increased resistance to flow among these samples which correlates well with their respective σ_y values of ≈90 MPa, ≈163 MPa and 221 MPa. These observations, coupled with the short t_{off} suggest that the calcium phosphates do not deform by a flow-based mechanism and that there is a negligible dependency of their deformation on strain rate. The most likely mechanism of deformation is therefore fracture of some type. The calcium phosphate powders have a low bulk volume, and the machine has to work for a much shorter period of time during compression (Fig. 5, page 43), the Emcompress curve), causing a relatively small energy expenditure in their compaction, hence the low W_C-W_D. Still, the compacts are fairly strong

presumably due to strong interparticulate bonds formed between the new surfaces exposed upon fracture.

In general, calcium phosphates can be classified as high yield-strength intrinsically brittle solids (see section 3.4.1 for explanation of intrinsically brittle behaviour). This mechanism allows a large pore volume in the compacts, and does not require the machine to expend a large amount of energy in continuously deforming the particles throughout the compression phase. Fracture only requires sufficient energy for crack initiation and propagation. Their intrinsically brittle nature would preferentially allow fracture rather than flow during compaction. There is, however, some likelihood of flow at low P_{max}, because at low P_{max} the porosities are very high, hence σ_T could be very high causing some flow consistent with the short t_{off} and small $\Delta P/V_T$ at these pressures.

It is not possible to correlate the deformation mechanism of calcium phosphates with their homologous temperature, because only the melting point of tricalcium phosphate can be determined. Other calcium phosphates undergo phase transitions such as dehydration or condensation of the orthophosphate groups to pyrophosphate groups (Rhone-Poulenc Product Information Manual, 1989), but at temperatures much higher than the melting points of organic substances listed in Table II. If the melting point of tricalcium phosphate (1943 K) and the transition temperatures of dicalcium phosphates (>670 K for the condensation reaction) are any indication of the strength of their structure, it is reasonable to expect that, at room temperature, their particles would not deform by a flow process.

3.8.3. Deformation mechanism of celluloses

Celluloses are characterised by low σ_y, long t_{off} values and a large $\Delta P/V_T$, high W_C-W_D, and relatively low E values (Table III, IV, VI, VIII). The low E and σ_y values indicate that celluloses deform easily, albeit not as easily as acetylsalicylic acid or ibuprofen. This is supported by the observation that the decrease in the porosity of cellulose compacts over the range of P_{max} applied is not as sudden as with acetylsalicylic acid or ibuprofen, even though the decrease is much larger (Table VIII). At low P_{max} the compacts of celluloses are quite porous ($p \approx 0.4$), but with increase in P_{max} the porosity gradually decreases to very low values ($p \approx 0.04$). The change in t_{off}, and $\Delta P/V_T$, with P_{max} are also gradual. The homologous temperature of celluloses is 0.54, indicating that there should be a certain degree of viscous flow, but not as significant as that of acetylsalicylic acid or ibuprofen. This, and the higher σ_y, indicates that the celluloses are much more viscous, i.e. less easily deformed, than these drugs. On the other hand they are much more readily deformed than materials such as lactose, sucrose or the calcium phosphates, which have generally much higher σ_y and E, and have comparable or lower homologous temperatures (≈ 0.60 for lactoses, ≈ 0.66 for sucroses, and 0.15 for tricalcium phosphate). The celluloses can therefore be classified as intermediate yield-strength viscoplastic solids, which have a significant degree of strain-rate dependent flow (hence long t_{off}), and also a certain degree of stiffness (hence intermediate σ_y).

Of the two types of celluloses commercially available for direct compression, the microcrystalline celluloses (different Avicels and Emcocel) form much stronger tablets than powdered cellulose (Elcema G250). There are small but obvious differences between the tableting parameters of

powdered cellulose and the microcrystalline celluloses. Powdered cellulose has slightly shorter t_{off}, and slightly higher σ_y and E suggesting that it is less easily deformed than microcrystalline cellulose. Powdered cellulose also consumes much less energy (lower W_C-W_D) during compression, which is partly why it forms much weaker tablets. Although the elastic expansion of powdered cellulose during decompression is similar to that of the microcrystalline celluloses, it has a significantly higher volumetric expansion during ejection (Fig. 36), which further weakens its tablets.

Cellulose has very strong hydrogen bonds between adjacent β-glucose chains (Talman, 1977). The strong inter-chain bonding, their partially amorphous nature, and the large amount of energy consumed (highest W_C-W_D) during compression of the microcrystalline celluloses results in high tablet strength. In fact, microcrystalline cellulose tablets are the strongest of all the materials used in this study. The viscoplastic behaviour and the high strength of their tablets makes the microcrystalline celluloses excellent direct compression agents.

3.8.4. Deformation mechanism of acetaminophen and its formulations

Crystalline acetaminophen has a short t_{off} and a small $\Delta P/V_T$ comparable to those of the calcium phosphates. The σ_y and E values are higher than those of the celluloses but much lower than those of the calcium phosphates. It is compacted to porosities almost as low as the celluloses. Tablets are formed only when large particles are compressed at low pressures. The amount of energy consumed (W_C-W_D) during compression is comparable to that of the calcium phosphates, and is much lower than the celluloses. The homologous temperature of acetaminophen ($\approx$0.66) is similar to that of the celluloses but is much higher than that of the tricalcium

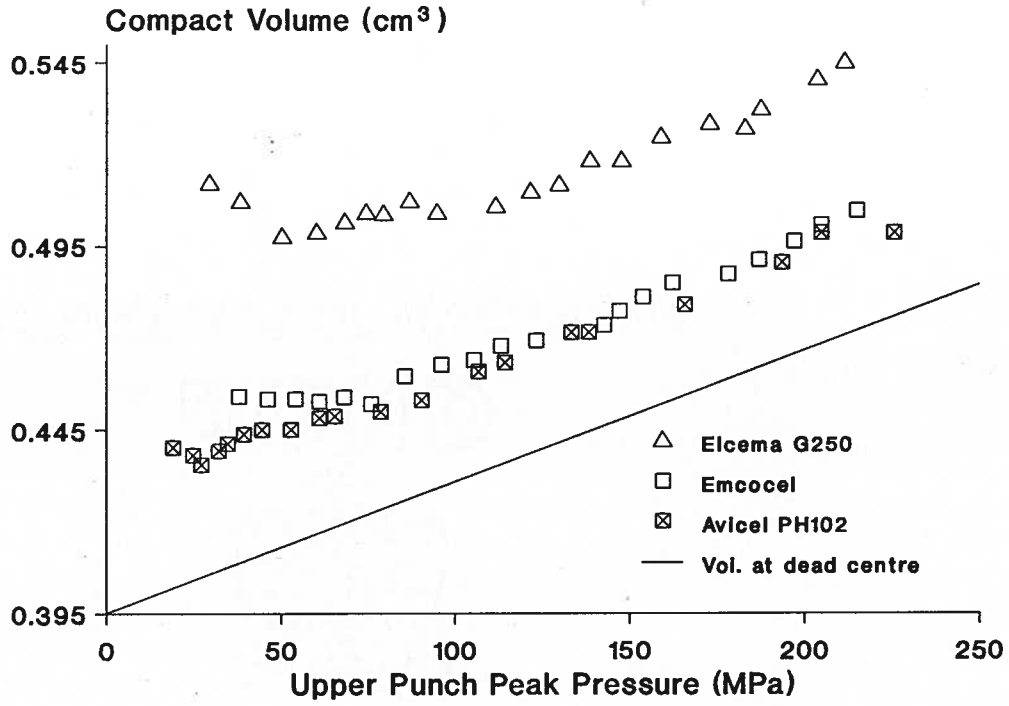

FIG. 36. Compact volume of celluloses determined from compact dimensions measured immediately post-ejection as a function of P_{max}. The solid line represents the compact volume at the dead centre position. This line was determined in a separate experiment by compressing lead shot (Section 2.6.5).

phosphate. Thus, acetaminophen appears to be fairly deformable at room temperature (hence the low porosities) and has a certain degree of flow (short t_{off}), but beyond a certain P_{max} the ability to flow diminishes (negligible t_{off}). Large crystals of Acetaminophen Granular readily yield at low pressures, at which the porosities are low, probably because the σ_T is very high, and eventually fail by fracture exposing new surfaces. Some bond formation occurs between these new surfaces and intact, but weak, tablets are formed. At high P_{max}, or when the particle size is decreased (as with Acetaminophen Fine Powder or Powder), these events do not occur and no tablet is formed. The brittle behaviour of acetaminophen is consistent with the observation that the fine particles of acetaminophen do not form tablets and have a slightly higher σ_y, because it is known that even the most brittle materials will not fracture once the particle size is reduced to below a critical value (Kendall, 1978; Roberts and Rowe, 1987). Crystalline acetaminophen can therefore be classified as an intermediate strength plastic/brittle solid, where the plastic flow results in low porosities and short t_{off}, and the plastic/brittle behaviour resulting in a relative lack of strain rate dependence after the initial yielding. Since the overall porosity changes are small, the machine does not have to expend a large amount of energy and W_C-W_D is low.

Crystalline acetaminophen has a higher E than celluloses, i.e., its elastic recovery during decompression is lower than that of the celluloses. Hence the inability of acetaminophen to form tablets is apparently not due to a high recovery as is commonly believed, but due to its inability to form bonds during compression, or due to the low strength of the bonds formed, if any. Using a flexible die to prolong decompression, Amidon *et al.* (1981) obtained intact tablets of an acetaminophen formulation. They

concluded that this process enabled the weak interparticulate bonds to withstand the tablet expansion. However an alternative explanation is that the longer contact time (time during which the die contents are under pressure; Jones, 1977) leads to increased deformation and an increase in the number of bonds.

When crystalline acetaminophen is formulated with other substances, t_{off} and $\Delta P/V_T$ are increased especially at low P_{max}, σ_y values are either similar or slightly decreased, and E is decreased. The porosity changes are much larger. Therefore, W_C-W_D increases significantly and the compacts are much stronger despite an increase in the elastic recovery during decompression as reflected by the low E values. An increase in t_{off} and in $\Delta P/V_T$ at low P_{max} suggests that the degree of strain rate dependency of the formulations is higher and the mechanism of deformation is more viscous than plastic/brittle. Some formulations do not form intact tablets at high P_{max}, at which their t_{off} values are very close to those of crystalline acetaminophen. This indicates a decrease in the degree of viscous flow, and this decrease, coupled with the greater recovery of the formulations during decompression, causes failure of the compacts at high P_{max}.

3.8.5. Deformation mechanism of lactoses

Lactose in its processed forms is commonly used as a direct compression excipient. The processing results in either α-anomer rich products (e.g., Fast-Flo Lactose, Spray-dried Lactose) or β-anomer rich products (e.g., Anhydrous Lactose and Lactose DCL 21) (Dwivedi and Mitchell, 1989). There are distinct differences between the tableting parameters of these forms. Alpha-lactose monohydrate has the shortest t_{off} and highest σ_y and E among all lactoses tested. The $\Delta P/V_T$ and the residual

porosities of the different lactoses are very similar. The processed forms have higher W_C-W_D values than α-lactose monohydrate, and the strength of their tablets is also higher. The small difference in W_C-W_D values, despite very similar porosities, indicates a slight degree of difference in the deformation mechanism of the various forms.

The σ_y and E values of the lactoses are higher than those of the celluloses, but much smaller than those of the calcium phosphates. Their t_{off} values, $\Delta P/V_T$, and W_C-W_D are much smaller than those of the celluloses but comparable to those of the calcium phosphates. This suggests that although the lactoses have a certain degree of flowability (short t_{off}), their deformation mechanism is predominantly fracture of some type. This is especially true of α-lactose monohydrate which has the highest σ_y among the various lactoses. According to the rank order of the σ_y values the rank order for the ease of deformation is: α-rich processed samples ≈ β-rich processed samples > α-lactose monohydrate. Alpha-lactose monohydrate can be classified as an intermediate strength plastic/brittle solid, while the processed samples have a greater degree of plastic flow. The increased deformation by flow is probably due to the amorphous content of the processed samples.

The homologous temperatures of the lactoses are in the intermediate range. Although the higher melting point and slightly higher σ_y values of β-rich samples indicate that they should be less readily deformed than the α-rich samples, they have comparable t_{off}, indicating that they deform equally well. The β-rich samples form stronger tablets presumably because the lattice bonds are much stronger than those of α-rich samples.

3.8.6. Deformation mechanism of sucroses

Relative to α-lactose monohydrate, the σ_y of sucrose is lower, E is higher, the t_{off} values and $\Delta P/V_T$ are comparable, the homologous temperature is slightly higher, and W_C-W_D is lower. The similarity of the various tableting parameters of crystalline sucrose and α-lactose monohydrate suggests a similar deformation mechanism. Therefore, sucrose is also classified as an intermediate yield-strength plastic/brittle solid, with perhaps a slightly greater ease of deformation than α-lactose monohydrate. Sucrose, however, forms much weaker tablets than α-lactose monohydrate. This can be correlated with the lower bond strength of sucrose as reflected by its lower temperature of melting with decomposition (≈175°C) relative to that of anhydrous α-lactose (dehydration of the monohydrate at ≈150°C followed by melting at ≈210°C).

The tableting parameters of crystalline sucrose are quite different from those of Sugartab and Di-Pac, the two types of compressible sugar used in this study. Sugartab is an agglomerated sugar product containing ≈90-93% sucrose with the rest being invert sugar, whereas Di-Pac is a crystallized product containing 98% sucrose with 2% dextrins (Handbook of Pharmaceutical Excipients, 1986). Compared with crystalline sucrose, the t_{off}, $\Delta P/V_T$ and W_C-W_D for the compressible sugars are much higher, but σ_y, E and the minimum residual porosities are lower, while the homologous temperature are almost identical. This suggests that the compressible sugars deform more readily. The agglomeration and inclusion of invert sugar, or co-crystallization with higher saccharides, evidently imparts a certain degree of viscoplastic flow. The original plastic/brittle behaviour is probably still maintained to a certain degree, the difference being that the samples perhaps fail by a fracture mechanism that shows some

degree of ductility. The degree of viscoplastic behaviour is not as pronounced as in the case of celluloses because W_C-W_D, although higher than that of crystalline sucrose, is much lower than that of the celluloses, and also the porosity changes are not as marked as with the celluloses. That increased flowability does not necessarily result in stronger compacts is evidenced by the weaker compacts of Sugartab relative to those of Di-Pac. This difference is presumably because the Di-Pac particles bond much more strongly due to the small content of polymeric dextrins, whereas the inclusion of invert sugar in Sugartab does not have a similar effect.

3.8.7. Deformation mechanism of polyols

Three monosaccharide-derived polyols, namely, mannitol, sorbitol and xylitol, are used in the crystalline state or in processed form as direct compression excipients. The tableting parameters of crystalline mannitol and xylitol, and direct compression forms Mannitol M.G. (mannitol) and Neosorb (sorbitol) are given in Table II-VI, and Table VIII. The t_{off}, $\Delta P/V_T$, and W_C-W_D of all samples are higher than those of calcium phosphates, but lower than those of celluloses, suggesting a certain degree of flowability. The homologous temperatures of xylitol, sorbitol and mannitol are ≈0.80, ≈0.77 and ≈0.66 respectively, which also suggests a deformation mechanism involving flow. The σ_y and porosities are higher than those of celluloses but much lower than those of calcium phosphates. The E values are generally higher than those of celluloses, and are similar to those of calcium phosphates, indicating a fair degree of stiffness in their lattice, which may cause fracture once a certain degree of flow has occurred. Thus, the polyols seem to have a certain degree of viscoplastic flow, although not as much as that of the celluloses, and also a certain

propensity to fracture, but not as much as of the calcium phosphates. The fracture is probably ductile and occurs only after an initial viscoplastic flow. The initial flow permits a rapid reduction in porosity, but the subsequent fracture does not allow this reduction to continue and locks a fair proportion of pore space in the compacts. The polyols used in this study can therefore be classified as intermediate yield-strength viscoplastic/brittle solids.

The t_{off} of the various polyols do not differ much from each other. The $\Delta P/V_T$ has the rank order: Neosorb > crystalline mannitol ≈ Mannitol M.G. > crystalline xylitol, which implies a difference in the rate of stress relief during t_{off}. The σ_y of mannitol and xylitol are similar, but the E value of mannitol is higher than that of xylitol. The σ_y and E of the direct compression formulations are lower than those of the crystalline samples. The σ_y of Neosorb is lower than that of Mannitol M.G.. The W_C-W_D values have the following sequence: crystalline mannitol > Neosorb > Mannitol M.G. > crystalline xylitol. Neosorb forms the strongest tablets, xylitol the weakest, and mannitol with intermediate strength. Small differences in their tableting parameters and also differences in other physical properties are the underlying causes of their different tablet strengths. For example, mannitol and sorbitol are isomers of each other, therefore they might be expected to produce tablets of nearly equal strength. However, the lower σ_y, slightly longer t_{off}, much higher $\Delta P/V_T$, and a higher homologous temperature of sorbitol indicate that it deforms with greater ease, which increases the probability of bond formation and hence sorbitol produce stronger tablets than mannitol. This suggests that differences in crystal structure, and the associated differences in the ability of deformation, can cause significant differences in the tablet

characteristics of materials with similar chemical structure. Xylitol tablets are weakest presumably due to the very low amount of energy consumed during its compaction and also due to the weaker nature (low m.p.) of its crystal lattice.

3.8.8. Deformation mechanism of miscellaneous other substances

Cellactose is a formulation of 25% microcrystalline cellulose with 75% lactose (Garr and Rubinstein, 1991). Its tableting parameters are intermediate between those of its constituent components. The t_{off}, $\Delta P/V_T$ and W_C-W_D of Cellactose are slightly smaller, and σ_y slightly higher, than the microcrystalline cellulose, indicating a slight reduction in the degree of viscoplastic flow due to the inclusion of lactose. The E value is similar to that of microcrystalline cellulose. A reduction in the viscoplastic flow and an equal degree of elastic recovery of Cellactose leads to the formation of weaker tablets compared with microcrystalline cellulose, but the tablets are still stronger than lactose alone. Cellactose can be classified as an intermediate yield strength viscoplastic solid which is essentially in the same category as microcrystalline cellulose.

Caffeine has a short t_{off} and a low $\Delta P/V_T$ indicating a low strain-rate dependency. It has intermediate σ_y, E, W_C-W_D, and porosity change suggesting it is a fairly stiff solid with the degree of stiffness very similar to that of the lactoses. This suggestion is supported by the similarity of its homologous temperature ($\approx$0.57) to that of the lactoses ($\approx$0.59). Hence it can be classified as an intermediate-strength plastic/brittle solid, with a lower tendency to flow than lactoses as its t_{off} and $\Delta P/V_T$ are lower than that of the lactoses. The compacts of

caffeine are slightly stronger than those of the lactoses, but they laminate at pressures above 127 MPa. This is perhaps due to the resistance to flow of caffeine which presumably forms fewer interparticulate bonds.

Emdex is made up of microcrystals of dextrose as porous spheres, with some amount of higher polysaccharides (Seugling, 1980). Its tableting parameters are slightly different from those of the celluloses. Compared with the celluloses the t_{off} are shorter, $\Delta P/V_T$ is lower, the porosity change is smaller, hence W_C-W_D is lower, and σ_y and E values are slightly higher. These differences suggest that Emdex is a viscoplastic material with a lower degree of rate of compaction dependency and higher stiffness than the microcrystalline celluloses, and can be classified as an intermediate yield-strength viscoplastic solid. The tablets of Emdex are weaker than those of microcrystalline celluloses, which suggests less viscoplastic flow into the voids and consequently a lower degree of bonding.

Starch is a polymer made up of partially linear and partially branched chains of α-glucose (The Merck Index, 1976). STA-Rx 1500 is a commercial form of pregelatinised starch. Its tableting parameters are intermediate between those of ibuprofen/acetylsalicylic acid and the microcrystalline celluloses. Its low σ_y and E values suggest that it is easily deformed and hence forms compacts of very low porosities. Its t_{off} and $\Delta P/V_T$ are low, which indicate that the compacts become very dense earlier on during the compression phase, and behave as a nearly incompressible solid. Thus STA-Rx 1500 can be regarded as a low yield-strength ductile solid. The W_C-W_D is intermediate, which means that the compacts should be fairly strong. In fact, they are very weak, implying that not much of the lost work is stored in the form of interparticulate

bonds, but is probably lost in other irreversible processes. Also, the bonds between the α-glucose chains may not be very strong. Evidence to support this is the difference in solubilities of starch and cellulose. Starch dissolves in boiling water, whereas cellulose does not. This would be true if α-glucose chains are much more weakly bonded in starch than the β-glucose chains in cellulose. The weak nature of the bonds coupled with a high elastic recovery of its compacts during decompression weaken the STA-Rx 1500 compacts. Lubrication with magnesium stearate is also known to weaken the compacts of STA-Rx 1500 (Ragnarsson and Sjorgen, 1985).

Two ionic salts, namely, potassium chloride and sodium chloride, were also studied on the Betapress. Both have low homologous temperatures ($\approx$ 0.28), which suggests that at room temperature the preferred mechanism of their deformation should be fracture, which would be consistent with their low W_C-W_D. Potassium chloride has longer t_{off} values and a greater $\Delta P/V_T$ than sodium chloride. It also has lower σ_y and E, and is compacted to much lower porosities. Therefore potassium chloride can be classified as a ductile solid, and sodium chloride as a plastic/brittle solid, both of which fail by a fracture process during compression at room temperature. The longer t_{off}, and larger $\Delta P/V_T$, of potassium chloride at low pressures are manifestations of its greater ductility.

The various materials and their general deformation behaviour is listed in Table IX. The above discussion of the various general classes of materials shows that it is possible to use a rotary press for a comprehensive analysis of the deformation mechanisms of pharmaceutical materials.

TABLE IX. Classification of deformation behaviour[a] of various solids on the Betapress.

Material	Classification of deformation behaviour
Acetylsalicylic acid, ibuprofen and their formulations, STA-Rx-1500	Low yield-strength ductile solids
Potassium chloride	Low yield-strength ductile/brittle solid
Cellactose, Celluloses, Emdex	Intermediate yield-strength ductile/viscoplastic solids
Formulations of acetaminophen	Intermediate strength plastic/brittle solids with some viscous flow
Polyols and their processed forms	Intermediate yield-strength viscoplastic/brittle solids
The processed forms of α-Lactose monohydrate and of Sucrose	Intermediate strength plastic/brittle solids with some viscoplastic flow
Acetaminophen, caffeine, α-Lactose monohydrate, Sodium chloride, Sucrose	Intermediate strength plastic/brittle solid
Calcium phosphates	High yield-strength brittle solids

a. This classification provides a simplified view of the general deformation behaviour of various solids. There are subtle differences in the extent of deformation within a given class. For a detailed analysis please see the discussion in section 3.8.

3.9. COMMENTS ON INTERPARTICULATE BOND FORMATION UNDER PRESSURE

An examination of the differences between the force of failure values of various tableted solids (Table VIII) and the differences in their deformation mechanisms (section 3.8, Table IX) indicate that, although the permanent deformation of a material under stress is considered a prerequisite for bond formation during compression, it does not guarantee the formation of strong tablets. For example, acetylsalicylic acid and ibuprofen are very readily deformed (section 3.8.1). Nevertheless, they form very weak tablets or no tablets at all. This is presumably because insufficient bonds are formed in spite of intimate interparticulate contact as indicated by the negligible residual porosities. Their highly elastic nature further aggravates the problem since the small number of bonds cannot withstand the substantial elastic expansion during decompression. It appears therefore that, along with an understanding of the deformation mechanisms under high speed compaction as outlined in this work, it is also necessary to understand the factors controlling bond formation between the surfaces newly created during compression.

4. SUMMARY

1. A high speed rotary tablet press, the Manesty Betapress, was used to analyse the powder compaction process while operating the press under speed.

2. After an initial calibration of the punch displacement profiles using an LVDT-slip ring system, the punch displacements on the Betapress were calculated using a relationship between machine deformation and punch force. Thus the analysis of powder compaction on the Betapress required only the measurement of upper and lower punch forces, and the position of the punches relative to the dead centre position where the punches are vertically aligned with the centres of the compression roll support pins.

3. Two types of punches, Manesty and IPT, were used at various machine speeds to study the influence of these variables on powder compaction characteristics over a range of pressures.

4. Several parameters from the compression phase were obtained and were related to particle deformation. These parameters included:
   i. Peak offset time (t_{off}): the time interval by which the position of the peak pressure preceded the dead centre position of the punches. The t_{off} is related to the ability of materials to undergo stress relaxation at constant strain during the time when the punch head flats are in contact with the compression rolls.
   ii. Decrease in pressure during t_{off} ($\Delta P/V_T$): this is an indication of the ease with which a compact material can flow into the residual pore spaces after P_{max} is achieved.

iii. The work of compression (W_C): this was corrected for the work of machine deformation and gives the energy expended by the machine in compressing the powder bed during the compression phase.

iv. Porosity change determined from the punch displacement analysis. The porosity change was used to calculate the maximum value of the Heckel term, H_{max}, at P_{max}. Heckel plots were constructed by plotting the values of H_{max} against P_{max}. These plots were linear and their slopes were used to calculate the yield stress (σ_y) of the material under pressure.

5. A new method of estimating compact expansion from the small differences between the decompression profiles of the various materials was developed by using the relationship between the machine deformation and force as follows:

   i. The machine recovery was obtained by 'compressing' an incompressible solid, a 'steel+Emcompress' tablet. The force applied during the compression phase deforms only the machine. Hence the force during the decompression phase corresponds primarily to the recovery of the press.

   ii. When a powder bed is compressed an additional force over and above the force due to machine recovery is recorded during decompression. This force, which causes an additional machine deformation during decompression, was obtained by subtracting the incompressible solid decompression profiles from the powder bed decompression profiles. The difference was translated into compact expansion by using the machine deformation constant.

iii. The expansion was also used to obtain stress-strain plots, the linear slopes of which provide a direct evidence that the expansion of a compact during decompression is elastic in nature. Hence there is no need for complex viscoelastic modeling to draw this conclusion.

iv. The slopes of the stress-strain plots gave the elastic modulus of the tablets at a given porosity, E_p. Plotting E_p against porosity and extrapolating these plots to zero porosity using a polynomial regression gave the Young's modulus of the solids compressed. This was a novel way of determining the Young's modulus of solids using a high speed rotary press, without the need of tests on single crystals or on large preformed compacts.

v. The compact expansion was used to calculate the work of decompression (W_D).

6. Over forty pharmaceutical solids were selected to cover a wide range of materials including direct compression excipients and their processed forms, and poorly compressible drugs and their formulations.

7. The solids were characterized by determining true and bulk densities, and melting and/or decomposition temperatures. Based on DSC, powder X-ray diffraction and a melting point-composition phase diagram, ibuprofen was found to be a 'racemic compound', and not a 'racemic mixture'. The USP description of ibuprofen as a '± mixture' is therefore misleading.

8. All solids, including S-ibuprofen and racemic ibuprofen, were compressed on the Betapress, and the various parameters mentioned above were obtained for each solid.

9. The parameters from the compression phase were related to the ability of the powder particles to deform permanently under pressure, and the parameters from the decompression phases were used to estimate the elastic behaviour of the solids under pressure.

10. A combination of these parameters with rate of compaction profiles was used to elucidate the deformation mechanisms of various categories of solids. These categories ranged from low yield-strength ductile solids such as acetylsalicylic acid, ibuprofen and their formulations to high yield-strength brittle solids such as the various calcium phosphates.

11. The difference between W_C and W_D, i.e., the work lost in irreversible processes during compression is an indication of the energy stored as bonds in the tablets, and correlated reasonably well with the force of failure of tablets in a diametral compression test.

12. The lost work W_C-W_D also correlated well with porosity change during compression. Materials with large porosity change, or high W_C-W_D, produced strong tablets, e.g., the microcrystalline celluloses relative to lactoses or calcium phosphates.

13. The lost work W_C-W_D was also correlated with the homologous temperatures of the various solids. Materials with a high homologous temperature had a low W_C-W_D indicating that solids are more easily compressed at temperatures close to their melting points.

14. The processed forms of the direct compression agents and direct compression formulations of poorly compressible drugs formed stronger tablets relative to the parent substances. The improvements in tablet strength were reflected in the parameters obtained from the compression and decompression phases.

15. S-ibuprofen and racemic ibuprofen have similar tableting properties, hence the decision to replace racemic ibuprofen with S-ibuprofen in commercial formulations should be based on the differences in their solubility and pharmacokinetics.

16. A simple and inexpensive system of analysis of powder compaction using only the force and time measurements on a rotary tablet press has been developed. This system is potentially applicable to any rotary press. Since the method uses data obtained under normal operating conditions, it can be used for the in-process monitoring of high speed compaction using all the tooling stations, provided the compaction cycles do not overlap. On the Betapress, overlapping seemed likely to be a problem only with fluffy materials such as the microcrystalline celluloses when, to obtain high P_{max}, the die was completely filled.

17. The method can be used for fundamental research on deformation behaviour, for the quality control of materials, for the development of tablet formulations and for the in-process monitoring of compaction.

5. REFERENCES

Agbada, C.O. and York, P. (1990) Theophylline hydrate/anhydrous system: effects of water of hydration on mechanical properties of compacted beams. J. Pharm. Pharmacol. 42(Suppl.): 76P.

Ahn, H.-Y., Amidon, G.L. and Smith, D.E., (1991) Stereoselective systemic disposition of ibuprofen enantiomers in the dog. Pharm. Res. 8: 1186-1190.

Amidon, G.E., Smith, D.P. and Hiestand, E.N. (1981) Rotary press utilizing a flexible die wall. J. Pharm. Sci. 70: 613-617.

Atkins, A.G. and Mai, Y.W. (1985) Elastic and Plastic Fracture: Metals, Polymers, Ceramics, Composites, Biological Materials. Ellis Horwood Ltd., Chichester, West Sussex. pp. 798-800.

Aulton, M.E., Travers, D.N., and White, P.J.P. (1973) Strain recovery of compacts on extended storage. J. Pharm. Pharmacol. 25(Suppl.): 79P-86P

Bangudu, A.B. and Pilpel, N. (1985) Effects of composition and stearic acid on the plasto-elasticity and tableting of paracetamol-microcrystalline cellulose mixtures. Ibid. 37: 289-293.

Bassam, F., York , P., Rowe, R.C. and Roberts, R.J. (1988) Effect of particle size and source on variability of Young's modulus of microcrystalline cellulose powders. Ibid. 40(Suppl.): 68P.

Bateman, S. (1988) High speed compression simulators in tabletting research. Pharm. J. May: 632-633.

Bateman, S., Rubinstein, M.H., Rowe, R.C., Roberts, R.J., Drew, P. and Ho, A.Y.K. (1989) A comparative investigation of compression simulators. Int. J. Pharm. 49: 209-212.

Beck, W.S., Geisslinger, G., Engler, H. and Brune, K., (1991) Pharmacokinetics of ibuprofen enantiomers in dogs. Chirality 3: 165-169.

Bettinetti, G., Giordano, F., Fronza, G., Italia, A., Pellegata, R., Villa, M. and Ventura, P., (1990) Sobrerol enantiomers and racemates: solid-state spectroscopy, thermal behavior, and phase diagrams. J. Pharm. Sci. 79: 470-475.

Bland, D.R. (1960) The theory of linear viscoelasticity. Pergamon Press, New York, N.Y.

Bridgman, P.W. (1949) Linear compression to 30,000 kg/cm^2, including relatively incompressible substances. Proc. Am. Soc. Arts. Sci. 77: 187-234.

Carroll, R.J. and Ruppert, D. (1988) Transformation and weighting in regression. Chapman and Hall, New York. pp 29-30.

Caspar, U. and Muller, F. (1984) Viskoelastizitat von Tabletten bei Statischer Belastung, Pharm. Acta Helv. 59: 329-334.

Celik, M. and Marshall, K. (1989) Use of a compaction simulator system in tabletting research. I. Introduction to and initial experiments with the system. Drug. Dev. Ind. Pharm. 15: 759-800.

Celik, M. and Travers, D.N. (1985) The use of an elastic recovery index as a criterion of compactional behaviour of some directly compression bases, Ibid. 11: 299-314.

Charlton, B. and Newton, J.M. (1984) Theoretical estimation of punch velocities and displacements of single-punch and rotary tablet machines. J. Pharm. Pharmacol. 36: 645-651.

Church, M.S. (1984) Mechanical characterization of pharmaceutical compacts, Ph.D. Thesis, Nottingham.

Church, M.S. and Kennerley, J.W. (1982) Flexure testing of compacted rectangular beams. J. Pharm. Pharmacol. 34(Suppl.): 50P.

Church, M.S. and Kennerley, J.W. (1983) A comparison of the mechanical properties of pharmaceutical materials obtained by the flexure testing of compacted rectangular beams. Ibid. 35(Suppl): 43P.

Cole, E.T., Rees, J.E and Hersey, J.A. (1971) Preliminary compaction studies using a device to simulate a rotary tabletting machine. Ibid. 23(Suppl): 258S.

Cole, E.T., Rees, J.E and Hersey, J.A. (1975) Relations between compaction data for some crystalline pharmaceutical materials. Pharm. Acta Helv. 50: 28-32.

Cook, G.D., Duffield, P.J. and Oliver, A. (1988) Mounting an inductive displacement transducer on a single punch tablet machine. J. Pharm. Pharmacol. 40(Suppl.): 119P.

Courtney, T.H. (1990) Mechanical behaviour of materials. McGraw-Hill, Inc. McGraw-Hill Series in Materials Science and Engineering. Eds. M.B. Bever and C.A. Wert. New York, U.S.A. p. 8, 16, 382.

Cutt, T., Fell, J.T., Rue, P.J. and Spring, M.S. (1987) Granulation and compaction of a model system II. Stress Relaxation. Int. J. Pharm. 39: 157-161.

Danielson, D.W., Morehead, W.L. and Rippie, E.G. (1983) Unloading and postcompression viscoelastic stress *versus* strain behavior of pharmaceutical solids. J. Pharm. Sci. 72: 342-345.

David, S.T. and Augsburger, L.L. (1974) Flexure test for determination of tablet tensile strength. Ibid 63: 933-936.

David, S.T. and Augsburger, L.L. (1977) Plastic flow during compression of directly compressible fillers and its effect on tablet strength. Ibid 66: 155-159.

Doroudian, A. (1991) Determination of compaction parameters of pharmaceutical powders with an instrumented hydraulic press. M.Sc. Thesis, The University of British Columbia, Vancouver, B.C., Canada.

Draper, N.R. and Smith, H. (1966) Applied Regression Analysis. John Wiley & Sons, Inc., New York. pp 88-90.

Duberg, M. and Nystrom, C. (1986) Studies on direct compression of tablets XVII. Porosity-pressure curves for the characterization of volume reduction mechanisms in powder compression. Powder Technol. 46: 67-75.

Duncan-Hewitt, W.C. and Grant, D.J.W. (1987a) Use of Hiestand's indices of tableting performance and the impact fracture wear test to evaluate the mechanical behaviour of labetalol·HCl compacts. Pharm. Res. 4: 22s.

Duncan-Hewitt, W.C. and Grant, D.J.W. (1987b) The impact fracture wear test: a novel method of tablet evaluation. Powder Technol. 52: 17-28.

Duncan-Hewitt, W.C. (1988) The use of microindentation techniques to assess the ability of pharmaceutical crystals to form strong compacts. Ph.D. Thesis, University of Toronto, Toronto, Canada.

Duncan-Hewitt, W.C. and Weatherly, G.C. (1989a) Evaluating the deformation kinetics of sucrose crystals using microindentation techniques. Pharm. Res. 6: 1060-1066.

Duncan-Hewitt, W.C. and Weatherly, G.C. (1989b) Evaluating the hardness, Young's modulus, and fracture toughness of some pharmaceutical crystals using microindentation techniques. J. Mat. Sci. Letters 8: 1350-1352.

Duncan-Hewitt, W.C. and Weatherly, G.C. (1990a) Modeling the uniaxial compaction of pharmaceutical powders using the mechanical properties of single crystals. I. Ductile materials. J. Pharm. Sci. 79: 147-152.

Duncan-Hewitt, W.C. and Weatherly, G.C. (1990b) Modeling the uniaxial compaction of pharmaceutical powders using the mechanical properties of single crystals. I. Brittle materials. Ibid 79: 273-278.

Dwivedi, S.K. (1988) Anomeric composition and solid state properties of lactose. M.Sc. Thesis, The University of British Columbia, Vancouver, B.C.

Dwivedi, S.K. and Mitchell, A.G. (1989) Gas-chromatographic analysis of anomeric composition of lactose. J. Pharm. Sci. 78: 1055-1056.

Ertel, K.D., Heasley, R.A., Koegel, C., Chakrabarti, A. and Carstensen, J.T. (1990) Determination of ibuprofen vapor pressure at temperatures of pharmaceutical interest. Ibid. 79: 552.

Fell, J.T. and Newton, J.M. (1968) The tensile srength of lactose tablets. Ibid. 20: 657-659.

Fell, J.T and Newton, J.M. (1970) Determination of tablet strength by the diametral-compression test. Ibid 69: 688-691.

Ferry, J.D. (1980) Viscoelastic properties of polymers. John Wiley and Sons, Inc., New York, N.Y.

Flugge, W. (1967) Viscoelasticity. A Blaisdell Book in Solid Mechanics, Blaisdell Publishing Co., Waltham, Massachusetts.

Garr, J.S.M. and Rubinstein, M.H. (1991) Compaction properties of a cellulose-lactose direct-compression excipient. Pharm. Technol. Int. 3: 76, 77, 80.

Guyot, J.C., Delacourte, A., and Marie, B. (1986) Computer determination and comparison of the compression behaviour of powder mixtures. Drug Dev. Ind. Pharm. 12: 1869-1884.

Handbook of Pharmaceutical Excipients (1986) published by American Pharmaceutical Association, Washington, DC, USA and The Pharmaceutical Society of Great Britain, London, England. p. 285, 309.

Heckel, R.W. (1961) Density-pressure relationships in powder compaction. Trans. Metall. Soc. A.I.M.E. 221: 671-675.

Hersey, J.A. and Rees, J.E. (1971) Deformation of particles during briquetting. Nature 230: 96.

Hiestand, E.N. (1985) Dispersion forces and plastic deformation in tablet bond. J. Pharm. Sci. 74: 768-770.

Hiestand, E.N., Bane, J.M., Jr. and Strzelinski, E.P. (1971) Impact test for hardness of compressed powder tablets. J. Pharm. Pharmacol. 60: 758-763.

Hiestand, E.N. and Smith, D.P. (1984) Indices of tableting performance. Powder Technol. 38: 145-149.

Hiestand, E.N., Wells, J.E., Peot, C.B. and Ochs, J.F. (1977) Physical process of tableting. J. Pharm. Sci. 66: 510-519.

Ho, A., Barker, J.F., Spence, J. and Jones, T.M. (1979) A comparison of three methods of mounting a linear variable displacement transducer on an instrumented tablet machine. J. Pharm. Pharmacol. 31: 471-472.

Ho, A.Y.K. and Jones, T.M. (1988a) Punch travel beyond peak force during tablet compression. Ibid 40S: 75P.

Ho, A.Y.K. and Jones, T.M. (1988b) Rise time: a new index of tablet compression. Ibid 40S: 74P.

Hunter, B.M., Fisher, D.G., Pratt, R.M. and Rowe, R.C. (1976) A high speed compression simulator. Ibid 28(Suppl.): 65P.

Hutt, A.J. (1991) Drug chirality: impact on pharmaceutical regulation. Chirality, 3: 161-164.

Jamali, F., Singh, N.N., Pasutto, F.M., Russel, A.S. and Coutts, R.T., (1988) Pharmacokinetics of ibuprofen enantiomers in man following oral administration of tablets with different absorption rates. Pharm. Res., 5: 40-43.

Jetzer, W.E., Leuenberger, H. and Sucker, H. (1983) The compressibility and compactibility of pharmaceutical powders. Pharm. Technol. 7: 33-39.

Jones, T.M. (1977) Formulation factors: Drugs given by oral route. In Formulation and Preparation of Dosage Forms: Proceedings of the 37th International Congress of Pharmaceutical Sciences of F.I.P. Eds. J. Polderman. The Hague, The Netherlands. Elsevier/North Holland, Amsterdam, The Netherlands. pp. 29-44.

Jones, T.M. (1978) Preformulation studies to predict the compaction properties of materials used in tablets and capsules. Acta Pharm. Technol. Supplement 6: 141-159.

Juslin, M.J. and Paronen, T.P. (1980) On the accuracy of displacement measurements by instrumented single-punch machines. J. Pharm. Pharmacol. 32: 796-798.

Kaneniwa, N., Imagawa, K. and Otsuka, M. (1984) Compression properties of cephalexin powder and physical properties of the tablet. Chem. Pharm. Bull. 32: 4986-4993.

Kendall, K. (1978) The impossibility of comminuting small particles by compression. Nature 272: 710-711.

Kerridge, J.C. and Newton, J.M. (1986) The determination of the compressive Young's modulus of pharmaceutical materials. J. Pharm. Pharmacol. 38(Suppl.): 79P.

Krycer, I., Pope, D.G. and Hersey, J.A. (1982a) An evaluation of the techniques employed to investigate powder compaction behaviour. Int. J. Pharm. 12: 113-134.

Krycer, I., Pope, D.G. and Hersey, J.A. (1982b) The interpretation of powder compaction data- a critical review. Drug. Dev. Ind. Pharm. 8: 307-342.

Kussendrager, K., De Hoog, P. and Van Leverink, J. (1981) Some physical properties of spray-dried lactose with respect to stability, compression. Acta Pharm. Suec. 18: 94-95.

Lammens, R.F., Polderman, J., De Blaey, C.J. and Armstrong, N.A. (1980) Evaluation of force-displacement measurements during powder compaction. Part II: Precision and accuracy of powder height and punch displacement measurements. Int. J. Pharm. Tech. & Prod. Mfr. 1: 26-35.

Lawn, B.R. and Wilshaw, T.R. (1975) Fracture of Brittle Solids. Cambridge University Press, Cambridge, London. p 77.

MacLeod, H.M. (1983) Compaction of ceramics. In: Enlargement and Compaction of Particulate Solids. Ed. N.G. Stanley-Wood. Butterworths Monographs in Chemical Engineering. Series ed. J.W. Mullin. Butterworths & Co, London, England. P. 259.

Malamataris, S., Bin Baie, S. and Pilpel, N. (1984) Plasto-elasticity and tableting of paracetamol, Avicel and other powders. J. Pharm. Pharmacol. 36: 616-617.

Marsh, D.M. (1964) Plastic flow in glass. Proc. R. Soc. London. A279: 420-435.

Marshall, K. (1986) Compression and consolidation of powdered solids. In The Theory and Practice of Industrial Pharmacy, L. Lachman, H.A. Lieberman, J.L. Kanig, Eds., Lea & Febiger, Philadelphia, PA, p. 66.

Marshall, K. (1989) Monitoring punch forces and punch movements as an aid to developing robust tablet formulations. Drug. Dev. Ind. Pharm. 15: 2153-2176.

Mashadi, A.B. and Newton. J.M. (1987) The characterization of the mechanical properties of microcrystalline cellulose: a fracture mechanics approach. J. Pharm. Pharmacol. 39: 961-965.

Morehead, W.T. and Rippie, E.G. (1990) Timing relationships among maxima of punch and die-wall stress and punch displacement during compaction of viscoelastic solids. J. Pharm. Sci. 79: 1020-1022.

Morita, M., Nakai, Y., Fukuoka, E. and Nakajima, S. (1984) Physicochemical properties of crystalline lactose. II. Effect of crystallinity on mechanical and structural properties. Chem. Pharm. Bull. 32: 4076-4083.

Oates, R.J. and Mitchell, A.G. (1989) Calculation of punch displacement and work of powder compaction on a rotary tablet press. J. Pharm. Pharmacol. 41: 517-523.

Oates, R.J. and Mitchell, A.G. (1990) Comparison of calculated and experimentally determined punch displacement on a rotary tablet press using both Manesty and IPT punches. Ibid. 42: 388-396.

Okada, J. and Fukumori, Y. (1975) Compaction of powders. II. Comparison of compaction behaviours among various powders, Chem. Pharm. Bull., 23: 326-332.

Parrott, E.L. (1985) Compression. In Pharmaceutical Dosage Forms: Tablets. H.A. Lieberman, L. Lachman, Eds., vol. 2., Marcell Dekker, Inc., New York, N.Y.

Peleg, M. and Moreyra, R. (1979) Effect of moisture on the stress relaxation pattern of compacted powders. Powder Technol. 23: 277-279.

Pitre, D. and Stradi, R., (1990) Racemic modification of (R,S)-3-(4-Phenyl-1-piperazinyl)-1,2-propandiol and melting point diagram. Arch. Pharm. (Weinheim), 323: 23-25.

Popov, E.P. (1968) Introduction to mechanics of solids. Prentice-Hall, Inc. Englewood Cliffs, N.J., pp. 116-120, p 554.

Prigogine, I. and Defay, R. (1954) Chemical Thermodynamics, D.H. Everett, translator, Longman Group Limited, London, pp. 373-375.

Ragnarsson, G. (1985) Evaluation of tabletting properties in preformulation and early formulation work. Acta Pharm. Suec. 22: 173

Ragnarsson, G. and Sjorgen, J. Force-displacement measurements in tableting. J. Pharm. Pharmacol. 37: 145-150.

Rees, J.E., Hersey, J.A. and Cole, E.T. (1972) Simulation devices for preliminary tablet compression studies. J. Pharm. Sci. 61: 1313-1315.

Rees, J.E. and Rue, P.J. (1978) Time-dependent deformation of some direct compression excipients. J. Pharm. Pharmacol. 30: 601-607.

Rhone-Poulenc Product Information Manual (1989) Calcium phosphate pharmaceutical ingredients. Rhone-Poulenc Basic Chemical Co., Shelton, CT.

Rhone-Poulenc Product Information Manual (1989) Calcium Phosphate Pharmaceutical Ingredients, Rhone-Poulenc Basic Chemicals Co., Shelton, CT, USA, p. 11.

Ridgway Watt, P. (1983) Tablet press instrumentation. Mnfg. Chem. 54: 42-43, 45.

Ridgway Watt, P. (1988) Tablet Machine Instrumentation in Pharmaceutics. Ellis Horwood Ltd., Chichester, West Sussex. pp 305-309.

Ridgway Watt, P. and Rue, P.J. (1979) The design and construction of a fully instrumented rotary tablet machine. International Conference on Pharmaceutical Technology and Product Manufacture, Copenhagen.

Ridgway, K., Shotton, E. and Glasby, J. (1969) The hardness and elastic modulus of some crystalline pharmaceutical materials. J. Pharm. Pharmacol. 21(Suppl.): 19S-23S.

Rippie, E.G. and Danielson, D.W. (1981) Viscoelastic stress/strain behavior of pharmaceutical tablets: analysis during unloading and post compression periods. J. Pharm. Sci. 70: 476-482.

Ritter, A. and Sucker, H.B. (1980) Studies of variables that affect tablet capping. Pharm. Technol. 4: 56-65, 128.

Roberts, R.J. and Rowe, R.C. (1985) The effect of punch velocity on the compaction of a variety of materials. J. Pharm. Pharmacol. 37: 377-384.

Roberts, R.J. and Rowe, R.C. (1987) Brittle/ductile behaviour in pharmaceutical materials used in tabletting. Int. J. Pharm. 36: 205-209.

Roberts, R.J. and Rowe, R.C. (1987a) The Young's modulus of pharmaceutical materials. Ibid 37: 15-18.

Roberts, R.J. and Rowe, R.C. (1987b) The compaction of pharmaceutical and other model materials- a pragmatic approach. Chem. Eng. Sci. 42: 903-911.

Rossi, R.C. (1968) Prediction of the elastic moduli of composites. J. Am. Ceram. Soc. 51: 433-439.

Seugling, E.W. (1980) The contribution of tableting aids to pharmaceutical development. Pharm. Technol. 4: 27-35, 62.

Shlanta, S. and Milosovich, G. (1964) Compression of pharmaceutical powders I. Theory and instrumentation. J. Pharm. Sci. 53: 562-564.

Simmons, G. and Wang, H. (1971) Single Crystal Elastic Constants and Calculated Aggregate Properties: A Handbook. The M.I.T. Press, Cambridge, Massachusetts. p 271.

Spriggs, R.M. (1961) Expression for effect of porosity on elastic modulus of polycrystalline refractory materials, particularly aluminum oxide. J. Am. Ceram. Soc. 44: 628-629.

Staniforth, J.N., Baichwal, A.R. and Hart, J.P. (1987) Interpretation of creep behaviour of microcrystalline cellulose powders and granules during compaction, Int. J. Pharm. 40: 267-269.

Swartz, C.J. (1969) Development of IPT standards for tableting tools. J. Pharm. Sci. 58: 473-477.

Talman, F.A.J. (1977) Formulation. In Bentley's Textbook of Pharmaceutics Ed. E.A. Rawlins. Bailliere Tindall, London, England. p. 644.

The Merck Index (1976) Starch. M. Windholz, Ed., 9th ed., Merck & Co., Inc., Rahway, N.J., p. 8574.

Toure, P., Puisieux, F., Duchene, D. and Carstensen, J.T. (1980) Energy terms in tablet compression cycles. Powder Technol. 26: 213-216.

Train, D. (1956) An investigation into the compaction of powders. J. Pharm. Pharmacol. 8: 745-760.

Travers, D.N., Celik, M. and Buttery, T.C. (1983) A computer aided investigation on strain movements in compacts under constant stress within the die. Drug. Dev. Ind. Pharm. 9: 139-157.

USP XXII (1990) Ibuprofen, Official Monographs. p. 682.

Vromans, H., Bolhuis, G.K., Lerk, C.F., Kussendrager, K.D. and Bosch, H. (1986) Studies on tableting properties of lactose. VI. Consolidation and compaction of spray dried amorphous lactose. Acta Pharm. Suec. 23: 231-240.

Wachtman, Jr., J.B. (1969) Elastic deformation of ceramics and other refractory materials. In Wachtman Jr., J.B. (Ed.), Mechanical and Thermal Properties of Ceramics, National Bureau of Standards Special Publication 303. National Bureau of Standards, Washington, D.C. pp 139-168.

Walter, J.T. and Augsburger, L. (1986) A computerized force-displacement instrumentation system for a rotary press. Pharm. Technol. 10: 26-34.

Wong, D.Y.T. and Aulton, M.E. (1989) Modification of the mechanical properties of alpha lactose monohydrate crystals by adjustment of growth conditions. J. Pharm. Pharmacol. 41(Suppl.) 124P.

York, P. (1979) A consideration of experimental variables in the analysis of powder compaction behaviour. Ibid 31: 244-246.

York, P. and Baily, E.D. (1977) Dimensional changes of compacts after compression. Ibid. 29: 70-74.

Yu, H.C.M., Rubinstein, M.H., Jackson, I.M. and Elsabbagh, H.M. (1988) Multiple compression and plasto-elastic behaviour of paracetamol and microcrystalline cellulose. Ibid. 40: 669-673.

Zar, J. H. (1984) Biostatistical Analysis. Prentice-Hall, Inc., Englewood Cliffs, New Jersey. pp. 268, 285-289.